Tectono-sedimentary evolution of Southern Mexico. Implications for Cretaceous and younger source-to-sink systems in the Mexican foreland basins and the Gulf of Mexico

Villagómez, D. [1,*], Steffensen, C. [2], Pindell, J. [1], Molina-Garza, R.S. [3], Gray, G. [4], Graham, R. [5], O'Sullivan, P. [6], Stockli., D. [7], Spikings, R. [8]

[1] Tectonic Analysis Ltd, Duncton, West Sussex GU28 0LH, UK
[2] Viking GeoSolutions LLC, Houston TX 77224 USA
[3] Centro de Geociencias, Universidad Nacional Autónoma de México, Juriquilla 76230, México
[4] Department of Earth, Environmental and Planetary Sciences, Rice University, Houston, TX 77055, USA
[5] Department of Geology, Imperial College, London SW7 2BP, UK
[6] GeoSep Services, Moscow, ID 83843, USA
[7] Department of Geological Sciences, University of Texas at Austin, TX 78712-1722, USA
[8] Department of Mineralogy, Faculty of Sciences, University of Geneva, 1205 Geneva, Switzerland

* Corresponding author (email: Diego.Villagomez@gmail.com)

Abstract

An extensive dataset of existing and new geo/thermochronological data from several areas in Southern Mexico constrains the tectonic history of the region, as well as various source-to-sink relationships and local burial histories. Our interpretation acknowledges that not all cooling/heating observed in the source areas is due to erosional exhumation/burial but, in some cases, due to advective heat transfer from magmatic sources, which potentially overprinted earlier events. In this work, we identified several areas that have been exhumed since the Early Cretaceous and potentially provided clastic material to the southern Gulf of Mexico area.

We help to document how the Mexican (Laramide) Orogeny propagated eastwards and southwards from the Late Cretaceous through the early Oligocene. The first sediments reaching the Tampico–Misantla and Veracruz basins derived mostly from eroded Cretaceous carbonate material that covered the Sierra Madre Oriental, the Sierra de Juárez Complex and the Cuicateco belts, as well as foredeep/intra-orogenic basin deposits formerly covering them. Possibly by the end of the Mexican Orogeny, the clastic Jurassic and older crystalline basement rocks became exposed and became the main sources of quartz-rich clastic material to the most easterly foreland basins and Gulf of Mexico. Exposure was probably assisted by higher angle basement thrusts such as the Vista Hermosa/Valle Nacional faults. The Mixtequita and Guichicovi blocks have also provided an important source of quartz-rich and metamorphic lithic-rich material to the southern Veracruz Basin possibly since the Eocene.

For most of the Cenozoic, the Chiapas and the Sureste basins were sourced from areas south of the Chiapas Massif, i.e., the North America–Caribbean plate boundary zone along today's Chiapas coastal plain. This plate boundary zone accommodated relative displacement between Mexico and the Chortis Block of the Caribbean Plate. Paleocene–middle Miocene sediments within the Chiapas Basin were at least partially sourced from i) metamorphic complexes in the northern Chortis Block; ii) the parautochthonous Chontal Complex, an oceanic-like basin sandwiched between Chortis and southern Mexico; iii) the elongating volcanic arc along southern Mexico and western Chortis; and iv) the Cretaceous and Jurassic sedimentary cover of the southern flank of the Chiapas Massif,

The westward telescoping of southern Mexico onto the Cocos Plate in the wake of Chortis has produced flat slab subduction geometry and eastwardly-younging uplift of the Xolapa Belt (Oligo–Miocene) and the Chiapas Massif (late Miocene). It also caused reorganization of the drainage systems providing material to the Chiapas and Sureste basins.

Our results highlight the importance of understanding relative block and plate boundary displacements in a dynamic hinterland and consider the role of major faults when interpreting source-to-sink relationships in the area. We describe the latter relationships for several geologic time intervals in which reservoir-prone sediments were delivered to the southern Gulf of Mexico. Finally, we integrate the source-to-sink history to provide an assessment of reservoir quality and hydrocarbon prospectivity in the region.

1 Introduction

Source-to-sink analyses aim to integrate the collective sedimentary systems that extend from eroding mountainous areas, through transfer zones and finally to depositional sink areas, usually deep-sea basins (Allen, 2017). Although these types of analyses are not a new concept (see Walsh et al., 2016; Helland-Hansen et al., 2016), their utility for the determination of the dispersal of sediments and potential resources contained in those sediments is unparalleled (Allen and Allen, 2013). Variations in the distribution and amount of sediments reaching the depositional areas reflect ultimately changes in tectonic activity and/or climate, particularly in active and highly dynamic areas such as the North American continental interior (Galloway et al., 2011).

The tectonic and/or erosional exhumation of continental and oceanic litho-tectonic units exposed in southern Mexico has significantly contributed to the sediment flux into the Gulf of Mexico and adjacent basins, beginning in the late Mesozoic (Winker and Buffler, 1988; Gray et al., 2021; Graham et al., 2020; Sierra-Rojas et al., 2020; Beltrán-Triviño et al., 2021). Although a number of individual studies have assessed the post-Jurassic uplift and exhumation history of certain areas in northern (Fitz-Díaz et al., 2014; 2018, Gray et al., 2001; 2021) and southern Mexico (Ducea et al., 2004; Witt et al., 2012; Abdullin et al., 2016; Gray et al., 2021; Villagómez and Pindell, 2020a, 2020b; Hernández-Vergara et al., 2021), we still lack a synthesis explaining when and how the continental margin was exhumed and where the potential sink areas were located.

We have determined the Cretaceous and younger exhumation history for southern Mexico by using a number of geochronological and thermochronological techniques on litho-tectonic units from the southern Sierra Madre Oriental to western Guatemala. We have linked these “source” areas to potential depositional areas based on published studies and industrial data. Our work also addresses some depositional aspects of clastic sediments reaching the Gulf of Mexico basins.

Our results show that the Cretaceous and younger exhumation history of the region directly relates to the progressive evolution of the Farallon/Cocos–North America–Caribbean plate boundaries, including the relative displacement of the Chortis Block along Mexico as part of the NW Caribbean Plate. This paper presents a series of paleogeographic and depositional reconstructions that account for i) regional tectonics, ii) exhumation-related information, iii) detrital provenance analysis, and iv) depositional studies in the different foreland basins of southern Mexico.

This work highlights the importance of sedimentary reworking as a fundamental aspect when determining provenance and reservoir quality in Southern Mexico. These “second cycle” sediments are more texturally and compositionally mature when re-deposited farther out into the basin, therefore with improved reservoir characteristics.

2 Geological setting

The following summary and **Appendix 1** synthesize the geology of the main litho-tectonic units in Southern Mexico, which are shown in **Figure 1**. Most of the litho-tectonic units described here are primarily identified based on their stratigraphy and deformation history, and do not necessarily carry any genetic implication even if some of them were allochthonous prior to a given time. Nonetheless, they are usually bounded by major faults (currently exposed at surface or not) with a clear geological relevance and displacement history based on geological mapping and/or exhumation-related information. For the purposes of this contribution, we have subdivided the Cuicateco Belt into several workable sub-units or sub-belts based on mapped faults and differential lithologies. The different regional-scale litho-tectonic units discussed below are characterized by internal geological homogeneity, tectonic style, exhumation, and deformation history and are bordered by the structures shown in **Figure 1**. Some of the most important litho-tectonic units and major structures are shown in cross sections (**Figures 2a and 2b**)

2.1 Geologic and tectonic aspects of the different litho-tectonic units

2.1.1 Xolapa

The Xolapa Complex records Jurassic–Cretaceous magmatism with concurrent Upper Jurassic–Lower Cretaceous sedimentation followed by an intense and eastwardly diachronous Cenozoic magmatism. This history suggests that Xolapa corresponds to a Jurassic–Cretaceous arc and associated peri-arc basin (Talavera-Mendoza et al., 2013; Peña-Alonso et al., 2018). The rocks also record several tectono-thermal events including: i) Late Jurassic tectonic foliation development, ii) a pre-129 migmatization (Herrmann et al., 1994; Solari et al., 2007), iii) Paleocene–early Eocene migmatization and ductile to brittle deformation (Peña-Alonso et al., 2017), and iv) conspicuous Eocene–Oligocene sinistral shearing (Peña-Alonso et al., 2017, 2021; Kazachkina et al., 2020).

The northern limit of the Xolapa Unit is a series of faults with ductile and brittle kinematic indicators such as (Las Ventas)–Tierra Colorada (Riller et al., 1992), and the Chacalapa mylonitic (Tolson, 2005) faults (**Figures 1 and 2a**). All of these faults may represent a strand of the long-lived North America–Chortis plate boundary (Graham et al., 2020), and seem to be offset by the offshore Chipehua Fault (Sánchez-Barreda, 1981).

2.1.2 Mixteca and Oaxaca blocks

The basement of these blocks comprises Late Mesoproterozoic gneisses and Paleozoic granitoids, amphibolite and metasediments (Keppie et al., 2003; Weber et al., 2010) intruded by Permian–Early Triassic anatectic granites. The Mixteca and Oaxaca blocks (which are separated by lithospheric Caltepec Fault; Elías-Herrera and Ortega-Gutiérrez, 2002) have likely behaved as a coherent crustal block at least since Middle Jurassic (Nieto-Samaniego et al., 2006; Peña-Alonso et al., 2017). The two blocks have a thick Mesozoic sedimentary cover with only limited evidence of Jurassic syn-rift extension (Martini and Ortega-Gutiérrez, 2018; Campos-Madrigal et al., 2013; Zepeda-Martínez et al., 2021), widespread Upper Jurassic shallow water deposition and a record of Early Cretaceous back-arc extension (Sierra-Rojas et al., 2016). On the east, the Oaxaca basement is covered by the deep-water Lower Cretaceous Jaltepetongo Fm. (Sierra-Rojas et al., 2020). Both blocks are covered by extensive Albian–Cenomanian platform deposits, as well as by a series of Coniacian to Paleogene clastic continental deposits. Late Cretaceous–Eocene compressional deformation is observed in both the Mixteca and Oaxaca blocks (Nieto-Samaniego et al., 2006; Fitz-Díaz et al., 2018; Ruiz-Arriaga, 2018). The latter deformation is related to the so-called Mexican Orogeny, traditionally referred to as the Laramide Orogeny (see discussion in Fitz-Díaz et al., 2018). The Oaxaca Block is widely intruded by Oligocene–Miocene arc-related intrusive bodies (e.g., Ejutla Batholith) and covered by Oligo–Miocene volcanic rocks which locally host magmatic-hydrothermal deposits mostly of Miocene age (Camprubí et al., 2019). The Oaxaca Block is bounded to the East by the brittle, west-dipping normal Oaxaca Fault (**Figures 1 and 2a**), which is possibly a late reactivation of a structure that may have been associated with the Jurassic strike-slip assembly of Southern Mexico (Pindell et al., 2020a) and the opening of the Gulf of Mexico (Fitz-Díaz et al., 2022).

2.1.3 Sierra de Juárez Complex

We consider the Sierra de Juárez Complex to include the crystalline rocks located along and between the Oaxaca Fault and the Siempre Viva Fault to the east. The Siempre Viva Fault is a major thrust that puts the Sierra de Juárez Complex above the Cuicateco Belt (**Figure 1**). The Sierra de Juárez Complex forms a ~170 km long and ~10–15 km wide migmatitic-mylonitic belt previously interpreted as a thrust zone reactivated by possibly dextral shearing during the opening of the Gulf of Mexico (Delgado-Argote, 1988; Alaniz-Alvarez et al., 1996). This complex includes a series of ortho- and para-gneisses that show evidence of partial migmatization and mylonitization. The metamorphic rocks have been separately named Sierra de Juárez Mylonitic Belt in the south (Alaniz-Alvarez et al., 1994) or Teotitlán Migmatitic Complex in the north (Ángeles-Moreno, 2006; Ángeles-Moreno et al. 2012). Most recently, they have been interpreted to share a common deformational history related to hyper-extension (Villagómez, 2014; Pindell et al., 2020a; Graham et al., 2020). The protoliths of the metamorphic rocks have Paleozoic, Neoproterozoic and Mesoproterozoic (Espejo-Bautista et al., 2021) ages and the rocks are intruded by Late Jurassic–earliest Cretaceous plutons (Pindell et al., 2020a; this work). Migmatization related to decompression has been dated at ~147–133 Ma (Ángeles-Moreno, 2006; Coombs, 2016; Pindell et al., 2020a) and was likely synchronous with mylonitization in the latest Jurassic–earliest Cretaceous (Graham et al., 2020; Pindell et al., 2020a).

2.1.4 Cuicateco Belt

The Cuicateco Belt, also known as the Juárez Terrane (Campa and Coney, 1983), includes a series of sub-belts located between the Siempre Viva Fault and the Valle Nacional/Soyaltepec thrusts (**Figure 1**). The southern region is dissected by a series of faults (e.g., Villa Alta, Vista Hermosa, Aloapán faults; **Figure 1**) that have brought the crystalline basement to surface levels. This deeper level of exposure in the southern region has removed much of the conspicuous Cretaceous–lower Cenozoic sedimentary cover observed in other regions of Southern Mexico. The northern region of the Cuicateco Belt is clearly less exhumed and preserves the so-called Cretaceous Córdoba Platform (Ortuño-Arzate et al., 2003).

Southern region: Although poor exposure prevents a better lithological discrimination, three main sub-belts (Units 4a–c; **Figure 1**) can be distinguished in the southern portion of the Cuicateco Belt, which from west to east are (see also **Appendix 1)**:
a) Paleozoic metasedimentary rocks covered by variably deformed sediments of the Todos Santos (Jurassic), Jaltepetongo, Chivillas (Lower Cretaceous) and Tamaulipas and Tecamalucán (mid–Upper Cretaceous). This sub-belt is pervasively intruded by Neogene plutons.
b) A massive sub-belt of Paleozoic schists named Mazateco Complex in the North (Ángeles-Moreno, 2006; Ángeles-Moreno et al., 2012) and Mazatlán Complex in the South, floored by Paleozoic metasediments and metaigneous rocks of the Tuxtepec Complex (Ordovician maximum depositional age; Molina-Garza et al., 2020a).
c) A plutonic metamorphic complex that includes serpentinized gabbros of the Tuxtepec Complex; thrust over and overlain by Jurassic Todos Santos Formation and partially covered by Lower Cretaceous back-arc volcanic rocks of the Xonamanca Fm.

*Northern region (*Unit 4d; **Figure 1***)*: The Córdoba Platform and Zongolica fold-and-thrust belt includes Upper Jurassic marine strata and Lower Cretaceous back-arc volcanic and sedimentary rocks of the Xonamanca and Chivillas formations followed by middle Cretaceous platform deposits and Upper Cretaceous siliciclastic deposits (Lawton et al., 2020). All of these Mesozoic sedimentary successions are deformed, forming a NNW–SSE oriented fold-and-thrust belt with eastward vergence. The origin of this belt, also known as the Zongolica fold-and-thrust belt, is related to the Mexican Orogeny and occurred during Late Cretaceous and early Cenozoic time (Fitz-Díaz et al., 2018; Carfantán, 1985). There are a few remnants of piggy-back basins with Paleocene and Eocene clastics deposited between thrusted carbonate rocks (Ortuño-Arzate et al., 2003).

2.1.5 Veracruz Basin

The western flank of this basin contains Cretaceous lithologies similar to those observed in the Córdoba platform, but the main depocenter is filled with Cenozoic foreland deposits above an uncertain Mesozoic stratigraphy. This is because drilling has rarely reached the Mesozoic, and some evolutionary models (e.g., Pindell and Kennan, 2001; 2009; Pindell et al., 2016; 2021) consider the eastern half of the basin as part of the Jurassic oceanic Gulf of Mexico. The Cenozoic deposits were dominated by deep-water submarine fans, at least until the latest Pliocene. Miocene re-activation of older structures is recognizable even beyond the deformation front into the western Veracruz Basin (**Figure 1**) and was responsible for the observed folding and thrusting beneath the coastal plain (Prost and Aranda, 2001; Graham et al., 2020).

2.1.6 Sierra Madre Oriental

The Sierra Madre Oriental remains one of the most prominent topographical expressions of the Mexican Orogeny (**Figure 1**). Folded and thrusted rocks currently exposed in the Sierra Madre Oriental Belt include Upper Triassic through middle Eocene strata. The Sierra Madre Oriental Belt grew during the Mexican Orogeny as a forward propagating system from ~90 Ma to ~43 Ma (Fitz-Díaz et al., 2014; Gray et al., 2021). This progressive but episodic deformation started in the western hinterland and propagated eastwards (Fitz-Díaz et al., 2014, 2018; Gray et al., 2001, 2021) forming various generations of km-scale folds. The frontal region of the southern Sierra Madre Oriental accommodated sedimentary and tectonic overburden throughout most of Mexican Orogeny times (Fitz-Díaz et al., 2018).

2.1.7 Tampico–Misantla Basin

This basin corresponds to the foreland basin related to the Mexican Orogeny, although Jurassic rifts form its deeper parts. Maastrichtian–Eocene synorogenic turbidites were deposited in foredeep depocenters and onlapped topographical highs (e.g., Tuxpan Platform; Carrillo, 1980; Horbury et al., 2003). The turbidites, composed of siliciclastic and calcareous detritus, were overlain by post-orogenic Oligocene–Miocene eastward propagating sedimentary wedges. It has been a depositional area throughout the Cenozoic with possibly a few episodes of erosion between 30 and 10 Ma (Gray et al., 2021; Villagómez et al., 2019).

2.1.8 Mixtequita Massif

Several authors (Pindell and Kennan, 2001, 2009; Nguyen and Mann, 2016) trace the landward expression of the East Mexico Transform (previously named Tamaulipas–Golden Lane–Chiapas fault by Pindell, 1985; or Western Main Transform fault by Martön and Buffler, 1994) through the Veracruz Basin and Tehuantepec as lying along the western side of the Mixtequita Massif (**Figure 1**). The metamorphic and granitic rocks located east of this fault zone (locally named the Petapa Fault; Molina-Garza et al., 2020a) include the Mixtequita Unit in the north (Permian and Jurassic granitoids) and the Guichicovi Unit in the south (Precambrian granulitic gneisses). The Mixtequita was probably derived from partial melting of the Guichicovi (Weber and Hecht, 2003). Both units are surrounded by Jurassic Todos Santos with some possible Todos Santos outliers upon them, suggesting strong extensional unroofing during rifting and after the partial melting (Pindell et al., 2021).

The northern border of the Mixtequita Block is buried beneath the southern Veracruz Basin (Pindell et al., 2016, 2020a) whereas the eastern border seems to be continuous with the greater Chiapas Massif, although beneath Cenozoic sediments (Molina-Garza et al., 2020a). The southern flank of the Guichicovi Block is overthrust by folded and cleaved Todos Santos, as well as by Cretaceous metasediments from the Chontal Complex (see below). The Mixtequita and Guichicovi units experienced a long history of sedimentary and tectonic burial during the Cretaceous and were arguably cooled and exhumed in the late Eocene (Molina-Garza et al., 2020a).

2.1.9 Chontal Complex

Upper Cretaceous metamorphosed volcanic and basinal sedimentary rocks, possibly extruded and deposited in an oceanic back-arc setting (Carfantán, 1981; Pindell et al., 2011; Molina-Garza et al., 2020a). These rocks are interpreted as being accreted to the paleo-Pacific continental margin of southern Mexico, forming the so-called Chivela Nappes (**Figure 1**; Molina-Garza et al., 2020a). As revealed by magnetic anomalies and field mapping, the Chontal Complex is thrusted tens of kilometres over the Mixtequita Block (Molina-Garza et al., 2020a).

Detrital zircon U–Pb ages from the Chontal metasediments have maximum depositional ages of 77 Ma (Pérez-Gutiérrez et al., 2009). The rocks experienced low-grade metamorphism (Molina-Garza et al., 2020a) and deformation after Maastrichtian times (protolith U–Pb age of 66 Ma age; Pérez-Gutiérrez et al., 2009). These metamorphic rocks are partially and unconformably overlain by continental Oligocene–late Eocene sediments (Carfantán, 1981) of the Huamelula Fm. The Huamelula sediments contain Chontal-like lithologies, as well as older granite boulders (Molina-Garza et al., 2020a), providing a minimum age constraint for the metamorphism and accretion of the Chontal Complex to the Mexican margin. These relationships indicate that the Chontal rocks were metamorphosed to low-grade conditions and then were exhumed to surface levels by the late Eocene, possibly during final accretion. All the units were subsequently intruded by Miocene granitoids.

2.1.10 Chiapas Massif and Basin

The Chiapas Massif is mainly composed of Permian granitoids, which intrude Upper Paleozoic metasedimentary rocks (Weber et al., 2006; 2007). The massif was likely detached from the basement of the Tampico–Misantla Basin (Tamaulipas Arch and other basement highs) in Bathonian times (Villagómez et al., 2019; Pindell et al., 2020a), when it began to rotate clockwise along with the Yucatán Block along the East Mexico Transform (**Figure 1**; Molina-Garza et al., 1992; Pindell et al., 2016). The Chiapas Massif has been roughly at North American paleo-latitudes since the Hauterivian. However, a small clockwise rotation (15–20°) has been recorded by paleomagnetic studies on overlying middle Eocene strata prior to late Miocene, probably in the middle Miocene (Molina-Garza et al., 2020b).

The Chiapas Basin developed above the southwest Yucatán Block since the Early Jurassic. Bed-plane shearing due to shortening and/or salt deformation in the Chiapas fold-and-thrust belt arguably started in the Eocene (Witt et al., 2012; Villagómez and Pindell, 2020a; Hernández-Vergara et al., 2021), although most deformation is middle Miocene to Recent (Chávez-Valois et al., 2009). Shortening in the Chiapas fold-and-thrust belt was most probably driven by the clockwise rotational translation of the Chiapas Massif, which in turn was likely caused by the onset of Cocos subduction beneath Chiapas in the wake of Chortis during middle to late Miocene times (Pindell and Miranda, 2011; Pindell et al., 2020b; Graham et al., 2020; Molina-Garza et al., 2021).

The Chiapas Massif is presently bounded to the South by the Tonalá Fault (**Figures 1 and 2b**), a sub-vertical ductile transcurrent shear zone (Molina-Garza et al., 2015, 2021), which, along with the Motagua and Baja Verapaz faults, is likely to represent major strands of the North America–Caribbean plate boundary zone (Graham et al., 2020).

2.1.11 Eastern Chiapas, Chortis (mobile) and the Tehuantepec Shelf

The geology of the southeasternmost tip of the morphological Chiapas Massif (south of the Polochic Fault) is composed of Lower Paleozoic metasedimentary rocks (Weber et al., 2008), which arguably resemble the lithologies of Chortis (**Appendix 1**). In Mexico, this tip of the Massif has been named the Huixtla Block and interpreted by Villagómez and Pindell (2020a) as more highly exhumed, allochthonous with respect to Chiapas Massif, and with a slightly older exhumation history than the rest of the massif.

In addition, two volcanoclastic rocks obtained from the Salina Cruz-1 well offshore Tehuantepec contained consistently unimodal U–Pb ages of 88 Ma and 69 Ma (Tectonic Analysis Ltd., pers. comm., 2022, unpublished data). This shows that the dated units correspond to Upper Cretaceous volcanoclastic rocks, which are not known in autochthonous onshore areas. However, these rocks are relatively close in age with plutons observed onshore in the Huixtla Block, south of the Polochic Fault (64.8±1.3 Ma; Villagómez and Pindell, 2020a), suggesting that offshore Tehuantepec Shelf and the Huixtla Block might be the western continuation or tail of the mobile Chortis Block.

3 Published thermochronology in Southern Mexico

3.1 Thermochronology basics and applications

Thermochronology provides information on the timing, duration and magnitude of heating and cooling events recorded by rocks (Braun et al., 2006). This information can be further used to evaluate the influence of tectonic and magmatic events, crustal or stratal exhumation of mountainous areas, basin-forming mechanisms, delivery of clastic material to sedimentary basins, as well as burial and erosion history of sedimentary basins (Armstrong, 2005). This information is therefore critical when determining the timing and possible pathways of sediments delivered to a depositional site, for instance the Gulf of Mexico.

All isotopic systems in minerals behave as open systems if the ambient temperature is sufficiently high. In such cases, isotopes are able to rapidly partition into fluid rich phases and solid phases with lower concentrations of the solute (i.e., daughter isotope). It is reasonable to assume that daughter isotope loss is dominated by thermally activated diffusion, hence we can define a temperature range where daughter isotopes are partially retained within their lattice of origin. It is also possible to define a closure temperature (Dodson, 1973), which lies within the temperature range of daughter isotope retention and is approximately equivalent to the temperature at which more than half of the daughter isotopes are retained.

Various geo- and thermo-chronometers with a wide range of retention temperatures are customarily employed in thermochronology in order to elucidate the thermal path of a rock within the middle and upper crust. Common methods currently used are U–Pb in zircon (closure temperatures >900˚C, considered a geochronometer, and usually a proxy for zircon crystallization), ^{40}Ar/^{39}Ar in a variety of mineral phases, and fission track and (U–Th)/He in zircon and apatite.

The closure temperature of the $^{40}Ar/^{39}Ar$ system depends on the dated mineral phase. For instance, temperatures for hydrous phases such as hornblende and muscovite range between ~545–511˚C and ~440±40°C respectively (McDougall and Harrison, 1999; Harrison et al., 2009). The retention temperatures of radiogenic ^{40}Ar are lower in K-feldspar, ranging from ~350˚C to ~150˚C (Lovera et al., 1991).

Other methods that are relevant to this study include the following: zircon fission track (ZFT), zircon (U–Th)/He, apatite fission track (AFT) and apatite (U–Th)/He, which provide thermal information on temperatures between ~290–210˚C, ~200–130˚C, ~120–60˚C and ~90–40˚C, respectively (Bernet and Garver, 2005; Wolfe and Stockli, 2010; Ketcham et al., 2007; Farley, 2002).

3.2 Published high- and medium-temperature thermochronological data in southern Mexico

Except for a few thermochronological studies focusing on Oaxaca/Mixteca (e.g., Vega-Granillo et al., 2007; Kirsch et al., 2014), Xolapa (Morán-Zenteno et al., 1996), the Sierra Madre Oriental (e.g., Fitz-Díaz et al., 2014, 2018) the Sierra Juárez Complex (Delgado-Argote et al., 1992; Ángeles-Moreno, 2006), and the Chiapas Massif and Basin (Villagomez and Pindell, 2020a; Hernández-Vergara et al., 2021; Fitz-Díaz et al., 2022), many uncertainties remain on the significance of the high- and medium-temperature thermochronological information (e.g., multi-phase $^{40}Ar/^{39}Ar$).

The most reliable and robust thermochronological data obtained in Sierra Juárez Complex were presented by Ángeles-Moreno (2006) and they correspond to undisturbed plateau $^{40}Ar/^{39}Ar$ ages in muscovite (closure temperature of ~440±40°C; Harrison et al., 2009) from three metamorphic rocks collected south of Tehuacán (one granitic gneiss, one granitic dike and one white mica schist). The muscovite $^{40}Ar/^{39}Ar$ ages are indistinguishable within error and range from 130 Ma to 133 Ma. A fourth hornblende $^{40}Ar/^{39}Ar$ age from a migmatitic gneiss from the same Sierra de Juárez Complex yielded an age (~144 Ma) which is older than its zircon U–Pb age (140 Ma; Ángeles-Moreno, 2006), suggesting that excess argon was present in the hornblendes (making the $^{40}Ar/^{39}Ar$ age suspect).

Hornblende $^{40}Ar/^{39}Ar$ ages obtained by Delgado-Argote et al. (1992) from three granitoid rocks collected from the road between Teotitlán and Vigastepec yielded slightly disturbed spectra (showing excess ^{40}Ar in the initial steps). Ages from the two less disturbed samples suggest that the rocks were cooled at the closure temperature of hornblende between 132 Ma and 134 Ma. All white mica and hornblende ages range from ~134 Ma and ~130 Ma, which undoubtedly indicates a regional period of rapid cooling during Hauterivian time in the western Cuicateco Belt.

3.3 Published low-temperature thermochronological data in Mixteca/Oaxaca, Xolapa, Chiapas and Chortis

There are a few reliable AFT and apatite U–Th/He data from the Mixteca and Oaxaca blocks. The Xolapa Block, on the contrary, has been extensively studied by a number of authors (e.g., Ducea et al., 2004; Shoemaker et al., 2004; Villagómez and Pindell, 2020b) and summarized in Villagómez and Pindell (2020b). The latter authors sampled for AFT and apatite and zircon (U–Th)/He a number of Eocene and older rocks along the whole extension of the Xolapa Block across three main traverses between Acapulco and Puerto Angel (**Figure 3**). Their thermochronological results yielded a clear eastward-younging trend with thermal models constraining cooling between ~32–20 Ma in the west (Acapulco location) and ~19–11 Ma in the east (Puerto Angel location). Villagómez and Pindell (2020b) demonstrated that cooling along the present-day Pacific margin was eastwardly diachronous. These authors explained cooling as a consequence of erosional exhumation with moderate exhumation rates of around 0.3 to 0.6 km/My during the previously mentioned periods of time.

Apatite Fission Track and U–Th/He cooling ages from the Chiapas Massif are mostly middle and late Miocene (Witt et al., 2012; Villagómez and Pindell, 2020a). The last and main period of cooling and exhumation observed in the northwestern and central portions of the Chiapas Massif probably started at around 10–8 Ma (Villagómez and Pindell, 2020a). Exhumation rates in these regions range from 0.7 to 0.4 km/My. The easternmost tip of the morphological Chiapas Massif (South of the Polochic Fault; an area that shows a geology which greatly resembles part of the Chortis Block) started to cool earlier (at 15–14 Ma) than the rest of the Chiapas Massif (<10 Ma; Villagómez and Pindell, 2020a). This middle Miocene cooling is relevant because it was obtained from rocks that are located away from thermal influences of Miocene magmatism emplaced along the Tonalá Shear Zone. Villagómez and Pindell (2020a) considered this block (so-called the Huixtla Block, south the Polochic Fault) to be part of the tail of the Chortis block rather than part of the Chiapas Massif.

Although it has not been thoroughly studied, there are a few publications that have dealt with thermochronological aspects of the Chortis Block in Central Guatemala, in particular from the Chuacús and Las Ovejas complexes (e.g., Ratschbacher et al., 2009; Simon-Labric et al., 2013). These regions are allochthonous with respect to present-day Guatemala (Solari et al., 2013). Published zircon U–Th/He and Ar–Ar data from the Chuacús Complex (north of the Motagua Fault and south of the Polochic Fault; **Figure 7a**) record early Paleocene–early Miocene cooling ages (Ratschbacher et al., 2009; Simon-Labric et al., 2013). In addition, zircon U–Th/He and AFT cooling ages from Las Ovejas Complex (south of the Motagua Fault; **Figure 7a**) suggest the region experienced cooling from 40 Ma to 10 Ma (Ratschbacher et al., 2009; Simon-Labric et al., 2013). Overall, these data suggest that the northern complexes of Chortis (Chuacús and Las Ovejas) cooled and were exhumed from early Paleocene to late Miocene, and possibly are still being exhumed today (Brocard et al., 2020).

3.4 Published thermochronological data in the southernmost Sierra Madre Oriental Belt and the northern Cuicateco Belt (eastern Córdoba platform)

The Sierra Madre Oriental has been considerably studied for thermochronology and the data show that the Mexican Orogeny deformation possibly started at ~90 Ma in the hinterland (western foothills) and at ~50 Ma along the eastern edge of the belt (Fitz-Díaz et al., 2014, 2018; Gray et al., 2001; 2021). This generally forward propagating system during the Mexican Orogeny saw the development of a syn-tectonic basin above the eastern toe of the active belt. This basin in the northern Sierra Madre Oriental (called Mayrán Basin by Gray et al., 2021) was buried and heated older rocks until at least ~40 Ma, when it was finally inverted. This inversion caused quick erosion of the basin, providing detrital material first eastward into the Gulf of Mexico, then southward toward the Tampico–Misantla Basin. The youngest (Oligocene–Miocene, post-Mexican Orogeny) compressional features affected pre-Miocene sedimentary units and are mainly observed in the adjacent foreland region (not in the interior parts of the fold belt; Gray et al., 2001). An interpreted northward-younging diachronous uplift and deformation during Oligocene–Miocene time along the length of the Sierra Madre Oriental is plausible from the thermochronological data (Gray et al., 2001).

Farther to the south, in the northern Cuicateco Belt (the Sierra de Zongolica s.s./Córdoba platform) only two AFT ages have been published (Gray et al., 2001). The AFT pooled ages were obtained from Santonian–Campanian sediments and yielded a partially reset age of 74±7 Ma and a fully reset age of 33±2 Ma. Fluid-inclusion homogenization temperatures suggest that the sample with the younger age was buried and heated above 130˚C, due to burial, prior to final exhumation. The older aged sample was probably not buried enough and recorded detrital AFT information (Gray et al., 2001).

4 New geochronological and thermochronological data

We have obtained 15 new geochronological ages (zircon U–Pb), two new K-feldspar ^{40}Ar/^{39}Ar ages, 13 new AFT ages, one new ZFT age, four new apatite (U–Th)/He and 14 new zircon (U–Th)/He ages (**Figure 3** and **Tables 1–6**). We have also reinterpreted AFT age data from four samples in the Tampico–Misantla Basin and 17 samples in the Cuicateco Belt published by Gray et al. (2021), considering the new geo and thermochronological data obtained in this work. The details of the methodologies used in this study are shown in **Appendix 2**. All the age results are shown in **Tables 1–6** and are grouped according to the litho-tectonic units described in **Figure 3**.

We have also run a controlled random search procedure (HeFTy; Ketcham, 2012) to identify thermal histories that closely match our medium- and low-temperature thermochronological analytical data within certain statistical parameters by using an inverse modelling procedure (Ketcham, 2005; Ketcham et al., 2007). By doing so, we have created time–Temperature paths (**Figures 4a and 4b**) that help us to identify periods of cooling and heating in southern Mexico described below.

4.1 Mixteca and Oaxaca blocks

We have obtained a few AFT ages in western Mixteca Block ranging from 62.4 Ma and 83.2 Ma (**Figure 3; Table 3**). Dated lithologies include low-grade metamorphosed and deformed sediments of the Cosoltepec Fm. of the Paleozoic Acatlán Complex (DH-23-12-3-11; DH-24-12-3-11) and fine-grained volcanoclastic sandstones of the Upper Paleozoic Olinalá Fm. (DH-22-12-3-11). Although the rocks did not yield enough AFT length information required for thermal modelling, consistent Campanian to early Paleocene AFT ages suggest that western Mixteca experienced cooling during the Mexican Orogeny.

Samples located farther to the east and close to the Oaxaca Fault (gneiss 18-01-18-01 covered by Jaltepetongo Fm.) record continuous heating from Early Cretaceous through the latest Cretaceous with cooling starting only at about 60 Ma (**Figure 4a**). We have also obtained zircon U–Pb from intrusive and volcanic rocks in central Oaxaca (samples 17-01-18-01, 17-01-18-04, 17-01-18-05, 17-01-18-06; **Table 1**). These crystallization ages span 33 Ma to 23 Ma, which attest to a continued Oligocene–early Miocene magmatism that has undoubtedly affected the Miocene paleo-geothermal gradient south of Oaxaca City (**Figure 3**). Thermal models from one Jaltepetongo Fm. sandstone (17-01-18-03) intruded by the Oligo–Miocene granites yielded middle Miocene elevated cooling rates (**Figure 4a**).

4.2 Sierra Juárez Complex (high and medium temperature data)

Alkali-feldspar from two orthogneiss samples 5-11-11-02A (zircon U–Pb age of 158±13 Ma, Pindell et al., 2020a) and 5-11-11-03A (zircon U–Pb age of 137.2 ± 2.2; Coombs, 2016) collected approximately 50 km SE of the city of Tehuacán (**Figure 3**) were dated by ^{40}Ar/^{39}Ar. Both samples present excess ^{40}Ar at the initial steps (sample 5-11-11-03A presents higher percentage of excess ^{40}Ar based on a more defined U-shaped spectrum; **Figure 5a**). Alkali-feldspar from sample 5-11-11-03A consequently presents a more disturbed spectrum with one hump at approximately 40% of the ^{39}Ar released. In contrast, sample 5-11-11-02A shows a more consistent stair-like spectrum with the younger reliable single step ages ranging from 90±9 Ma to 133±5 Ma (2-sigma error; **Figure 5a**; **Table 2**). We consider the latter as a more representative and less disturbed sample.

Higher temperature domains (closure temperature of ~350˚C) within the K-feldspar yielded a single-step age of 133±5 Ma (5-11-11-02A), which overlaps within error with muscovite and hornblende ^{40}Ar/^{39}Ar ages of 134–130 Ma, previously reported by Ángeles-Moreno (2006) and Delgado-Argote et al. (1992). This reinforces the idea that the K-feldspar age data successfully complement the thermal history of the region at least since ~130 Ma.

Alkali-feldspars degassed by step heating with a CO_2–IR laser arguably provide a semi-quantitative thermal history of the sample within the zone of partial ^{40}Ar retention (see discussion in Villagómez et al., 2019). Age spectra show that there might be some excess ^{40}Ar at the initial steps, but alkali-feldspar from crystalline samples from the Sierra de Juárez Complex record a slow protracted cooling from ~130 Ma to ~90 Ma (**Figure 5a**).

4.3 Sierra Juárez Complex (low-temperature data)

Orthogneiss 5-11-11-02A and migmatitic orthogneiss 5-11-11-03A from the Teotitlán Migmatitic Complex (northern Sierra de Juárez Complex) were also dated by AFT yielding indistinguishable ages within error (51.9±5.6 Ma and 57.2±6.0 Ma, respectively; **Table 3**). Apatite (U–Th)/He was obtained from one sample (5-11-11-02A) and yielded a weighted mean age of 16.4±0.5 Ma (**Table 4**). Inverse thermal modelling using AFT data and Apatite (U–Th)/He in both samples shows similar patterns. The good solutions and best-fitting thermal models (**Figure 4a**) show: i) an onset of moderate cooling in the latest Cretaceous–Paleocene, lasting until about 50 Ma as observed in the best constrained model; ii) that there is no evidence of significant late Eocene–early Miocene cooling in those rocks; and iii) a renewed cooling at about 10 Ma.

4.4 Cuicateco Belt

4.4.1 West of Villa Alta and Aloapán faults, East of Siempre Viva Fault

We dated a number of samples for thermochronology including deformed/low-grade metamorphosed Jurassic sediments (Todos Santos-like units) and Cretaceous sedimentary rocks (Jaltepetongo Fm.), which are conspicuously intruded by Oligo–early Miocene plutons. In order to precisely determine the timing of Cenozoic magmatism, we dated two San Juan Juquila plutons, which yielded U–Pb zircon crystallization ages of 17.3–17.5 Ma (**Table 1**). We also dated by zircon U–Th/He an undeformed dacitic porphyry (26Feb16-6B) collected near the locality of Las Animas, which gave a middle Miocene crystallization age (15.7 Ma; **Table 5**).

All the thermal models show that the Jurassic and Cretaceous rocks (16-01-18-05A; 16-01-18-08A; 16-01-18-09A; 18-01-18-03; 26Feb16-7A) were continuously heated after deposition to temperatures above ~120°C until about 30–20 Ma, after which they were finally cooled (**Figure 4a**).

4.4.2 Between Villa Alta/Aloapán and Vista Hermosa faults (Mazateco Complex)

We modelled AFT age data published by Gray et al. (2021), including new apatite and zircon U–Th/He data (**Tables 3–5**). The new thermal models from Paleozoic metamorphic rocks, as well as from Todos Santos red beds, show cooling starting at 45 Ma and continuing through the latest Miocene (**Figure 4a**). The best constrained sample is a low-grade Paleozoic metamorphic rock (21-01-18-01), which included AFT, apatite and zircon U–Th/He constraints. Its thermal model shows that the rocks experienced continuous cooling possibly from 45 Ma, with probable pulses after 10 Ma. The late Eocene onset of cooling is also supported by a different Paleozoic sample (21-01-18-04), which yielded a ZFT age of 40.6 Ma (**Table 6**). This continuous cooling starting in the middle Eocene is also recorded in red beds from the Todos Santos Fm. (27Feb16-3B), which yielded early Oligocene zircon U–Th/He cooling ages (**Table 5**).

4.4.3 Between Vista Hermosa and Valle Nacional faults

Two Jurassic sandstones from the Todos Santos (20-01-18-08 and 19-01-18-10) and a Cretaceous litharenite from the Xonamanca Fm. (19-01-18-06) yielded AFT ages of 27.6 Ma and 19.7 Ma. Samples of similar lithologies (27Feb16-4B and 27Feb16-5B) were dated by zircon U–Th/He but they yielded partial reset ages with uninterpretable discordant single grain ages (**Table 5**). This points out that the region never reached sufficient temperatures to fully reset the zircon U–Th/He system (~200°C). Nonetheless, the AFT modelling suggests that samples were heated since deposition until about 35 Ma, when they were subsequently cooled (**Figure 4a**).

4.4 Remodelling of published data from the Tampico–Misantla Basin

We have dated detrital zircons (DZ) for U–Pb from a number of Chicontepec sandstones (COAP17-1, SANT17-2A, SANT17-2B, SFRAN17-1; **Table 1**) and our results consistently indicate that the basal Chicontepec has a Paleocene maximum depositional age, while middle and upper Chicontepec members have lower Eocene maximum depositional ages. We modelled the Time–temperature history from key samples (COAP17-1, ACAT17, SANT17-1, ALTO17-2; **Figure 3**) also reported in Gray et al. (2021). Our models (**Figure 4b**) show an eastward younging trend in both heating and cooling in the region, in line with Gray et al. (2021) interpretation. The most relevant samples are described below.

4.4.1. Samples located close to the Sierra Madre Oriental fold-thrust-belt

Lower Chicontepec samples located close to the Sierra Madre Oriental fold-thrust-belt were heated after deposition to 100°C (probably even to 120°C) and started cooling between 45 Ma and 25 Ma according to Gray et al. (2021). The middle Chicontepec sample ACAT17 shows minor reworking and includes sub-angular carbonate and volcanic clasts rich in euhedral zircons, which suggests that a large component of the grains were sourced from a proximal, contemporaneous volcanic source. It is very likely that the middle Chicontepec units experienced only some partial thermal resetting (temperatures above 60°C but below ~120˚C) after deposition based on its AFT length distribution. Since then, the sample underwent final cooling in mid Miocene time, as suggested by the U–Th/He data.

4.4.2 Samples from more central regions of the Tampico–Misantla Basin

Thermal models from basal Chicontepec samples (COAP17-1), as well as older samples, such as a Cretaceous breccia straddling the K/T boundary (SANT17-1) and the Jurassic Cahuasas red-beds (ALTO17-2) show cooling in the late Oligocene–Miocene. The pre-Chicontepec units were heated enough to reset the AFT system (temperatures above 120°C) but not enough to reset the zircon U–Th/He age (temperatures below ~200˚C; see sample SANT17-1).

4.5 Guichicovi and Mixtequita blocks

We dated one Mixtequita Permian granitoid (27Mar17-3A) by a number of methods in order to unravel the thermal history of this block. The granitoid yielded a zircon U–Th/He age of 108.6 Ma, AFT age of 42 Ma, and apatite U–Th/He age of 8.2 Ma. The Jurassic Todos Santos Fm. was deposited on the flanks of the Guichicovi and Mixtequita blocks, indicating that this sample was located near the surface in the Jurassic. The composite thermal models (**Figure 4b**) suggest that the rocks reached temperatures of around 180°C prior to mid Cretaceous. The Mixtequita granitoid was subsequently cooled from ~70 Ma through 30 Ma, with increased cooling rates from 10 Ma to Present.

On the other hand, samples from the Guichicovi Block experienced a different Cenozoic thermal history than that of the Mixtequita Block. Precambrian Guichicovi metasediments (26Mar17-3A and 26Mar17-5A) yielded zircon U–Th/He cooling ages ranging from 31 Ma and 43 Ma. A different Guichicovi sample (Precambrian granulitic gneiss 19-07-04-1) yielded an AFT age of 23 Ma. All U–Th/He ages and the AFT thermal model (**Figure 4b**) suggest that the Guichicovi samples were heated prior to Middle Eocene and it was subsequently cooled during the late Eocene–Miocene (with increased rates from ~27 Ma till ~16 Ma).

4.6 Chontal Complex (Western Tehuantepec)

We sampled for AFT (**Table 3**) a few middle Miocene plutons (U–Pb crystallization ages presented in Pindell et al., 2020b) in the western Tehuantepec region, as well as one Cretaceous phyllite (19-07-03-2B) from a complex lithodeme south of the Chivela Nappe. The thermal modelling systematically shows that all samples in Western Tehuantepec were cooled from ~15 Ma with increased rates of cooling from ~10–7 Ma to the Present (**Figure 4b**).

4.7 Chiapas Massif

One porphyritic granite (19-07-05-4) located in westernmost Chiapas Massif yielded an AFT age of 8.3 Ma (**Table 3**), attesting to late Miocene–Recent cooling. Moreover, one Triassic migmatite (25Mar17-1A) and one Triassic granitoid (27Mar17-2A) yielded a zircon U–Th/He and apatite U–Th/He age of 7.7 Ma and 13.3 Ma, respectively (**Table 5**). The two samples are located approximately 150 km apart (**Figure 3**), and these ages suggest an important middle to late Miocene cooling event.

5 Interpretation and discussion

Heating and cooling periods constrained by our data are related to burial and exhumation (either erosional or tectonic) or to advective heat transfer (e.g., thermal relaxation due to in-situ or nearby magmatism). We use the term erosional exhumation to mean vertical upward movement of rocks with respect to the Earth’s surface, representing a reduction of overburden due to erosion (England and Molnar, 1990; Braun et al., 2006).

Several regions, such as the easternmost outcrops of the Oaxaca Block and the westernmost Cuicateco sub-belts (south of Villa Alta and Aloapán faults) are extensively intruded by Oligo–Miocene magmatic rocks and affected by hydrothermal fluids (Camprubí et al., 2019; and references therein). We consider the Cenozoic heating observed in some host rocks in the previously mentioned regions to be a consequence of advective heat transfer from the plutons, leaving the pre-Oligocene thermal history nearly completely erased. Similarly, we treat the observed cooling from these two regions with a degree of scepticism, as Miocene cooling might record sub-solidus thermal relaxation following the emplacement of the plutons (see for instances sample 17-01-18-06 Ejutla pluton, which yielded zircon U–Pb and apatite fission track ages that are similar within error).

5.1 Sierra de Juárez Complex and the Cuicateco Belt

5.1.1 Pre-Mexican Orogeny

Muscovite and hornblende ^{40}Ar/^{39}Ar data suggests that the migmatitic–mylonitic rocks of the Sierra de Juárez Complex were cooled at extremely fast rates during Hauterivian (~134–130 Ma) until ~350–300˚C. Alkali-feldspar ^{40}Ar/^{39}Ar data show that migmatites subsequently cooled slowly from the Barremian and reached temperatures of ~150˚C by ~90 Ma. This indicates that the migmatites were not exposed at surface levels when the Lower Cretaceous Chivillas Fm. was deposited in the northern Cuicateco Belt.

Any model on the tectonics of Sierra de Juárez Belt should explain the existence of these mid-crustal rocks (migmatites and mylonites) and their emplacement into higher crustal levels at extremely fast rates during the Hauterivian. The two existing models, Ángeles-Moreno (2006) and Mendoza-Rosales et al. (2010), do not explain the quick exhumation of mid-crustal rocks of the Sierra de Juárez Complex. It would be unlikely for mid-crustal rocks to be elevated in multiple small pull-apart basins (Ángeles-Moreno 2006), or along a transform margin (Mendoza-Rosales et al., 2010) to expose the migmatites and mylonites to nearly the surface, while allowing the deposition of the overlying Lower Cretaceous Chivillas Fm. in such a short period. Our K-feldspar ^{40}Ar/^{39}Ar data show, in fact, that the migmatites from the Sierra de Juárez Complex only reached the 150˚C-isotherm (~5 km depth) in the Late Cretaceous (~90 Ma), meaning that these rocks were not close to the surface during most of the Cretaceous.

The Hauterivian cooling in migmatitic rocks cannot be solely a consequence of magmatic cooling because there was an ongoing tectonic deformation (shearing and deformation D2 of Ángeles-Moreno, 2006), along with a decrease of the metamorphic grade (amphibolitic to greenschist facies; Ángeles-Moreno, 2006). The only mechanism fast enough to allow quick cooling (from ~550˚C to 350˚C, during ~134–130 Ma) concurrent with the observed deformation is tectonic unroofing on low-angle detachment faults during regional-scale extension, perhaps in a similar way to metamorphic core complexes (Lister and Davis, 1989). However, the orientation of the stretching lineation in the mylonites indicates N–S shear on west-dipping planes, pointing to sinistral transtension as the driver (Graham et al., 2020). The fast cooling (from ~134 Ma through ~130 Ma) indicates large-scale hyper-transtension possibly accompanied with retrograde metamorphism (**Figures 5b and 6**).

Syn-extensional supra-detachment basins usually develop above the exposed detachment surface (Friedmann and Burbank, 1995; Gawthorpe and Leeder, 2000), and they are probably represented by the Jaltepetongo Fm. and possibly by the basal units of the Chivillas Fm. (Graham et al., 2020). While the migmatitic rocks exposed in the north possibly did not reach the surface during the stretching process, our field evidence suggests that the mylonitic rocks (mainly proto-mylonites) exposed in the south possibly reached surface levels in the Early Cretaceous, based on clasts observed in the Jaltepetongo Fm. Nevertheless, it appears that the quick stretching process decelerated drastically by ~130 Ma (**Figures 5b and 6**).

Subsequently, slower but protracted cooling from ~130 Ma to ~90 Ma in the Sierra Juárez Complex was contemporaneous with more stable platform and basinal depositional conditions in the northern Cuicateco area, and in particular the Córdoba Platform. This precludes any possibility of an important exhumation phase between ~130 Ma and ~90 Ma. We propose that the thermal relaxation of the crust (lowering of the geothermal gradients) that followed the high thermal (migmatization at ~147–134 Ma) and the rapid extensional (~134–130 Ma) events was responsible for overall basement cooling (**Figure 5b and 6**). This cooling accompanied long wavelength thermal subsidence of the Cuicateco Belt and probably the neighbouring Oaxaca Block during the middle and Late Cretaceous. Thermal relaxation and cooling probably lasted >40 My (as shown by the feldspar ^{40}Ar/^{39}Ar data) and reflect a slow decay of geothermal gradients in the mid–upper crust. Net cooling was not greatly affected by the moderate sediment burial that accompanied the subsidence itself in quasi-stable conditions (maximum thickness of 2 km of middle–Upper Cretaceous carbonate platform). Depositional burial lasted until the Maastrichtian, when samples from the Sierra de Juárez Complex began to be cooled further during Mexican Orogeny-related exhumation.

5.1.2 Syn-Mexican Orogeny

Thermochronological data from the basement rocks of the Sierra de Juárez Complex show that cooling probably started as early as Maastrichtian (**Figure 4a**) with increased rates (~5˚C/My) observed during ~60–50 Ma. Cooling was likely driven by erosional exhumation and this produced contemporaneous foredeep sediments that were deposited to the east and fed the Veracruz Basin. If we convert cooling into exhumation assuming a normal geothermal gradient of 30˚C/km, then it is estimated that this hinterland region exhumed at low rates of ~0.2 km/My during the early Paleocene–middle Eocene.

There is no evidence of the late Eocene exhumation within the Sierra de Juárez Complex (**Figure 6**), in contrast to the Mazateco Complex (this work) and the foreland Veracruz Basin (Gray et al., 2001). This may suggest that the deformation and exhumation migrated in-sequence as thrusting propagated eastwards, away from the Sierra de Juárez Complex.

Mexican Orogeny-related thrusting and deformation in the Sierra de Juárez Complex appears to have continued to slightly younger times (early Paleocene–middle Eocene) than compressional deformation observed in other regions (**Figure 6**) such as in the Mixteca and Oaxaca blocks (Campanian–early Paleocene; this work) and the Guerrero–Morelos platform (Latest Cretaceous; Nieto-Samaniego et al., 2006; Ruiz-Arriaga, 2018). Although the direction of shortening during the Mexican Orogeny may be variable (E–W in the Guerrero–Morelos platform and NE–SW in the Zongolica fold-and-thrust belt), there is a slight eastward migration of the deformation as proposed by Nieto-Samaniego et al. (2006). It seems that regional deformation was preferentially partitioned along the main basement structures within the Cuicateco Belt.

Exhumation of the Mazateco Complex (sub-belt 4b in **Figure 1**) from samples near the Vista Hermosa Fault began in the middle Eocene (~45 Ma) and lasted through the latest Miocene. This exhumation phase is not observed in the hinterland region (Sierra de Juárez Complex). This delayed cooling compared with the western hinterland regions supports the idea that Mexican Orogeny related-exhumation propagated eastwards.

Rocks from the easternmost Cuicateco belt (sub-belt 4c in **Figure 1**) were most likely heated due to sedimentary burial (possibly in a foredeep setting) and/or thrust imbrication until about 35 Ma, when they were finally cooled (due to tectonic uplift and erosional exhumation) and brought to present-day surface levels. We envisage that the Cenozoic heating of sub-belt 4b and 4c (**Figure 4b**) involved development of piggy-back basins and imbrication of nappes as a consequence of the Mexican Orogeny compressional deformation, mostly eroded today. Most of the Cretaceous–Paleogene sedimentary pile was eroded from ~35 Ma onwards in sub-belt 4c (**Figure 4b**). This suggests that the first stages of the Mexican orogenesis in the Cuicateco Belt led to the development of a topography dominated by folding, thrusting and nappe piling, while the erosional exhumation phase in the easternmost Cuicateco sub-belt came at the very end of the Mexican Orogeny (**Figure 6**) and it was probably renewed in Miocene times (see below).

Cretaceous sediments from the Córdoba Platform (sub-belt 4d) record Oligocene AFT ages that are fully reset (reaching T>130°C, Gray et al., 2001). This resetting suggests that either sediment accumulation in the foreland was thicker than the present-day preserved section or, alternatively, thrust stacking provided significant tectonic burial prior to the Oligocene. It is likely that migration of deformation towards the Zongolica foreland occurred only after the Eocene and was possibly responsible for partial erosion of the early Mexican Orogeny molasse (Gray et al., 2001).

It is worth noting that the amount of exhumation in the Mazateco Complex (sub-belts 4b and c) was higher than in the northern regions of the Cuicateco Belt such as the Zongolica Belt/Córdoba platform (sub-belt 4d). This might imply steeper thrust ramps or greater shortening toward the south, the latter of which could suggest minor anti-clockwise rotation of the thrusts during shortening.

5.1.3 Post Mexican Orogeny

The high-angle Oaxaca (normal) Fault (**Figure 1**) started to grow and propagate in the Oligocene (Nieto-Samaniego et al., 2006; Dávalos-Álvarez et al. 2007) down-dropping the Oaxaca Block as a hanging-wall relative to the Cuicateco Belt. This extension also formed several grabens on the Oaxaca Complex during the Oligo–Miocene (Nieto-Samaniego et al., 2006). It is impossible to quantitatively determine the amount of exhumation experienced in the westernmost sub-belt of the Cuicateco (sub-belt 4a) during Oligo–Miocene times given the conspicuous presence of Oligocene–early Miocene plutons in the region (Camprubí et al., 2019; and references therein). Given that these plutons east and south of Oaxaca City are currently exposed at surface, we estimate that this region experienced at least 4–5 km (plausible pluton emplacement depths) of exhumation since the middle Miocene (approx. 16 Ma).

On the other hand, the easternmost Cuicateco Belt (sub-belt 4c) underwent exhumation since the early Oligocene, probably peaking in the early–middle Miocene. This was contemporaneous with rapid exhumation in the Xolapa–Oaxaca blocks (Villagómez and Pindell, 2020b). We estimate that exhumation was a consequence of establishing Farallon/Cocos flat-slab subduction behind the Chortis Block, with interplate coupling at the position of Cuicateco such that Cuicateco was uplifted rather than Oaxaca being downdropped (Pindell and Kennan, 2009; Pindell and Miranda 2011; Graham et al. 2020; Molina-Garza et al., 2020b). Given the geometry of some of the faults involved in this post-Mexican Orogeny deformation (e.g., Vista Hermosa Fault and Valle Nacional faults) it is plausible that some back-stepped high-angle faulting occurred after the thin-skinned process (Graham et al., 2020).

The Oligocene–early Miocene magmatism in the Cuicateco Belt is arc-related, documenting the flattening of the Farallon/Cocos slab as SW Mexico overthrust its own Benioff Zone. We interpret the early–middle Miocene cooling and exhumation of the Cuicateco Belt as a whole relate to this slab flattening.

5.2 Mixteca/Oaxaca, the Sierra Madre Oriental and the Tampico–Misantla Basin

5.2.1 Syn-Mexican Orogeny

The earliest record of deformation and exhumation related to the Mexican Orogeny is dated as Campanian and is found in rocks located in the vicinities of the western border of the Mixteca Block (Ruiz-Arriaga, 2018). Similarly, our samples within the Mixteca and Oaxaca blocks (those located away from the influence of Cenozoic plutons) record cooling starting in Campanian times. Their thermal history paths (**Figure 4a**) and geological record might suggest that Mixteca/Oaxaca were heated (probably due to burial) throughout most of the Cretaceous and its overburden was partially exhumed from the latest Cretaceous through the early Paleocene due to the Mexican Orogeny. As for the southernmost extension of the Sierra Madre Oriental fold-thrust-belt (Mexican Orogeny), Gray et al. (2021) demonstrated that some regions in the central part of the belt also record this earliest stage of the orogeny.

In general, the Time–temperature history paths of sedimentary samples from the Tampico–Misantla Basin show consistent patterns, with post-depositional heating and subsequent Oligocene–Miocene cooling (**Figure 4b**). We ascribe heating and cooling to be due to burial and exhumation, respectively. There is an along- and across-strike variation in the amount of burial and subsequent exhumation within the basin. Cooling due to erosional exhumation shows an eastward-younging trend, with late Eocene–Oligocene cooling in the foothills of the Sierra Madre Oriental fold-and-thrust belt (Gray et al., 2021) and Oligocene–Miocene cooling in the lower coastal plains of the Tampico–Misantla Basin.

5.3 Chontal, Guichicovi and Mixtequita blocks

5.3.1 Mexican Orogeny phase

The Mixtequita and the Guichicovi blocks experienced heating during the Cretaceous. We assume that this heating was due burial by continental and then marine deposits (akin to the evolution of the neighbouring Chiapas Massif and Basin). The thermal models (**Figure 4b**) show that, unlike the Mixtequita Block, the Guichicovi Block underwent continuous heating through Paleocene to Middle Eocene.

Field observations and geophysical data indicate that some Guichicovi-like rocks are partially buried by the Chontal Complex (Pérez-Gutiérrez et al., 2009; Molina-Garza et al., 2020a). Molina-Garza et al. (2020a) argued that Paleocene–middle Eocene is the time when slices from the Chontal litho-tectonic unit and the Jurassic Todos Santos Fm. were overthrust above the Guichicovi along the Chivela Nappe front, now deeply eroded, forming a thin-skinned Mexican Orogeny thrust front above the Guichicovi. We therefore assume that the continuous Paleocene–middle Eocene heating observed in the Guichicovi Block was a consequence of overthrusting and tectonic burial from the south or southwest.

The allochthonous Chontal litho-tectonic unit has a maximum depositional age of 77 Ma (Pérez-Gutiérrez et al., 2009) and was deformed and metamorphosed prior to the Oligocene, given that it is unconformably covered by the Eocene–Oligocene Huamelula conglomerates (Tectonic Analysis Ltd., pers. comm., 2022, unpublished data). It is therefore plausible that i) low-grade metamorphism of the

Chontal Complex, and ii) the main period of exhumation of the Chontal occurred from Paleocene through Eocene. This is exactly the time when the Guichicovi Block was heated, arguably corroborating its overthrusting by the Chontal along the Chivela Nappes proposed by Pérez-Gutiérrez et al. (2009) and Molina-Garza et al. (2020a).

The Guichicovi and Mixtequita blocks record distinct cooling histories during the Cenozoic, at least until the late Miocene (see **Figure 6**). Cooling was likely due to erosional exhumation. While the Mixtequita Block underwent exhumation from Paleocene through early Oligocene, the Guichicovi Block experienced exhumation from the late Eocene through late Miocene (**Figure 6**). Summing up, exhumation seems to be younger and of higher magnitudes in the Guichicovi Block (late Eocene–late Miocene) compared to the Mixtequita Block (Paleocene–early Oligocene). This difference on the timing and magnitude of the exhumation between the two blocks (or between the northern and southern ends of a composite block behaving as one) might be the result of northward propagation of minor thrusting (and uplift) of the Mixtequita portion of the composite massif, with the Todos Santos and Chivela nappes riding piggy-back on the Guichicovi prior to erosion.

5.4 Chiapas and Chortis areas

5.4.1. Syn and post-Mexican Orogeny

The Tonalá Shear Zone represents one of the primary fault strands of the North America–Chortis (Caribbean) plate boundary zone (Molina-Garza et al., 2015), at least since early Miocene times (Graham et al., 2020). However, the long-lived sinistral displacement of Chortis involved a number of other faults during and prior to the Miocene, including "paleo-Motagua" faults possibly encompassing the Jocotán–Chamelecón and Baja Verapaz faults (**Figure 7a**). All the post-mid Miocene magmatic, hydrothermal, and tectonic events along the Tonalá Shear Zone constrained by Villagómez et al. (2020a), Witt et al. (2011), and Ratschbacher et al. (2009) have unfortunately overprinted older (Late Cretaceous–mid Miocene) thermal histories that could have potentially been recorded by higher temperature thermochronometers.

The southernmost tip of the Chiapas Massif (the Huixtla Block of Villagómez and Pindell, 2020a) located south of the Polochic and Tonalá Shear Zone records an earlier onset of exhumation (middle Miocene). Moreover, rocks located away from the Polochic Fault in the Chortis Block, including the Chuacús and Las Ovejas complexes, also record continued middle Eocene to late Miocene exhumation (Simon-Labric et al., 2013; Ratschbacher et al., 2009). We believe that the northern Chortis Block has consequently experienced exhumation since at least the Paleocene and most of this exhumation occurred long before the arrival of the Chortis Block at its present-day position (Villagómez and Pindell, 2020b). Thus, the Chortis Block has very likely supplied detrital material to the Chiapas Basin while located south of the Chiapas Massif since the Paleocene, and prior to the late Miocene uplift of the massif.

The Chiapanecan folding event that created the Chiapas fold-and-thrust belt started in middle Miocene times (Mandujano-Velázquez and Keppie, 2009), prior to the main period of uplift observed in the Chiapas Massif itself (<10 Ma). The folding event was driven by the onset of subduction beneath Chiapas in the wake of the eastwardly migrating Chortis Block, and the younger uplift of the massif pertains to the encroachment of slab flattening into Chiapas from Oaxaca (Pindell and Miranda, 2011; Pindell et al., 2020b; Graham et al., 2020; Molina-Garza et al., 2020b). The Chiapas Massif has become an effective topographic barrier starting at around 10 Ma (Pindell et al., 2020b).

Such a mechanism for the younger exhumation of the Chiapas Massif is also validated by the northward sweep of arc magmatism, from about 15 Ma in western Tehuantepec (Damon and Montesinos, 1978; Pindell et al., 2020b), 9–11 Ma along the Tonalá Fault Zone (Molina-Garza et al., 2015), and Pliocene to Recent times within the Chiapas fold-and-thrust belt (Mora et al., 2012; Garduño-Monroy et al., 2015). Similarly, the Chontal Block has been cooling since the late Miocene, and this also probably pertains to the increasingly flat subduction of the Cocos slab beneath the Tehuantepec area.

6 Paleogeographic reconstructions and sediment delivery pathways to the foreland basins and Gulf of Mexico

We present a detailed description of the source-to-sink interpretation and the evolution of southern Mexico from the Late Cretaceous at eight different times (**Figures 7b–i**).These reconstruction maps are based on the models of Pindell and Kennan (2009), Villagómez and Pindell (2020b) and Graham et al. (2020), within the context of the approximate relative displacement history of the Chortis Block. Our reconstructions include the block rotations as indicated by the paleomagnetic data of Molina-Garza et al. (2019a) for the core of Chortis and Molina-Garza et al. (2020b) for the Chiapas Massif.

The sediment source terrains (active exhumation and presumed erosion) are represented by the horizontal ruled pattern in **Figures 7a–i**. In general, hinterland uplift and exhumation becomes progressively younger from west to east along the southern Mexican margin, with uplift of the Xolapa and Mixteca/Oaxaca blocks beginning in the earliest Cretaceous, uplift of the Mixtequita in Paleocene and uplift of the Guichicovi and Chiapas Massif possibly beginning in the Eocene–Oligocene but with greatly increased rates since the middle Miocene. We complement the maps with information from key wells drilled by the state-owned petroleum company (Pemex) and other international operators in onshore and offshore areas, as further described in Section 7.

Various Paleogene and Neogene depositional systems in the southern Gulf of Mexico, as described by Ambrose et al. (2003), Arreguín-López et al. (2011), Escalera-Alcocer (2010), CNH (2014, 2015, 2017a, 2017b, 2019), González and Medrano (2014), Snedden and Galloway (2019), Brito and Luysterburg (2019), Shann et al. (2020), and Davison (2021) have been integrated with the uplift and exhumation data presented here (**Figure 6**). Our analysis is also supported by incorporating additional geochronological evidence, such as detrital zircon and heavy mineral analyses (Beltrán-Triviño et al., 2021). Our aim is to build an initial framework for connecting the primary sediment source terrains with their respective depositional systems (transport routes and sinks).

The locations of the present-day drainage system entry points (**Figure 7a**) into the southern Gulf of Mexico are probably largely representative of the main entry points throughout the Paleogene and Neogene in the region (Shann et al., 2020). Accepting this, and looking at current drainage basins, it is possible to identify three main entry points that likely delivered sediment into the Gulf of Mexico from the Veracruz and Sureste basins during those times. Similarly, the Tampico–Misantla Basin was fed during the Eocene by channels that flowed southwards (Cantú-Chapa, 2001; Cossey et al., 2021), and which potentially originated in the Tamaulipas or Río Grande embayment area (Gray et al., 2021). Considering the impact of the Mexican Orogeny and later morphologic and tectonic development, the drainage basins associated with those entry points could have been as much as 30% larger prior to final compressional deformation, thus increasing the potential sediment input significantly, especially during the earlier part of the Paleogene. Also, the potential contribution from the Chortis Block across the plate boundary during relative displacement along the southern Mexico could add significantly more drainage area to the hinterland south of the Sureste basins and the Chiapas Massif (see also Snedden et al., 2021; Stockli et al., 2021).

Deposition into the southern Gulf of Mexico during the Paleogene and Neogene occurred primarily via deep water (bathyal) channel and fan (turbidite) depositional systems (e.g., Snedden and Galloway, 2019), which in most cases developed in response to hinterland tectonics and further influenced by structured slope and basinal topography (e.g., Mayall et al., 2010) and active volcanism. Cenozoic depositional environments in the Veracruz Basin, for instance, are dominantly upper slope. The shelf and coastal environments have been eroded due to continued uplift and erosion of the Cuicateco and Zongolica belts (González and Medrano, 2014). The same can be said for the Paleogene sequences in the onshore Sureste Basin, although Neogene fluvial and deltaic (coastal) depositional environments have been encountered in numerous wells (Chávez-Valois et al., 2009).

Sedimentary reworking is a fundamental aspect that should be taken into consideration when determining provenance and reservoir quality. The Eocene–Oligocene foreland in the Sureste Basin is involved in the middle Miocene to recent Chiapas folding, implying the potential for recycling those sediments into younger (post-middle Miocene) deposits. Such “second cycle” sediments are more texturally and compositionally mature once they are re-deposited farther out into younger basins.

6.1 Latest Cretaceous–Eocene (Figures 7b and 7c)

Source

Our data from the Mixteca and Oaxaca blocks suggest that uplift and exhumation in those areas started as early as the Campanian. This may coincide with the Mexican Orogeny deformation (i.e., uplift of the Oaxaquian region) which propagated eastwards to form the southern Sierra Madre Oriental Belt (Cuicateco). Our first evidence for exhumation in the southern Sierra Madre Oriental belt dates to the Maastrichtian, although the northern region of the Sierra Madre Oriental possibly started to deform and exhume earlier in Coniacian times (Fitz-Díaz et al., 2018; Gray et al., 2021).

As the Sierra Madre Oriental Belt developed into a topographic high, it also started to provide carbonate clastic debris to the foreland basins. Whether or not the Sierra Madre Oriental was uplifted in discrete pulses (Fitz-Díaz et al., 2018), several intra-orogenic basins developed throughout the belt's Mexican Orogeny history (Gray et al., 2021).

Deformation during the Mexican Orogeny also appears to be younger to the south. The Cretaceous sedimentary cover of the Oaxaca and Sierra de Juárez Complex started to erode in the Maastrichtian and delivered the first clastic carbonate material (Méndez Fm.) to the nascent Veracruz foredeep basin (Sierra-Rojas et al., 2020).

As deformation continued throughout the Paleocene, some intra-orogenic basins of the Sierra Madre Oriental began to be eroded (Gray et al., 2021) and this material also contributed to the Paleocene–Eocene synorogenic turbidites of the Chicontepec Fm. deposited in foredeep depocenters of the Tampico–Misantla Basin (**Figure 7b**). Similarly, the Paleocene–lower Eocene denudation of Cretaceous sediments capping the Oaxaca Block and the Sierra de Juárez Complex continued providing material to the Veracruz Basin along submarine fans (González and Medrano, 2014).

"In-sequence" propagation of thrusts and exhumation is observed in the Oaxaca and Cuicateco regions throughout the Paleogene. Unroofing of the Oaxaca Complex and the Mazateco Complex in the Cuicateco Belt continued in the middle Eocene and led to a continuous supply of material toward the foreland basin (Chapopote, Aragón and Guayabal formations.; **Figure 7c**). The detrital material initially consisted of the Cretaceous sedimentary cover. Graham et al., (2020) postulate that Oaxacan basement formed the uppermost nappe of the western Cuicateco Belt, the erosion of which may have potentially contributed to Eocene some clastic supply reaching the Veracruz Basin and Gulf of Mexico. It is very likely that the southern Veracruz Basin also received material coming from the denudation of the Mixtequita Massif during most of the Eocene (González and Medrano, 2014). We estimate that the source material coming from Mixtequita consisted of Cretaceous marine deposits and arguably northwardly-vergent overthrust Jurassic Todos Santos siliciclastics that once covered the Mixtequita Massif. The late Eocene marks the culmination of the Sierra Madre Oriental thrusting (Fitz-Díaz et al., 2018), concurrent with strong transpression along the Chortis–Southern Mexico plate boundary zone.

Farther south, our analyses suggest that the allochthonous Chontal litho-unit (present-day western Tehuantepec area) cooled in the Paleocene–Eocene, possibly during final emplacement onto the southern Mexican margin. Although many of the rocks and detritus of Chontal may require a Maastrichtian arrival of the Greater Antilles arc along the margin, the cooling data suggest that the final emplacement onto the margin was more likely due to Mérida Andes-style transpression between Chortis and Mexico once displacement was underway (Graham et al., 2020). The Chontal rocks were eroded and provided material of oceanic affinity to the western Sureste and Chiapas basins, such as that seen in the Maastrichtian Cerebro Mb. of the Ocozocuautla Fm., the Paleocene Soyaló Fm., the Eocene Uzpanapa conglomerate (Michaud and Fourcade, 1987; Molina-Garza et al., 2019b, 2020b), and the Eocene El Bosque Fm. (Tectonic Analysis Ltd., pers. comm., 2022, unpublished data; **Figure 7b**),

The continental core of Chortis migrated towards the east in a highly transpressive setting due to rapid Farallon–North America convergence rates and the westward drift of North America over the mantle (e.g., Engebretson et al., 1984). The erosional exhumation of the Chortis metamorphic complexes during the Paleogene (Simon-Labric et al., 2013) probably provided quartz-rich and metamorphic lithic-rich material to the Chiapas Basin through marine turbiditic channels. We believe, however, that an important proportion of material feeding the Chiapas Basin's Soyaló/Sepúr and El Bosque formations derived from the denudation of Cretaceous (Sierra Madre Fm.) and Jurassic units (Todos Santos Fm.) that once covered the Chiapas Massif and were possibly involved in thrusting on the massif's southern flank. This partial denudation of the sedimentary cover of the Chiapas Massif is suggested by the initial cooling history of its basement (Witt et al., 2012; Villagómez and Pindell, 2020b) as a very slow and restricted late Eocene–early Oligocene exhumation pulse, possibly related the passage of the Chortis Block (Villagómez and Pindell, 2020b).

The Late Cretaceous–Eocene magmatic arc that bordered both western and eastern Chortis after arc collision also provided volcanic and pyroclastic rocks to the Paleogene Soyaló/Sepúr and Eocene El Bosque formations of the Chiapas Basin, as shown in **Figure 7b**.

Sink

The Chortis Block was actively migrating east at this time coincident with the advance of the Sierra Madre Oriental, generating robust depositional systems that fed sediment eroded from the impinging highlands directly into the Gulf of Mexico across a narrow foreland shelf and into deep water.

In the Tampico–Misantla Basin, the Bejuco–La Laja, Chicontepec and Nautla (also known as San Andrés) paleo-canyons were channels for submarine fan systems coming from the erosion of the Sierra Madre Oriental (Cantú-Chapa, 2001; Rosenfeld and Pindell, 2003; Graham et al., 2020). The fans propagated into deep water, depositing turbiditic sandstones and shales throughout the Eocene. Within the submarine facies that reached deep water zones, it is possible to observe meandering channels, crevasse splays, lobes, basin floor fans, as well as mass transport complexes (CNH, 2019).

In the Veracruz and Chiapas basins, bathyal water conditions prevailed during the Paleocene–Eocene (Velasco, Chicontepec and Guayabal formations in Veracruz; Soyaló Fm. in Chiapas), in continental slope and rise environments, ultimately connecting the developing foreland basins with the Gulf of Mexico. This allowed the deposition of material derived from the sedimentary cover of the uplifting blocks to be deposited as calcareous and siliciclastic lithic-rich turbidites interbedded with deep marine shales farther out in the basin (Pemex, 2013a, 2013b; Martens et al., 2021).

Sedimentary reworking played a major role in the Paleocene–Eocene depositional systems. As mentioned previously, in the Chiapas Basin, one of the main sources of material feeding the Paleocene Soyaló/Sepúr were derived from the denudation of Cretaceous (Sierra Madre carbonates) and Jurassic (Todos Santos siliciclastic) units that once covered the Chiapas Massif and were actively deforming along the massif's southern flank.

Similarly, the erosion of the Soyaló/Sepúr foredeep units also provided second/third-cycle siliciclastic sediments (e.g., into the Eocene El Bosque Fm. and the Nanchital shale) from the southeast, delivered across a somewhat broader coastal and shelfal region in the Chiapas and Sureste area. El Bosque Fm. sandstones (deposited in fluvial, littoral and possibly bathyal environments; García-Molina, 1994; Meneses-Rocha, 2001) were originally transported from the south across the Chiapas Massif to the Chiapas foredeep, the accommodation space for which was possibly aided by northwardly evacuating salt. This siliciclastic fairway was northwest trending towards the western Sureste basins (Isthmus Saline Basin, s.s.), promoting the formation of an early salt canopy.

Large Eocene channel systems have been mapped from seismic data, extending far into the Campeche Salt Basin mainly along the western margin of the basin (CNH, 2015; **Figure 7c**). These channels consist of deep water turbidite system sandstones. Seismic interpretations allow for the identification of sedimentary fairways related to turbidite deposition and include elements such as amalgamated channels, crevasse splays and channelized lobes oriented southwest to northeast. Outboard of the Campeche Salt Basin, these amalgamated/anastomosed channel systems are largely straight and unconfined but tend to turn eastward towards the distal end of the salt province (**Figure 7c**), where deposition is controlled by incipient halo-kinetic activity (CNH, 2019). In addition to these robust depositional systems, intrusive volcanic bodies (of undetermined age) within the Eocene section have been locally identified on industry seismic images, particularly in the northwest Isthmus Saline Basin.

Towards the east of the Campeche Salt Basin, calcarenite flows shed from the Yucatán shelf margin (**Figure 7c**) were deposited in a slope apron adjacent to the platform (middle Eocene Kumaza: the Ku, Maloob, Zaap fields; Ríos-López and Cantú-Chapa, 2009).

6.2 Oligocene–middle Miocene (Figures 7d, 7e and 7f)

Source

New and published data show that deformation (e.g., Fitz-Díaz and Van der Pluijm, 2013) and exhumation in the western and central portions of the southern Sierra Madre Oriental waned by the latest Eocene. However, our thermochronological and detrital geochronological data suggest that the westernmost regions of the Tampico–Misantla Basin remained tectonically active during the Oligocene–Miocene. In fact, some of the former Paleogene foredeep deposits from the Sierra Madre Oriental thrust front were probably eroded and reworked, feeding more easterly depocenters and possibly the Gulf of Mexico during the Oligocene–Miocene.

Subduction beneath southern Mexico in the migrating wake of the Chortis Block led to the onset of arc-magmatism first in Guerrero and western Oaxaca states (Martiny et al., 2000) and later in eastern Oaxaca/western Cuicateco in late Oligocene–Miocene times (Morán-Zenteno et al., 2005, 2018). This was concurrent with uplift and erosional exhumation of the eastern Cuicateco sub-belts, the Guichicovi, and the Mixtequita blocks that resulted in a continued supply of sediment directly into the Veracruz Basin (**Figure 7d**). Oligocene onset of motion on the high-angle Oaxaca Fault, which cut pre-existing low-angle detachment faults in the Sierra de Juárez Complex (Dávalos-Álvarez et al., 2007; Graham et al., 2020), as well as initial movement on the left-lateral Chacalapa Fault (Tolson, 2005) downdropped the Oaxaca Block relative to the neighbouring blocks (**Figure 7d**).

The Oligocene material that entered the Veracruz Basin (Horcones Fm.) mostly consisted of the (presently eroded) Cretaceous platform that had still covered the Cuicateco Belt (remains of the platform are preserved north of the Valle Nacional Fault). We estimate that by the earliest Miocene, the eastern Cuicateco sub-belts had had much of their Cretaceous carbonate cover fully removed; therefore, their Lower Cretaceous and Jurassic siliciclastic cover and metamorphic core were finally becoming exposed. This might have important implications for reservoir quality especially in the Veracruz Basin because the early Miocene was probably the time when feldspar and quartz clastics, possibly derived from the Todos Santos and Xonamanca formations, were first delivered to the basin from the west (Martínez-Medrano et al., 2009).

The volcanic arc jumped northward to the Trans-Mexican Volcanic Belt in the latest early Miocene (~20 Ma; Ferrari et al., 2012; **Figure 7e**), with the first volcaniclastic detritus feeding the northern Veracruz Basin in the middle Miocene (Martínez-Medrano et al., 2009). It is worth noting that the Cordoba Platform was not deeply exhumed during the Neogene based on its current preservation; therefore, its detrital input towards the northern Veracruz Basin was limited. The southern Veracruz Basin probably continued to receive siliciclastic material from the exhumation of the Guichicovi and Mixtequita massifs throughout the Miocene (CNH, 2017a).

Exhumation of the Chontal litho-tectonic unit, as well as exhumation of some metamorphic complexes within Chortis, continued during the Oligocene–middle Miocene (Ratschbacher et al., 2009; Simon-Labric et al., 2013). We believe that these regions located south of the Chiapas Massif were important sources of material for the Oligocene La Laja, the lower Miocene Depósito Fm., and the mid-Miocene Encanto Fm. (including the Nanchital conglomerate; Pindell et al., 2020b) in the Chiapas Basin (**Figure 7d–f**), suggesting low relief for the Chiapas Massif at those times.

As explained previously, the amount of material reworked from older sedimentary units should not be underestimated, and it is probably the main reason why mineral detrital provenance studies have led to disparate interpretations in the Chiapas Basin (Ortega-Flores et al., 2018, 2020; Molina-Garza et al., 2019b). Moreover, Oligocene–Miocene arc magmatism along the southern Mexican margin provided contemporaneous volcanic material to sedimentary units in the Chiapas Basin as well, contributing to the different detrital zircon populations.

The main deformational event in the Chiapas Basin (Chiapanecan orogeny) began in the middle Miocene (Ángeles-Aquino et al., 1994; Mandujano-Velázquez and Keppie, 2009). The deformation was driven by the clockwise rotation of the Chiapas Massif, which acted as an indenter prior to the late Miocene (Molina-Garza et al., 2020b), and ultimately was a consequence of the onset of subduction beneath Chiapas. Folding and thrusting of the Chiapas Basin provided, therefore, a proximal source for second-cycle sediments.

Sink

Fine-grained sandstones continued to be transported to deep water settings through submarine fan systems. The most observed sedimentary facies in the Oligo–middle Miocene turbiditic system in the Tampico–Misantla Basin include channels, crevasse splays, and basin floor fans (CNH, 2019).

The Oligo–Middle Miocene sediments in the Veracruz Basin were deposited as basin-floor fans that were fed from multiple areas. In onshore Veracruz Basin, the high-energy upper Oligocene–Miocene deposits usually contain subangular to rounded clasts of Cretaceous carbonates with minor presence of metamorphic and igneous rock fragments in a sandy or shaly matrix (IHS, 2010; Sánchez-Hernández, 2013).

In the Veracruz Basin, volcanic material derived from the Trans-Mexican Volcanic Belt started to become important by the middle Miocene (Martínez-Medrano et al., 2009). Similarly, volcanic activity in the Los Tuxtlas and Anegada volcanic centers probably started in the middle Miocene (Ferrari et al., 2005), providing volcaniclastic material to the neighbouring areas. Moreover, the Los Tuxtlas and Anegada centers became bathymetric highs that resulted in a constriction of sedimentary entry points into the Gulf of Mexico from the Veracruz Basin (Winter, 2018), as shown in **Figure 7f**.

Sandstone-prone submarine channel complexes up to 10 km wide fed these deep-water deposits that comprise turbidites and debrites (Winter, 2018). For instance, middle Miocene reservoirs (Encanto Fm.) have been described as deltaic and turbiditic sandstone with minor conglomerate lenses that were confined to submarine canyons (Martínez-Medrano et al., 2009). In addition, shale diapirism and deformation continued offshore Veracruz, enhancing the structure of the slope environment and having a dramatic impact on sediment dispersal patterns throughout the Neogene.

In the Campeche Salt Basin and the Catemaco Foldbelt, the lower–middle Miocene sandstones and shales include high-density deep-water turbidites, debris flow deposits, low-density turbidites, slumps, tuff-rich debrites and distal volcaniclastic turbidites (Sosa-Patrón et al., 2009; Sánchez-Hernández, 2013). The lower Miocene high-density turbidity currents have been encountered unconfined outboard (to the west) of the Campeche salt, but their distribution is controlled by salt tectonics in mini-basins within the salt province itself (CNH, 2017a, 2019).

Middle Miocene deposition in the Campeche Basin was very similar to that of the lower Miocene, with perhaps more robust systems delivering coarse sands and conglomerates even farther out into the different basins due to increased hinterland deformation. Confined and unconfined fans and channels of varying thickness have been encountered, likely reflecting the fact that many wells have been drilled on anticlinal highs that were actively growing during the time of deposition (particularly in the Catemaco Foldbelt). Contemporaneous salt movement also played an important role in sedimentation, locally restricting flow and impacting direction of sediment fairways (CNH, 2019).

Recent studies in the Campeche Salt Basin have delineated extensive Oligo–Miocene fans sourced from the southern Veracruz Basin (Brito and Luysterburg, 2019) and arguably also from the Chiapas basin (Clark et al., 2019) extending across the deep water Gulf of Mexico and reaching as far north as U.S. waters. Deposition of these compensating fan systems began in the upper Oligocene (**Figure 7d**), peaked during the middle Miocene (**Figure 7f**), and ceased by the late Miocene (**Figure 7g**), as documented in Winter (2018). Detrital zircon U–Pb ages derived from DSDP cores tie these sediments to southern continental Mexico (Clark et al., 2019), implying that the sediments were delivered more than 600 km northward into the basin. DSDP Leg 10 Sites 87, 90, and 91 (**Figure 7f** and **Table 7**) encountered middle Miocene aged turbidite sands and gravels ranging in thickness from 20cm (Site 87) to more than 10m (Site 91). The turbidite sandstones from the DSDP sites are coarse-grained and they are characterized by high percentages of quartz, plagioclase and a diverse heavy mineral assemblage including biotite and hornblende. They also have a minor and fine gravel component of carbonate rock fragments, volcanic rock fragments and chert (Worzel et al., 1973). While such large volumes of sediment being derived from drainage areas potentially limited in scale may seem counter-intuitive, earlier research has shown that tectonics and climate, among other things, can be significant controlling factors in such short-runoff systems as were present throughout the Cenozoic in the Veracruz and Sureste Basin areas (Sømme et al., 2009; Covault and Graham, 2010).

6.3 Late Miocene–Present (Figures 7g, 7h and 7i)

Source

Several regions of Southern Mexico experienced variable amounts of uplift and exhumation during the late Miocene–Pliocene, and they, along with widespread volcanic centers located along Gulf of Mexico margin, provided a continued supply of detrital material to the basins.

By the late Miocene there was a major reorganization of drainage patterns in the southern margin because the Chiapas Massif had become a positive topographic high (Pindell et al., 2020b). The early late Miocene marks then the onset of material coming directly from the crystalline basement of the Chiapas Massif towards the Chiapas Basin and the Sureste basins. Upper Miocene turbidite sandstones from the offshore Zama discovery (**Figure 7g**) also exhibit a major input from the Chiapas mountainous areas (Stockli et al., 2021).

In the absence of high-resolution 3D seismic data, it is difficult to establish whether the late Miocene exhumation of the Guichicovi and Mixtequita massifs sourced fluvial channels towards the Veracruz Basin, the Sureste/Chiapas basins, or to all of them. However, our data record an important erosional exhumation of both massifs; therefore, quartz-rich material sourced from these areas should have been distributed generally towards the Gulf of Mexico.

The Veracruz Basin was surrounded by active volcanic centres including Los Tuxtlas, which continued providing volcanoclastic material to the offshore basin (**Figure 7g**). The southern Veracruz Basin continued to receive siliciclastic and metamorphic detritus from the erosion of the easternmost Cuicateco sub-belts (the primary outlet for fluvial flow was possibly the original river that is now dammed as the Lake Miguel Alemán). However, the volcanic lithic component became dominant in the upper Miocene sequences and took over the plutonic and metamorphic provenance (Gutiérrez-Paredes et al., 2009).

Sink

The upper Miocene sandstones in the Veracruz Basin were deposited as basin-floor progradational submarine fans, which formed channels and over-bank deposits. Subsequent Pliocene submarine fans were dominated by meandering channels (Martínez-Medrano et al., 2009) and they are more limited in extent than the Miocene fans (Jennette et al., 2003a, 2003b).

Although the erosion of the Cuicateco Belt continued to provide sediment to depositional systems in the Veracruz basin during the late Miocene, the basin experienced a significant change in depositional patterns during this time. Prior to the middle Miocene (**Figure 7e**), the Cenozoic depositional fairways fed directly into the deeper Gulf of Mexico Basin in a dip-oriented sense, i.e., running southwest to northeast. With the emergence of the Anegada and Los Tuxtlas volcanic centers in the latest middle Miocene, entry points into the Gulf of Mexico became restricted, and depositional systems in the Veracruz Basin became axially oriented, running northwest–southeast before exiting the basin between the volcanic highs (**Figures 7f–7g**; Martinez-Medrano et al., 2009).

In the Isthmus Saline Basin, the upper Miocene sequences are characterized by lateral and vertical facies variations, which evolved from deeper to shallower waters (Sosa-Patrón et al., 2009). This progradation accelerated in the lower Pliocene with the shelf margin advancing towards the northwest. The upper Miocene–Pleistocene sandstones of the Reforma–Comalcalco–Macuspana depocenters were deposited mostly in proximal turbidite, prograding transitionally into deltaic environments. The shelf margin migrated progressively northward in the Sureste basins throughout the Miocene, making particularly substantial advancement during the late Miocene and Pliocene. Upper Miocene fine-grained sandstones are interbedded with siltstones and shales in very thin layers and were deposited in a relatively confined depositional environment (Chávez-Valois et al., 2009).

The upper Miocene–Pleistocene sandstones in the Sureste basins are distributed along NE–SW trends (**Figures 7g–7h)** controlled by normal growth faults (Pemex, 2013c). Development and growth of the Macuspana supra-salt extensional basin (beginning in the latest middle Miocene; Pindell and Miranda, 2011) and the Comalcalco–Pescadores extensional system (mainly Pliocene) appears to have captured a considerable amount of siliciclastic sediment derived from the south/southeast. When underfilled, the two basins likely inhibited the coarsest detrital fractions of south-derived material from reaching farther north into the Campeche salt province.

Considering the constriction of depositional fairways in the Veracruz Basin and that near-coast Comalcalco and Pescadores extensional systems in Sureste were actively growing during the Pliocene, it is not surprising that there is little evidence of robust Pliocene reservoir deposition in deep water tests to date. However, Pliocene sands are encountered inboard of these extensional systems and can be good reservoirs. Further entrapment of sediment may have occurred due to continued anticlinal growth in the Chiapas fold-and-thrust belt onshore and concurrent salt deformation offshore, creating paleobathymetric relief. Pliocene deposits in the Campeche Salt Basin appear to be dominated by deposition of mass transport deposits (Sickmann and Snedden, 2021). Pliocene sands tend to be rich in carbonate lithic grains and quartz (Hessler et al., 2018), with reservoirs developed in amalgamated channels, crevasse splays, and channelized lobe facies possibly also associated with turbidite depositional systems.

Within the Chiapas Basin, the transtensional Ixtapa Graben captured a significant volume of littoral and deltaic coarse-grained sediments (Ixtapa Fm.) during the latest middle Miocene to the earliest Pliocene, derived from acidic plutonic, metamorphic and volcanic rocks (Meneses-Rocha, 2001; Sánchez-Hernández, 2013).

7. Clastic reservoir characteristics

Oil and gas have been under production from Cenozoic reservoirs in southern Mexico for decades, both onshore and in the shallow offshore. Pemex and other international operators have stepped out into water depths exceeding 500m since the reform of the Mexican petroleum industry in 2013. New wells have provided additional data and evidence for the extension of the Cenozoic depositional systems farther out into the Gulf of Mexico.

We have integrated these wells into the interpretations of both provenance and potential reservoir quality presented below. Many of these wells have discovered hydrocarbons. The most important Cenozoic wells that have proven important prospects are listed in **Table 7**.

7.1 Eocene clastic reservoirs

Tampico–Misantla Basin: The Chicontepec sandstones are considered immature and contain a predominance of lithic clasts. The majority of the lithic clasts are reportedly fragments of limestones, with a lesser proportion of siliciclastic fragments (Bitter, 1993; Santillán-Pina and Aguayo-Camargo, 2011).

Veracruz Basin: Porosity preservation in Eocene sediments seems to be relatively good (porosities vary between 10% and 25%; González and Medrano, 2014) even at burial depths approaching 5,000m, as observed in the Tepaxtli-1EXP (deep pools in Perdiz Field) and Heim-1 wells, onshore Veracruz Basin (**Figure 7g**). The impact of varying sediment source terrains could be significant with respect to compositional and textural make-up of Eocene sediment offshore and in deep water. Core descriptions of middle Eocene conglomerates and breccias in the onshore Perdiz Field include carbonate and igneous rock fragments supported in a calcareous clay matrix and cemented with calcite (industry reports). Small gas and condensate accumulations are also reportedly found in mass flow deposits of the upper Eocene Chapopote Fm. in the Mata Espino-2 onshore well (IHS, 2010).

Campeche Salt Basin and Chiapas Basin: Recently, the deep water Bukma-1SON well discovered gas and condensate in middle Eocene siliciclastic reservoirs. In the Chiapas Basin, the Eocene sediments include fine to coarse conglomeratic sandstones of the El Bosque Fm., which are conspicuously found in onshore outcrops (García-Molina, 1994).

7.2 Oligo–middle Miocene reservoirs

Veracruz Basin: Oligocene reservoirs are represented by deep water turbidite system deposits, although they have not received considerable attention as an exploration target. Oligocene deep clastic reservoirs have been reported in several wells in the offshore Catemaco Foldbelt (Shann, 2021). Oligocene potential reservoirs in the onshore region of the Veracruz Basin show porosity values between 15% and 20% (González and Medrano, 2014).

Lower Miocene conglomerates and sandstones are reportedly rich in calcareous clasts. The samples also show the onset of quartz and feldspar delivery to the basin, and an increased presence of metamorphic and plutonic rock fragments (Martínez-Medrano et al., 2009; Sánchez-Hernández 2013). Gas is reportedly produced from five clastic Miocene sequences. Some lower Miocene producing horizons (La Laja Fm.) show average porosity ranging from 6–8% (IHS, 2010) to 23% (Martínez-Medrano et al., 2009). The middle Miocene reservoirs show maximum porosity values of 29% (Martínez-Medrano et al., 2009). Summing up, lower and middle Miocene sandstones average porosity in the range of 6 to 29%.

As observed in several onshore fields in the Veracruz Basin (Playuela, Apertura–Madera), the onset of delivery of quartz and feldspar was in the early Miocene, reaching a period of maximum supply in the middle Miocene (Martínez-Medrano et al., 2009). Middle Miocene was also the time when sediments in the northern Veracruz Basin started to receive the first volcaniclastic input coming from the Trans-Mexican Volcanic Belt (Martínez-Medrano et al., 2009), although the main contribution to the sandstones still came from the erosion of the Cuicateco sub-belts (carbonates, metamorphic and siliciclastic clasts).

Campeche Salt Basin: In general, Neogene sediments are poorly sorted and mineralogically immature. They correspond to feldspathic litharenites with abundant volcanic lithics, feldspar, quartz, metamorphic and sedimentary fragments (CNH, 2019). The lower Miocene play is considered to be the most prospective in the deep-water region of Campeche Salt Basin and has been the focus of many wells drilled in recent years (e.g., Kabili-1, Labay-1, Leek-1, Polok-1EXP, Tabscoob-101 and Yoka-1 wells). Well logs and cores reveal upward-fining stacking patterns of massive coarse-grained sandstones, plus siltstone and shale, with some channels exhibiting erosive bases and basal conglomerates.

7.3 Upper Miocene–Pliocene reservoirs

Veracruz

Upper Miocene–Pliocene reservoirs show an increased contribution of mafic and felsic volcanic lithics at expenses of carbonate and metamorphic lithics (Martínez-Medrano et al., 2009; Jennette et al., 2003a; Gutiérrez-Paredes et al., 2009). The same is observed in the Catemaco Foldbelt, where most of the detrital material was supplied by Los Tuxtlas Volcanic Complex. Maximum porosity determined in upper Miocene–Pliocene sandstones in the Veracruz Basin reach up to 34% (Martínez-Medrano et al., 2009).

Sureste and Campeche Salt Basins

The Upper Miocene–Pleistocene sandstones of the Reforma–Comalcalco–Macuspana are classified as arkoses and subarkoses, with a lesser proportion of litharenites (Pemex, 2013c). The main constituents of the sandstones are quartz, feldspars, and rock fragments of igneous and metamorphic provenance according to Pemex (2013c).

Reservoir quality highly depends on the depositional facies and the depth of burial (Chávez-Valois et al., 2009). In the Isthmus Saline Basin (onshore) porosity values in upper Miocene reservoirs range from 10% to 30% (Sosa-Patrón et al., 2009), similarly as in the Reforma–Comalcalco–Macuspana region, where porosity reaches up to 30% in the coarsest upper Miocene–Pleistocene horizons (Chávez-Valois et al., 2009).

The percentage of volcanic rocks fragments in sandstones from offshore wells (e.g., Chuktah-1, Chuktah-201, Tibil-1, Lakmay-1, Lakach-1, Kunah-1; CNH, 2019; Beltrán-Triviño et al., 2021) indicates the increased presence of a significant calc-alkaline volcanic source likely sourced from the Los Tuxtlas Volcanic Complex and the scattered arc-related volcanoes and domes present in the Chiapas Basin. Nevertheless, the Upper Miocene–Pliocene reservoirs are deemed good (CNH, 2019). Eni's Sayulita-1EXP discovery in shallow waters contains 150–200 mmboe reportedly in good quality upper Miocene sands approximately 70km from the coast. The Tabscoob-1 discovery located near the transition from shallow to deep water produces gas and condensate from middle Pliocene sandstones (CNH, 2019).

7.4 Summary on reservoir potential

Cenozoic siliciclastic reservoir quality tends to improve from older to younger units due to progressive exposure of basement rocks following the erosion of their overlying sedimentary cover (mainly Cretaceous carbonates). Cenozoic siliciclastic reservoirs are typically classified as litharenites or feldspathic litharenites due to the abundance of lithic fragments contained in the sediments (often exceeding 50% of constituent grains; Shann et al., 2020). Porosity types identified include intergranular porosity, secondary porosity (due to the dissolution of unstable lithic grains, feldspars, and bioclasts), fracturing, and microporosity (Gutiérrez-Paredes et al., 2018). Analyses of core data indicates that a 10% porosity cutoff for reservoir effectiveness is appropriate for these rocks; porosity-depth relationships thereby suggest a reservoir floor of approximately 4,000m below mud line (Shann et al., 2020). Quartz cementation does not seem to be a significant contributor to porosity reduction, but rather the high lithic content of most of these sands can result in substantial porosity loss due to compaction of ductile lithics with burial (Mousavi and Bryant, 2013).

8 Conclusions

The extensive geo- and thermo-chronological data set that we have generated allows us to determine with confidence all areas in southern Mexico that have potentially provided carbonate and clastic material towards the onshore and offshore foreland basins of southern Mexico and the Gulf of Mexico, including the Tampico–Misantla, Veracruz, Sureste and Chiapas basins.

We outline an Early Cretaceous rapid low-angle extensional event in the Sierra de Juárez Complex that was followed by cooling from ~130 Ma to ~90 Ma, as well as platform and basinal depositional conditions in the Cuicateco Belt. Subsequently, the onset of the Mexican Orogeny deformation in Mixteca/Oaxaca blocks and the Sierra Madre Oriental occurred from the Campanian–Maastrichtian through the early Oligocene and propagated eastward and southward towards the foreland regions and the Cuicateco Belt. Erosional exhumation of these regions provided carbonate detrital material to the Tampico–Misantla and Veracruz basins.

Although relatively local sources such as the Mixtequita and Guichicovi Blocks possibly provided first-order quartz-rich material to the southernmost Veracruz Basin from the Eocene, most of the quartz-rich and metamorphic-rich material feeding the Veracruz basins came from the Cuicateco sub-belts and was only supplied from the earliest Miocene. This clastic material has been subsequently overtaken by volcaniclastic material derived from the Trans-Mexican Volcanic Belt since the middle Miocene.

During most of the Cenozoic, the Chiapas Basin and the Sureste basins were sourced from the Chontal Complex (western Tehuantepec), the mobile Chortis Block, as well as volcanic-arc rocks that bordered Chortis during the Cenozoic. Moreover, older sedimentary material covering the Chiapas Massif and Basin has been partially eroded throughout the Cenozoic and provided second-cycle material to the Chiapas and the Sureste basins.

Our results highlight the importance of understanding relative block and plate boundary displacements and ponder the role of major faults when interpreting source-to-sink relationships in the area. This work documents how foredeep deposits in the Mexican foreland basins have been involved in late deformational events, and how those sediments are very often re-incorporated into younger deposition. This has traditionally led to incorrect detrital provenance conclusions. This synthesis should help to predict the physical nature and lithologic characteristics of turbidites and fluvial channels from several Late Cretaceous–Cenozoic fairways along the southern Gulf of Mexico rim.

Future work should seek an improved determination of the offshore limits of the Chortis Block, such as along the Pacific margin and the Honduras Shelf regions because they were source areas for Mexican basins throughout most of the Cenozoic. Also, more robust determinations of the thermal histories in onshore regions of the Chortis Block will not only aid exploration in Central America, but will impact our understanding of potential provision of detritus to Mexico, as well.

Acknowledgments

This work is dedicated to our dear colleague and friend Roberto Molina Garza, whose life was taken from us too soon. His memory will last forever in our hearts. We thank Elisa Fitz Díaz (Universidad Nacional Autónoma de México, UNAM), Goran Andjic (Utrecht University) and Editor Douwe van Hinsbergen (Utrecht University) for a thorough and enriching review of this manuscript. We also thank the sponsors of the 11-year Cordilleran (Mexico) Research Program, in particular Phase 3 corporate sponsors (BHP, Chevron, Equinor and ExxonMobil). We wish to acknowledge the contribution and knowledge shared with us by Uwe Martens (UNAM). We also thank Juliana Estrada Carmona and María Isabel Sierra Rojas (UNAM) for processing some of the samples presented herein.

Figure captions

Figure 1

Tectonic map of southern Mexico modified from Reed et al. (2004) showing the main litho-tectonic units defined in this work. Inset shows the extent of the Mexican Orogen (after Fitz-Díaz et al., 2018). Abbreviations: AF, Aloapán Fault (possibly a reactivated subvertical structure) ; BGB, Barranca Grande Backthrust ; CB, Cuicateco Belt ; ChT, Chivela Trust; CF, Caltepec Fault ; CP, Córdoba Platform ; OF, Oaxaca Fault (steep westerly dipping structure of Tertiary age) ; PF, Papalutla Fault ; PeF : Petapa Fault ; SF, Soyaltepec Fault ; SVF, Siempre Viva Fault (thrust carrying basement rocks of the Sierra de Juárez Complex over the Cuicateco Belt) ; TF, Tehuantepec Fault ; TV, Tehuacán valley (a Tertiary half-graben) ; VAF, Villa Alta Fault (possibly a reactivated subvertical structure) ; VHF, Vista Hermosa Fault (thrust); VNF, Valle Nacional Fault (oblique inversion structure). Geographic Coordinate System: Mexico ITRF2008; Projection: Lambert Conformal Conic.

Figure 2 a,b

a) Oaxaca cross section A1–A4; b) Chiapas cross section B1–B5 (lines shown on Figure 1). Modified from Graham et al. (2020, figures 7b and 15b).

Figure 3

Tectonic map of southern Mexico modified from Reed et al. (2004) showing the main litho-tectonic units and new samples analysed in this work for geo- and thermochronology (red squares). We also include sample locations with published thermochronological data (blue squares) used in our interpretations. Published data include Villagómez et al. (2019); Villagómez and Pindell (2020a, 2000b) and Gray et al. (2021). Geographic Coordinate System: Mexico ITRF2008; Projection: Lambert Conformal Conic.

Figures 4 a,b

Thermal history models for the different litho-tectonic units using HeFTy© software. Input data included AFT age, track length data, and Dpar (a proxy for chemical composition), as well as apatite and zircon U–Th/He when available. The good-fit envelope of solutions (all solutions with a goodness of fit of 0.5 and higher) are shown in pink. Acceptable solutions (goodness of fit between 0.05 and 0.5) are shown in green. For more details on the dating methods and thermal modelling see **Appendix 2**. Most thermal models are unpublished although input AFT data in the Tampico–Misantla and the Cuicateco models include data from Gray et al. (2021) and Villagómez (2014).

Figure 5 a, b

a) New K-feldspar $^{40}Ar/^{39}Ar$ ages from the Sierra de Juárez Complex. b) Cooling history of the Sierra de Juárez Complex and interpretation.

Figure 6

Stratigraphic columns and post-Jurassic rock cooling periods observed in southern Mexico, as well as an interpretation of the causes of cooling. Geologic time scale used is the International Chronostratigraphic Chart of the International Commission on Stratigraphy, version 2013/01 (Cohen et al., 2013). Sources are listed in the text and in **Appendix 1.** For more details on the stratigraphy see **Appendix 1**.

Figures 7 a–i

Present-day configuration (**Figure 7a**) and Late Cretaceous to Recent (**Figures 7b–i**) reconstruction of southern Mexico and Chortis. Litho-tectonic units represented using the same colours as in **Figure 1**. Areas that were potentially eroded are colour filled. The horizontal line patterns represent litho-tectonic units which experienced known erosional exhumation for a given map. The maps show the present-day outline of continental core of Chortis (Chortis s.s.) according Andjic et al. (2018) and Romito and Mann (2020), as well as our preferred outline based on onshore geology. Key wells drilled offshore Chortis are also shown on the present-day configuration. Paleo-position of Chortis and movement relative to North America are from Pindell and Kennan (2009), Villagómez and Pindell (2020b), Graham et al. (2020). Our reconstruction maps include basic palinspastic corrections that account for possible rigid and nonrigid deformation of the different block boundaries. Rotation of Chortis since early Paleocene is about 40° counter-clockwise, in line with data from Molina-Garza et al. (2019a). Rotation (and translation) of Chiapas is about 15° clockwise (possible moving pole at around 14.7°N/92.7°W) between early and mid-Miocene (Molina-Garza et al., 2020b). Paleogene channels are based on Rosenfeld and Pindell (2003). Depositional axes of the most relevant fairways are shown with coloured arrows and are compiled from Arreguín-López et al., 2011; Ambrose et al., 2003; Escalera-Alcocer, 2010; CNH, 2014, 2015, 2017a, 2017b, 2019, González and Medrano, 2014; Snedden and Galloway, 2019; Brito and Luysterburg, 2019; Shann et al., 2020; Davidson, 2021 and unpublished industry data. The depositional facies areas are based on multiple published interpretations (*incl.* Quezada-Muñetón, 1987; Meneses-Rocha, 2001; Witt et al., 2012; CNH, 2017b) and our own fieldwork observations.

Geographic Coordinate System and datum used in this map are WGS84. Abbreviations: BVF: Baja Verapaz Fault; JChF: Jocotán–Chamelecón Fault; MF: Motagua Fault; PFZ: Polochic Fault Zone. Figure 7a. Inset: Modern river drainage system of southern Mexico, indicating the extent of drainage into the Gulf of Mexico. These drainage systems were probably considerably larger prior to compressional deformation (possibly as early as Eocene but peaking in middle Miocene) and could deliver vast volumes of sediment to offshore areas.

Appendixes

Appendix 1
Litho-tectonic unit details

Appendix 2
Methodologies

Appendix 3
Analytical data

References

Alaniz-Álvarez, S.A., van der Heyden, P., Nieto-Samaniego, A.F. and Ortega-Gutiérrez, F. 1996. Radiometric and kinematic evidence for Middle Jurassic strike-slip faulting in southern Mexico related to the opening of the Gulf of Mexico. Geology, 24(5), pp. 443–446. https://doi.org/10.1130/0091-7613(1996)024%3C0443:RAKEFM%3E2.3.CO;2

Allen, P.A. 2017. *Sediment routing systems: The fate of sediment from source to sink*. Cambridge University Press. 442 pp.

Allen, P.A. and Allen, J.R., 2013. *Basin analysis: Principles and application to petroleum play assessment*. John Wiley & Sons.

Ambrose, W.A., Wawrzyniec, T.F., Fouad, K., Talukdar, S.C., Jones, R.H., Jennette, D.C., Holtz, M.H., Sakurai, S., Dutton, S.P., Dunlap, D.B. and Guevara, E.H., 2003. Geologic framework of upper Miocene and Pliocene gas plays of the Macuspana Basin, southeastern Mexico. *AAPG bulletin*, *87*(9), pp.1411–1435.

Andjić, G., Baumgartner, P.O. and Baumgartner- Mora, C., 2018. Rapid vertical motions and formation of volcanic arc gaps: Plateau collision recorded in the forearc geological evolution (Costa Rica margin). *Basin Research*, *30*(5), pp.863–894.

Ángeles-Aquino, F.J., Reyes-Nunez, J., Quezada-Muneton, J.M. and Meneses-Rocha, J.J., 1994. Tectonic evolution, structural styles, and oil habitat in Campeche sound, Mexico.

Ángeles-Moreno, E., 2006. *Petrografía, geología structural y geocronología del borde noroccidental del terreno Cuicateco, Sierra Mazateca, estado de Oaxaca, México.* Universidad Nacional Autónoma de México, Posgrado en Ciencias de la Tierra, Instituto de Geología, unpublished M. Sc. Thesis.

Ángeles-Moreno E., Elías-Herrera M, Macías-Romo C, Sánchez-Zavala JL, Ortega-Gutiérrez F. 2012. Geological Map of the Western Border of Cuicateco Terrane, Southern Mexico*. Geological Society of America*, Map & Chart Series MCH102.

Armstrong, P.A., 2005. Thermochronometers in sedimentary basins. *Reviews in Mineralogy and Geochemistry*, 58(1), pp.499–525.

Arreguín-López, M.A., Reyna-Martinez, G., Sanchez-Hernandez, H., Escamilla-Herrera, A. and Gutierrez-Araiza, A., 2011. Tertiary Turbidite Systems in the Southwestern Gulf of Mexico. *Gulf Coast Association of Geological Societies Transactions*, v. 61, p. 45–53.

Beltrán-Triviño, A., U. Martens, and A. von Quadr, 2021, Siliciclastic provenance of the Cenozoic stratigraphic succession in the southern Gulf of Mexico: insights from U-Pb detrital zircon geochronology and heavy minerals analysis. In: Martens, U. and Molina-Garza, R.S. (eds) Southern and Central Mexico: Basement Framework, Tectonic Evolution, and Provenance of Mesozoic–Cenozoic Basins. Geological Society of America, Special Papers, 546.

Bernet, M., Garver, J. I., 2005. Fission-track Analysis of Detrital Zircon. *Reviews in Mineralogy and Geochemistry* 58, 205–237.

Bitter, M.R., 1993. Sedimentation and provenance of Chicontepec sandstones with implications for uplift of the Sierra Madre Oriental and Teziutlan Massif, east-central Mexico. Mesozoic and Early Cenozoic Development of the Gulf of Mexico and Caribbean Region–A Context for Hydrocarbon Exploration, James L. Pindell, Bob F. Perkins. p. 155–172. https://doi.org/10.5724/gcs.92.13.0155

Braun, J., Van der Beek, P. and Batt, G., 2006. *Quantitative thermochronology: numerical methods for the interpretation of thermochronological data*. Cambridge University Press. 254 pp.

Brito, M. and Luysterburg, C., 2019, April. Evaluation of Sediment Fairways Along the Western Margin of the Saline Basin. *In* Second EAGE (European Association of Geoscientists & Engineers) *Workshop on Deepwater Exploration in Mexico: Knowledge transfer and collaboration from shelf to deepwater*. Vol. 2019, No. 1, pp. 1–5.

Brocard, G.Y., Willenbring, J.K., Salles, T., Cosca, M., Guttiérez-Orrego, A., Cacao-Chiquín, N., Morán-Ical, S. and Teyssier, C., 2020. Top-down and bottom-up controls on mountain-hopping erosion: insights from detrital 10 Be and river profile analysis in Central Guatemala. *Earth Surface Dynamics Discussions*, pp.1–46.

Campa-Uranga, M.F., and Coney P.J. 1983. Tectono-stratigraphic terranes and mineral resource distribution in Mexico: Canadian Journal of Earth Sciences, **v. 20**, pp. 1040–1051.

Campos-Madrigal, E., Centeno-García, E., Mendoza-Rosales, C.C. and Silva-Romo, G., 2013. Sedimentología, reconstrucción paleoambiental y significado tectónico de las sucesiones clásticas del Jurásico Medio en el área de Texcalapa, Puebla-Huajuapan de León, Oaxaca: Revisión de las formaciones Ayuquila y Tecomazúchil. *Revista mexicana de ciencias geológicas*, *30*(1), pp.24–50. 24–50. ISSN 2007-2902.

Camprubí, A., Cabrera-Roa, M.Á., González-Partida, E. and López-Martínez, M., 2019. Geochronology of Mexican mineral deposits. VIII: the Zacatepec polymetallic skarn, Oaxaca. Boletín de la Sociedad Geológica Mexicana, 71(1), pp.207–218.

Cantú-Chapa, A. 2001, Paleocanyons in the subsurface of eastern Mexico: Facts and uncertainties, *in* C. Bartolini, R. T. Buffler, and A. Cantú-Chapa, eds., The western Gulf of Mexico Basin: Tectonics, sedimentary basins, and petroleum systems: AAPG Memoir 75, p. 421–430.

Carfantán, J.C., 1981. Evolución estructural del sureste de México, Paleogeografía e historia tectónica de las zonas internas mesozoicas. *Revista mexicana de Ciencias Geológicas*, *5*(2), pp.207–216.

Carfantán, J.C. 1985. Du Système Cordilleran nord-american au domaine Caraibe. Etude Geologique du Mexique Meridional. PhD thesis, Université de Savoie, France.

Carrillo-Bravo, J.C., 1980. Paleocanones terciarios de la planicie costera del Golfo de Mexico. *Boletin de la Asociacion Mexicana de Geologos Petroleros*, *32*(1), pp.27–55. https://shar.es/aWxtC1

Chávez-Valois, V. M., M. d. L. C. Valdés, J. I. Juarez-Placencia, I. A. Ortiz, M. M. Jurado, R. V. Yanez, M. G. Tristan, and S. Ghosh. 2009. A new multidisciplinary focus in the study of the tertiary plays in the Sureste Basin, Mexico*, in* C. Bartolini and J. R. Romá- Ramos, eds., *Petroleum systems in the southern Gulf of Mexico*: AAPG Memoir 90, p. 155–190.

Clark, J., Ochoa, J., Stockli, D., Fildani, A., Gerber, T., Covault, J., Guzman, J., Vinnels, J. and Marshall, J., 2019. Provenance and Morphology of Extensive Oligocene-Miocene Deep-Water Fan Systems Sourced from Chiapas-Veracruz and Sierra Madre Oriental, Gulf of Mexico. In *2019 AAPG Annual Convention and Exhibition.*

CNH. 2014. Cuencas del Sureste Aguas Someras - Síntesis Geológica Petrolera. Comisión Nacional de Hidrocarburos (CNH), Mexico City, 64 p. https://www.rondasmexico.gob.mx/media/1418/atlas.pdf

CNH. 2015. Saline Basin - Petroleum Geological Synthesis. Comisión Nacional de Hidrocarburos (CNH), Mexico City, 47p. https://rondasmexico.gob.mx/media/1557/geological-atlas-cs.pdf

CNH. 2017a. Atlas Geológico Cuenca Veracruz. Comision Nacional de Hidrocarburos (CNH), Mexico City, 57p. https://hidrocarburos.gob.mx/media/3092/atlas_geologico_cuenca_veracruz_v3.pdf

CNH. 2017b. Atlas Geológico Cuencas Del Sureste - Cinturón Plegado de la Sierra de Chiapas.. Comision Nacional de Hidrocarburos (CNH), Mexico City, 54p. https://hidrocarburos.gob.mx/media/3094/atlas_geologico_cuencas_sureste_v3.pdf

CNH. 2019. Prospective Resources of Mexico: Perdido Area, Mexican Ridges and Saline Basin, deepwater Gulf of Mexico. Comisión Nacional de Hidrocarburos (CNH), 160p.https://www.gob.mx/cms/uploads/attachment/file/527025/Deepwater_Prospective_Resources_of_Mexico_Publishing_2019_DGEPP_low.pdf

Cohen, K.M., Finney, S.C., Gibbard, P.L. and Fan, J.-X. 2013. The ICS International Chronostratigraphic Chart. Episodes, 36, 199–204, http://www.stratigraphy.org/ICSchart/ChronostratChart2018-07.pdf; https://doi.org/10.18814/epiiugs/2013/v36i3/002

Coombs, H. 2016. Geochemical and geochronological constraints on terrane definition in Mexico. PhD thesis. Cardiff University, 378 p.

Cossey, S., Rosenfeld, J., Bitter, M., and Pindell, J., 2021. Update on the Paleogene Water-Level Drawdown Hypothesis, Gulf of Mexico. *Gulf Coast Association of Geological Societies Journal, 10,* pp.123-141.

Covault, J.A. and Graham, S.A., 2010. Submarine fans at all sea-level stands: Tectono-morphologic and climatic controls on terrigenous sediment delivery to the deep sea. *Geology*, *38*(10), pp.939–942.

Damon, P. and Montesinos, E., 1978. Late Cenozoic volcanism and metallogenesis over an active Benioff zone in Chiapas, Mexico. *Arizona Geological Society Digest*, *11*, pp.155–168.

Dávalos-Álvarez, O.G., Nieto-Samaniego, Á.F., Alaniz-Álvarez, S.A., Martínez-Hernández, E. and Ramírez-Arriaga, E., 2007. Estratigrafía cenozoica de la región de Tehuacán y su relación con el sector norte de la falla de Oaxaca. *Revista mexicana de ciencias geológicas*, *24*(2), pp.197–215.

Davison, I., 2021. Salt tectonics in the Sureste Basin, SE Mexico: some implications for hydrocarbon exploration. *Geological Society, London, Special Publications*, *504*(1), pp.147–165. https://doi.org/10.1144/SP504-2019-227

Delgado-Argote, L.A., López-Martínez, M., York, D. and Hall, C.M. 1992. Geologic framework and geochronology of ultramafic complexes of the southern México. Canadian Journal of Earth Sciences 29(7), 1590–1604, https://doi.org/10.1139/e92-125

Delgado-Argote, L.A., 1988. Geología preliminar de la secuencia volcanosedimentaria y serpentinitas asociadas del Jurásico (?) del área de Cuicatlán–Concepción Pápalo, Oaxaca. Rev. - Inst. Geol., UNAM 7, 127–135.

Dodson, M.H., 1973. Closure temperature in cooling geochronological and petrological systems. Contributions to Mineralogy and Petrology, 40(3), pp.259–274.

Ducea, M.N., Valencia, V.A., Shoemaker, S., Reiners, P.W., DeCelles, P.G., Campa, M.F., Morán-Zenteno, D., and Ruiz, J., 2004, Rates of sediment recycling beneath the Acapulco trench: Constraints from (U-Th)/He thermochronology: Journal of Geophysical Research, v. 109, B09404, https://doi.org/10.1029/2004JB003112.

Elías- Herrera, M. and Ortega- Gutiérrez, F., 2002. Caltepec fault zone: An Early Permian dextral transpressional boundary between the Proterozoic Oaxacan and Paleozoic Acatlán complexes, southern Mexico, and regional tectonic implications. *Tectonics*, *21*(3), pp. 1–18.

Engebretson, D.C., Cox, A. and Gordon, R.G. 1984. Relative motions between oceanic plates of the Pacific Basin. Journal of Geophysical Research, 89, 10291–10310, https://doi.org/10.1029/JB089iB12p10291

England, P. and Molnar, P., 1990. Surface uplift, uplift of rocks, and exhumation of rocks. *Geology*, *18*(12), pp.1173–1177.

Escalera-Alcocer, J.A., 2010. Estrategia, Logros y desafios de la exploracion petrolera en Mexico. *Trabajo de Ingreso a la Academia de Ingeniería México. Especialidad: Ingeniería Geológica*. 70 p.

Espejo-Bautista, G., Ortega-Gutiérrez, F., Solari, L.A., Maldonado, R. and Valencia-Morales, Y.T., 2021. The Sierra de Juárez Complex: a new Gondwanan Neoproterozoic-early Palaeozoic metamorphic terrane in southern Mexico. *International Geology Review*, pp.1-23. https://doi.org/10.1080/00206814.2020.1870172

Farley, K.A., 2002, (U-Th)/He dating: Techniques, calibrations, and applications: Reviews in Mineralogy and Geochemistry, v. 47, no. 1, p. 819–844, https://doi.org/10.2138/rmg.2002.47.18.

Ferrari, L., Tagami, T., Eguchi, M., Orozco-Esquivel, M.T., Petrone, C.M., Jacobo-Albarrán, J. and López-Martínez, M. 2005. Geology, geochronology and tectonic setting of late Cenozoic volcanism along the southwestern Gulf of Mexico: The Eastern Alkaline Province revisited. *Journal of Volcanology and Geothermal Research*, *146*(4), pp.284–306. https://doi.org/10.1016/j.jvolgeores.2005.02.004

Ferrari, L., Orozco-Esquivel, T., Manea, V. and Manea, M., 2012. The dynamic history of the Trans-Mexican Volcanic Belt and the Mexico subduction zone. *Tectonophysics*, *522*, pp.122-149. https://doi.org/10.1016/j.tecto.2011.09.018

Fitz-Díaz, E. and van der Pluijm, B., 2013. Fold dating: A new Ar/Ar illite dating application to constrain the age of deformation in shallow crustal rocks. *Journal of Structural Geology*, *54*, pp.174–179. https://doi.org/10.1016/j.jsg.2013.05.011

Fitz- Díaz, E., Hudleston, P., Tolson, G. and Van Der Pluijm, B., 2014. Progressive, episodic deformation in the Mexican Fold–Thrust Belt (Central Mexico): evidence from isotopic dating of folds and faults. *International Geology Review*, *56*(6), pp.734–755.

Fitz-Díaz, E., Lawton, T.F., Juárez-Arriaga, E. and Chávez-Cabello, G., 2018. The Cretaceous-Paleogene Mexican orogen: Structure, basin development, magmatism and tectonics. *Earth-Science Reviews*, *183*, pp.56–84.

Fitz-Díaz, E., Hernández-Vergara, R., Ortega-Gutiérrez, F., Sanz-Valencia, J. Albarrán-Santos, M.A., Pi-Puig, T., 2022. Kinematics and Ar–Ar illite age of deformation in the late Paleozoic Chicomuselo Fold-Thrust Belt (CFTB), Chiapas, Mexico and tectonic implications. *Journal of South American Earth Sciences*, *113*, p.103648.

Friedmann, S.J., and Burbank, D.W., 1995, Rift basins and supra detachment basins: Intracontinental extensional end-members. Basin Research, v. 7, p. 109–127

Galloway, W.E., Whiteaker, T.L. and Ganey-Curry, P. 2011. History of Cenozoic North American drainage basin evolution, sediment yield, and accumulation in the Gulf of Mexico basin. *Geosphere*, *7*(4), pp.938–973.

García-Molina, G., 1994. *Structural evolution of SE Mexico (Chiapas-Tabasco-Campeche) offshore and onshore*. Doctoral dissertation, Rice University. 494 pp.

Garduño-Monroy, V.H., Macías, J.L. and Garza, R.M., 2015. Geodynamic setting and pre-volcanic geology of active volcanism in Chiapas. In *Active Volcanoes of Chiapas (Mexico): El Chichón and Tacaná* (pp. 1-23). Springer, Berlin, Heidelberg.

Gawthorpe, R.L., and Leeder, M.R., 2000, Tectonosedimentary evolution of active extensional basins. Basin Research, v. 12, p. 195–218.

González, E. and Medrano, M. 2014. Structural slope fans resulting from Palaeogene compression in the Veracruz Basin, Mexico. AAPG Search and Discovery Article #50963, AAPG 2014 Annual Convention and Exhibition, April 6–9, 2014, Houston, Texas, USA, http://www.searchanddiscovery.com/pdfz/documents/2014/50963gonzalez/ndx_gonzalez.pdf.html

Graham, R., Pindell, J., Villagómez, D., Molina-Garza, R., Granath, J. and Sierra-Rojas, M., 2020. Integrated Cretaceous–Cenozoic plate tectonics and structural geology in Southern Mexico. *Geological Society, London, Special Publications*, *504*(1), pp. 285–314. https://doi.org/10.1144/SP504-2020-70

Gray, G.G., Pottorf, R.J., Yurewicz, D.A., Mahon, K.I., Pevear, D.R., Chuchla, R.J., 2001, Thermal and chronological record of syn- to post-Laramide burial and exhumation, Sierra Madre Oriental, Mexico, *in* Bartolini, C., Buffler, R.T., Cantú-Chapa, A. (eds.), The western Gulf of Mexico Basin: Tectonics, sedimentary basins, and petroleum systems: American Association of Petroleum Geologists Memoir, 75, 159–181.

Gray, G., Villagómez, D., Pindell, J., Molina-Garza, R., O'Sullivan, P., Stockli, D., Farrell, W., Blank, D. and Schuba, J. 2021. Late Mesozoic and Cenozoic thermotectonic history of eastern, central and southern Mexico as determined through integrated thermochronology, with implications for sediment delivery to the Gulf of Mexico. Geological Society of London *Special Publications* 504, no.1. 255–283. https://doi.org/10.1144/SP504-2019-243

Gutiérrez Paredes, H. C., Martinez Medrano, M. and Sessarego, H. L. 2009, Provenance for the middle and upper Miocene sandstones of the Veracruz Basin, Mexico, in C. Bartolini and J. R. Roman Ramos, eds., Petroleum systems in the southern Gulf of Mexico: AAPG Memoir 90, p. 397–407. https://doi.org/10.1016/j.jsames.2017.10.007

Gutiérrez-Paredes, H. C., O. Catuneanu, and U. Hernandez Romano. 2018. Controls on the quality of Miocene reservoirs, southern Gulf of Mexico. *Journal of South American Earth Sciences*, *81*, pp.45–65.

Harrison, T.M., Célérier, J., Aikman, A.B., Hermann, J. and Heizler, M.T., 2009. Diffusion of ^{40}Ar in muscovite. Geochimica et Cosmochimica Acta 73, 1039–1051.

Helland-Hansen, W., Sømme, T.O., Martinsen, O.J., Lunt, I. and Thurmond, J. 2016. Deciphering Earth's natural hourglasses: perspectives on source-to-sink analysis. *Journal of Sedimentary Research*, *86*(9), pp.1008–1033.

Hernández-Vergara, R., Fitz-Díaz, E., Brocard, G. and Morán-Zenteno, D.J., 2021. Illite 40Ar–39Ar dating of Eocene deformation in the Chiapas Fold and Thrust Belt, southern Mexico. *Geological* Society, London, Special Publications, 504(1), pp.315–341.

Herrmann, U.R., Nelson, B.K. and Ratschbacher, L., 1994. The origin of a terrane: U/Pb zircon geochronology and tectonic evolution of the Xolapa complex (southern Mexico). *Tectonics*, *13*(2), pp.455-474. https://doi.org/10.1029/93TC02465

Hessler, A.M., Covault, J.A., Stockli, D.F. and Fildani, A., 2018. Late Cenozoic cooling favored glacial over tectonic controls on sediment supply to the western Gulf of Mexico. *Geology*, *46*(11), pp.995–998. https://doi.org/10.1130/G45528.1

Horbury, A.D., Gonzalez-P, S.H.F., Rodriguez-F, D., Reyes-F, A., Ortiz-G, P., Martinez-M, M. and Quintanilla-R, G. 2003, Tectonic sequence stratigraphy of the western margin of the Gulf of Mexico in the late Mesozoic and Cenozoic: Less passive than previously imagined, in C. Bartolini, R. T. Buffler, and J. Blickwede, eds., The Circum-Gulf of Mexico and the Caribbean: Hydrocarbon habitats, basin formation, and plate tectonics: AAPG Memoir 79, p. 184–245.

IHS. 2010. Basin Monitor – Veracruz Basin, IHS Markit Basin Dataset. Mexico. https://ihsmarkit.com/Info/en/a/mexico/e-p-data.html

Jennette, D.C., Fouad, K., Wawrzyniec, T., Dunlap, D., Muñoz, R. and Meneses-Rocha, J. 2003a. Slope and basin-floor reservoirs from the Miocene and Pliocene of the Veracruz Basin, southeastern Mexico. Marine and Petroleum Geology, 20(6-8), pp.587–600. https://doi.org/10.1016/j.marpetgeo.2003.01.001

Jennette, D., Wawrzyniec, T., Fouad, K., Dunlap, D.B., Meneses-Rocha, J., Grimaldo, F., Muñoz, R., Barrera, D., Williams-Rojas, C.T. and Escamilla-Herrera, A., 2003. Traps and turbidite reservoir characteristics from a complex and evolving tectonic setting, Veracruz Basin, southeastern Mexico. AAPG bulletin, 87(10), pp.1599–1622. https://doi.org/10.1306/05130302010

Kazachkina, E., Kostoglodov, V., Cotte, N., Walpersdorf, A., Ramirez-Herrera, M.T., Gaidzik, K., Husker, A. and Santiago, J.A., 2020. Active 650-km long fault system and Xolapa sliver in Southern Mexico. *Frontiers in Earth Science*, *8*, p.155. https://doi.org/10.3389/feart.2020.00155

Keppie, J.D., Dostal, J., Cameron, K.L., Solari, L.A., Ortega-Gutiérrez, F., and López, R., 2003, Geochronology and geochemistry of Grenvillian igneous suites in the northern Oaxacan Complex, southern Mexico: Tectonic implications: Precambrian Research, v. 120, p. 365–389, https://doi.org/10.1016/S0301-9268(02)00166-3.

Ketcham, R.A., 2005, Forward and inverse modelling of low-temperature thermochronometry data: Reviews in Mineralogy and Geochemistry, v. 58, p. 275–314.

Ketcham, R.A., 2012. User’s manual for HeFTy Version 1.7.5.

Ketcham, R.A., Carter, A., Donelick, R.A., Barbarand, J., and Hurford, A.J., 2007, Improved modeling of fission-track annealing in apatite: The American Mineralogist, v. 92, no. 5–6, p. 799–810, https://doi.org/10.2138/am.2007.2281.

Kirsch, M., Helbig, M., Keppie, J.D., Murphy, J.B., Lee, J.K.W., Solari, L.A., 2014. A Late Triassic tectonothermal event in the eastern Acatlán Complex, southern Mexico, synchronous with a magmatic arc hiatus: the result of flat-slab subduction? Lithosphere 6, 63–79.

Lawton, T.F., Sierra-Rojas, M.I. and Martens, U., 2020. Stratigraphic correlation chart of Carboniferous–Paleogene rocks of Mexico, adjacent southwestern United States, Central America, and Colombia. *Southern and Central Mexico: Basement Framework, Tectonic Evolution, and*

Provenance of Mesozoic–Cenozoic Basins. Geological Society of America, Special Papers, *546*, p.28.

Lister, G., and Davis, A.G., 1989, The origin of metamorphic core complexes and detachment faults formed during Tertiary continental extension in the northern Colorado River region, USA: Journal of Structural Geology, v. 11, p. 65–94.

Lovera, O. M., Richter, F. M., Harrison, T. M., 1991. Diffusion Domains Determined by ^{39}Ar Released During Step Heating. Journal of Geophysical Research 96, 2057–2069.

Mandujano-Velázquez, J.J. and Keppie, J.D., 2009. Middle Miocene Chiapas fold and thrust belt of Mexico: a result of collision of the Tehuantepec Transform/Ridge with the Middle America Trench. *Geological Society, London, Special Publications*, *327*(1), pp.55–69.

Martens, U. and Molina-Garza, R., 2021. Mexico: Basement Framework and pre-Cretaceous Stratigraphy. *Southern and Central Mexico: Basement Framework, Tectonic Evolution, and Provenance of Mesozoic–Cenozoic Basins. Geological Society of America, Special Papers*, *546*. https://doi.org/10.1130/2021.2546(01)

Martini, M. and Ortega-Gutiérrez, F., 2018. Tectono-stratigraphic evolution of eastern Mexico during the break-up of Pangea: A review, in Gómez-Tuena, A. and Ortega-Gutiérrez, F., Tectonic Systems of Mexico. Origin and Evolution. Earth-Sciences Reviews, 183, 1–182.

Martiny, B., Martínez-Serrano, R.G., Morán-Zenteno, D.J., Macías-Romo, C. and Ayuso, R.A., 2000. Stratigraphy, geochemistry and tectonic significance of the Oligocene magmatic rocks of western Oaxaca, southern Mexico. *Tectonophysics*, *318*(1-4), pp.71–98. https://doi.org/10.1016/S0040-1951(99)00307-8

Martínez-Medrano, M., Vega-Escobar, R., Flores-Cruz, F., Angeles-Marin, D. and Lopez-Martinez, C., 2009. Integrated seismic and petrographic analyses of the sandstone reservoirs of the Tertiary Veracruz Basin, Mexico. *in* C. Bartolini and J. R. Roman Ramos, eds., Petroleum systems in the southern Gulf of Mexico: AAPG Memoir 90, p. 217–235. DOI:10.1306/13191085M903335

Martön, G.L. and Buffler, R.T. 1994. Jurassic reconstruction of the Gulf of Mexico Basin. International Geology Review, 36, 545–586, https://doi.org/10.1080/00206819409465475

Mayall, M., Lonergan, L., Bowman, A., James, S., Mills, K., Primmer, T., Pope, D., Rogers, L. and Skeene, R., 2010. The response of turbidite slope channels to growth-induced seabed topography. *AAPG Bulletin*, *94*(7), pp.1011–1030. https://doi.org/10.1306/01051009117

McDougall, I., and Harrison, T., 1999, Geochronology and Thermochronology by the 40Ar/39Ar Method.: Oxford University Press, New York, v. 2nd ed.

Mendoza-Rosales, C.C., Centeno-García, E., Silva-Romo, G., Campos-Madrigal, E., and Bernal, J.P., 2010. Barremian rift-related turbidites and alkaline volcanism in southern Mexico and their role in the opening of the Gulf of Mexico: Earth and Planetary Science Letters, 295, 419–434, https://doi.org/10.1016/j.epsl.2010.04.020.

Meneses-Rocha, J. J., 2001, Tectonic evolution of the Ixtapa graben, an example of a strike-slip basin in southeastern Mexico: Implications for regional petroleum systems, in C. Bartolini, R. T. Buffler, and A. Cantú- Chapa, eds., The western Gulf of Mexico Basin: Tectonics, sedimentary basins, and petroleum systems: AAPG Memoir 75, p. 183–216.

Michaud, F. and Fourcade, E.R.I.C., 1989. Stratigraphie et paléogéographie du Jurassique et du Crétacé du Chiapas (Sud-Est du Mexique). Bulletin de la Société géologique de France, (3), pp.639-650. https://doi.org/10.2113/gssgfbull.V.3.639

Molina-Garza, R.S., Van der Voo, R. and Urrutia-Fucugauchi, J., 1992. Paleomagnetism of the Chiapas Massif, southern Mexico: Evidence for rotation of the Maya Block and implications for the opening of the Gulf of Mexico. Geological Society of America Bulletin, 104(9), pp.1156–1168.

Molina-Garza, R.S., Geissman, J.W., Wawrzyniec, T.F., Pena Alonso, T.A., Iriondo, A., Weber, B. and Aranda-Gómez, J., 2015. Geology of the coastal Chiapas (Mexico) Miocene plutons and the Tonalá shear zone: Syntectonic emplacement and rapid exhumation during sinistral transpression. *Lithosphere*, *7*(3), pp.257–274.

Molina-Garza, R.S., van Hinsbergen, D.J., Boschman, L.M., Rogers, R.D. and Ganerød, M., 2019a. Large-scale rotations of the Chortis Block (Honduras) at the southern termination of the Laramide flat slab. *Tectonophysics*, *760*, pp.36-57.

Molina-Garza, R.S., Pindell, J. and Villagómez, D. 2019b. Discussion of Ortega-Flores et al. (2018) ‘Provenance analysis of Oligocene sandstone from Cerro Pelón area, southern Gulf of Mexico’. International Geology Review, 62, 415–420, https://doi.org/10.1080/00206814.2019.1616620

Molina-Garza, R.S., Pindell, J., Coombs, H., Weber, B., Peña Alonso, T. 2020a. Definition of tectonic elements in Tehuantepec, southeast Mexico: An integrated geophysical, geochronological, and stratigraphic perspective. *Southern and Central Mexico: Basement Framework, Tectonic Evolution, and Provenance of Mesozoic–Cenozoic Basins. Geological Society of America, Special Papers*, *546.*

Molina-Garza, R.S., Pindell, J. and Cortés, P.C.M., 2020b. Slab flattening and tractional coupling drove Neogene clockwise rotation of Chiapas Massif, Mexico: Paleomagnetism of the Eocene El Bosque Formation. *Journal of South American Earth Sciences*, *104*, p.102932.

Molina Garza, R.S., Geissman, J.W., Peña Alonso, T., Aranda Gómez, J. and Wawrzyniec, T., 2021. Structural Setting, Paleomagnetism, and Magnetic Fabric of Miocene Plutons in a Transpressional Sinistral Shear Zone, Tonalá, Chiapas, Mexico: Evidence of Shortening During Magma Emplacement. *Tectonics*, *40*(2), p.e2020TC006559. https://doi.org/10.1029/2020TC006559

Mora, J.C., Layer, P.W. and Jaimes-Viera, M.D.C., 2012. New 40Ar/39Ar ages from the central part of the Chiapanecan Volcanic Arc, Chiapas, México. *Geofísica internacional*, *51*(1), pp.39–49.

Morán-Zenteno, D.J., Corona-Chávez, P., and Tolson, G., 1996, Uplift and subduction erosion in southwestern Mexico since the Oligocene: Pluton geobarometry constraints: Earth and Planetary Science Letters, v. 141, p. 51–65, https://doi.org/10.1016/0012-821X(96)00067-2.

Morán-Zenteno, D.J., Cerca, M. and Keppie, J.D., 2005. La evolución tectónica y magmática cenozoica del suroeste de México: avances y problemas de interpretación. *Boletín de la Sociedad Geológica Mexicana*, *57*(3), pp.319–341. https://doi.org/10.18268/bsgm2005v57n3a4

Morán-Zenteno, D.J., Martiny, B.M., Solari, L., Mori, L., Luna-González, L. and González-Torres, E.A., 2018. Cenozoic magmatism of the Sierra Madre del Sur and tectonic truncation of the Pacific margin of southern Mexico. *Earth-Science Reviews*, *183*, pp.85-114. https://doi.org/10.1016/j.earscirev.2017.01.010

Mousavi, M.A. and Bryant, S.L., 2013. Geometric models of porosity reduction by ductile grain compaction and cementation. *AAPG Bulletin*, *97*(12), pp.2129–2148. https://doi.org/10.1306/05171311165

Nguyen, L.C. and Mann, P. 2016. Gravity and magnetic constraints on the Jurassic opening of the oceanic Gulf of Mexico and the location and tectonic history of the Western Main transform fault along the eastern continental margin of Mexico. Interpretation, 4, SC23–SC33, https://doi.org/10.1190/INT-2015-0110.1

Nieto-Samaniego, A.F., Alaniz-Álvarez, S.A., Silva-Romo, G., Eguiza-Castro, M.H. and Mendoza-Rosales, C.C., 2006. Latest Cretaceous to Miocene deformation events in the eastern Sierra Madre del Sur, Mexico, inferred from the geometry and age of major structures. *Geological Society of America Bulletin*, *118*(1-2), pp.238–252.

Ortega-Flores, B., Martini, M., Solari, L., Colás, V., Guerrero-Moreno, S., Centeno-Garcia, E., Silva-Romo, G., Grajales-Nishimura, M. 2018. Provenance analysis of Oligocene sandstone from the Cerro

Pelón area, southern Gulf of Mexico. International Geology Review, 61, 915–935, https://doi.org/10.1080/00206814.2018.1476922

Ortega-Flores, B., Martini, M., Solari, L., Colás, V., Guerrero-Moreno, S., Centeno-Garcia, E., Silva-Romo, G., Grajales-Nishimura, M. 2020. Reply to Molina- Garza et al. (2019) 'Discussion of: Ortega-Flores et al. (2018) "Provenance analysis of Oligocene sandstone from the Cerro Pelón area, southern Gulf of Mexico"'. International Geology Review, 62, 421–427, https://doi.org/10.1080/00206814.2019.1616621

Ortuño-Arzate, S., Ferket, H., Cacas, M.-C., Swennen, R., and Roure, F. 2003. Late Cretaceous carbonate reservoirs in the Cordoba Platform and Veracruz Basin (eastern Mexico). *In* C. Bartolini, R. T. Buffler, and J. Blickwede, eds., *The Circum-Gulf of Mexico and the Caribbean: Hydrocarbon habitats, basin formation, and plate tectonics*, AAPG Memoir 79, p. 476–514. https://doi.org/10.1306/M79877C22

Pemex. 2013a. Provincia Petrolera Veracruz. Petróleos Mexicanos (Pemex). Exploración y Producción Subdirección de Exploración Versión 2.0, 2013. 38p.

Pemex. 2013b. Provincia Petrolera Cinturón Plegado de Chiapas. Petróleos Mexicanos (Pemex). Exploración y Producción Subdirección de Exploración Versión 2.0, 2013. 33p.

Pemex. 2013c. Provincia Petrolera Sureste (Salina del Istmo, Reforma-Akal y Macuspana). Petróleos Mexicanos (Pemex). Exploración y Producción Subdirección de Exploración Versión 2.0, 2013. 57p.

Peña-Alonso, T.A., Estrada-Carmona, J., Molina-Garza, R.S., Solari, L., Levresse, G., and Latorre, C., 2017, Lateral spreading of the middle to lower crust inferred from Paleocene migmatites in the Xolapa Complex (Puerto Escondido, Mexico): Gravitational collapse of a Laramide orogen?. Tectonophysics, v. 706–707, p. 143–163, https://doi.org/10.1016/j.tecto.2017.04.010.

Peña-Alonso, T.A., Molina-Garza, R.S., Villalobos-Escobar, G., Estrada-Carmona, J., Levresse, G. and Solari, L., 2018. The opening and closure of the Jurassic-Cretaceous Xolapa basin, southern Mexico. *Journal of South American Earth Sciences*, *88*, pp.599–620.

Peña-Alonso, T.A., Latorre, C., Estrada-Carmona, J., Molina-Garza, R.S., Solari, L. 2021. Multi-stage, Upper Eocene-Oligocene anatexis in the Xolapa metamorphic belt (Puerto Escondido, Mexico): Dynamics of the Xolapa Complex as the decoupled lower crust of the Chortís Block upper crust during its tectonic migration. Tectonophysics. https://doi.org/10.1016/j.tecto.2021.229004

Pérez-Gutiérrez, R., Solari, L.A., Gómez-Tuena, A., and Valencia, V.A., 2009, The Cuicateco terrane: Upper Cretaceous oceanic basin with subduction influence in southern Mexico? New structural, geochemical and geochronological data: Revista Mexicana de Ciencias Geológicas, v. 26, p. 222–242.

Pindell, J.L. 1985. Alleghanian reconstruction and the subsequent evolution of the Gulf of Mexico, Bahamas, and Proto-Caribbean Sea. Tectonics, 4, 1–39, https://doi.org/10.1029/TC004i001p00001

Pindell, J.L. and Kennan, L. 2001. Kinematic evolution of the Gulf of Mexico and Caribbean. In: Fillon, R.H., Rosen, N.C. et al. (eds) Petroleum Systems of Deep-Water Basins: Global and Gulf of Mexico Experience. Transactions of the 21st Annual GCSSEPM Foundation Bob F. Perkins Research Conference. Gulf Coast Section SEPM, Houston, TX, 193–220.

Pindell, J.L. and Kennan, L. 2009. Tectonic evolution of the Gulf of Mexico, Caribbean and northern South America in the mantle reference frame: an update. Geological Society, London, Special Publications, 328, 1–55, https://doi.org/10.1144/SP328.1.

Pindell, J.L. and Miranda, E. 2011. Linked kinematic histories of the Macuspana, Akal-Reforma, Comalcalco, and deepwater Campeche Basin tectonic elements, southern Gulf of Mexico. Gulf Coast Association of Geological Societies Transactions, 61, 353–361.

Pindell, J., Maresch, W.V., Martens, U. and Stanek, K., 2011. The Greater Antillean Arc: Early Cretaceous origin and proposed relationship to Central American subduction mélanges: implications for models of Caribbean evolution. *International Geology Review*, *54*(2), pp.131-143. https://doi.org/10.1080/00206814.2010.510008

Pindell, J., Miranda E., Cerón, A., and Hernandez, L. 2016. Aeromagnetic Map Constrains Jurassic-Early Cretaceous Synrift, Breakup, and Rotational Seafloor Spreading History in the Gulf of Mexico. *In* Lowery, C.M., Snedden, J.W., and Rosen, N. (eds.). *Mesozoic of the Gulf Rim and Beyond: New progress in Science and Exploration of the Gulf of Mexico Basin. Transactions 35th Annual Gulf Coast Section of the Society of Economic and Paleontological Mineralogists Foundation*, Perkins-Rosen Research Conference, Houston, Texas, p. 123–153.

Pindell, J., Villagómez, D., Molina-Garza, R., Graham, R., Weber, B. 2020a. A revised synthesis of the rift and drift history of the Gulf of Mexico and surrounding regions in the light of improved age dating of the Middle Jurassic salt. In: Davidson I., Pindell J. (eds). The Geology and Hydrocarbon Potential of Mexico and the Northern Caribbean. Geological Society of London Special Publication.

Pindell, J., Molina-Garza, R., Villagómez, D., Martens, U., Graham, R., Stockli, D., Weber, B., Sierra-Rojas, M.I. 2020b. Provenance of the Miocene Nanchital Conglomerate, western Chiapas Foldbelt, Mexico: implications for reservoir sands in the Sureste Basin, greater Campeche Province. In: Davidson I., Pindell J. (eds). The Geology and Hydrocarbon Potential of Mexico and the Northern Caribbean. Geological Society of London Special Publication.

Pindell, J., Martens, U., Molina Garza, R., Villagomez, D., Beltrán, A., Stockli, D., Wildman, M., Solari, L., 2022 (submitted). Late Cretaceous–Paleogene depositional evolution of Chiapas, Mexico: a foreland controlled by collision of Greater Antilles Arc and the subsequent relative migration of the Chortís Block.

Prost, G., and Aranda, M. 2001, Tectonics and hydrocarbon systems of the Veracruz Basin, Mexico, *in* C. Bartolini, R. T. Buffler, and A. Cantú-Chapa, eds., The western Gulf of Mexico Basin: Tectonics, sedimentary basins, and petroleum systems: AAPG Memoir 75, p. 271–291. https://shar.es/aWwoHn

Quezada-Muñetón, J.Q., 1987. El Cretacico Medio–Superior, y el limite Cretacico Superior–Terciario Inferior en la Sierra de Chiapas. *Boletin de la Asociación Mexicana de Geólogos Petroleros (AMGP), vol. 39*, pp.3–98. https://shar.es/aWYHmk

Ratschbacher, L., Franz, L., Min, M., Bachmann, R., Martens, U., Stanek, K., Stübner, K., Nelson, B.K., Herrmann, U., Weber, B., López-Martínez, M., Jonckheere, R., Sperner, B., Tichomirowa, M., McWilliams, M.O., Gordon, M., and Meschede, M. 2009. The North American-Caribbean plate boundary in Mexico-Guatemala-Honduras. *In* James, K., Lorente, M.A., and Pindell, J., eds., Origin and evolution of the Caribbean Region: Geological Society of London, Special Publication, **328**, p. 219–293. https://doi.org/10.1144/SP328.11

Reed, J.C., Wheeler, J.O., Tucholke, B.E. and Compilers. 2004. Geological Map of North America: Decade of North American Geology. Continental Scale Map 001. Geological Society of America, Boulder, CO. Scale 1:5 000 000, 1 sheet.

Riller, U., Ratschbacher, L. and Frisch, W., 1992. Left-lateral transtension along the Tierra Colorada deformation zone, northern margin of the Xolapa magmatic arc of southern Mexico. *Journal of South American Earth Sciences*, *5*(3–4), pp.237–249.

Ríos-López, J. J., and A. Cantu-Chapa, 2009, Stratigraphy and sedimentology of Middle Eocene Kumaza Calcarenites Member in the Ku, Maloob, and Zaap oil fields, offshore Campeche, Mexico, in C. Bartolini and J. R. Roman Ramos, eds., Petroleum systems in the southern Gulf of Mexico: AAPG Memoir 90, p. 257–277. Doi:10.1306/13191087M903336

Romito, S. and Mann, P. 2020. Tectonic terranes underlying the present-day Caribbean plate: their tectonic origin, sedimentary thickness, subsidence histories and regional controls on hydrocarbon resources. Geological Society, London, Special Publications, 504, 343–377. https://doi.org/10.1144/SP504-2019-221

Rosenfeld, J., and J. Pindell, 2003, Early Paleogene isolation of the Gulf of Mexico from the world's oceans? Implications for hydrocarbon exploration and eustasy, in C. Bartolini, R. T. Buffler, and J. Blickwede, eds., The Circum-Gulf of Mexico and the Caribbean: Hydrocarbon habitats, basin formation, and plate tectonics: AAPG Memoir 79, p. 89–103.

Ruiz-Arriaga, D., 2018. *Historia de deformación de la margen Oriental de la Plataforma Morelos-Guerrero.* Msc Thesis. Universidad Nacional Autónoma de México. 132 pp.

Sanchez-Barreda, L.A., 1981. *Geologic evolution of the continental margin of the Gulf of Tehuantepec in Southwestern Mexico*. Doctoral dissertation, The University of Texas at Austin. 272 pp.

Sánchez Hernández, H., 2013. Stratigraphic characterization and evolution of a Mid-tertiary age deep water system, Holok area, SW Gulf of Mexico. Doctoral dissertation, University of Aberdeen, 358 pp.

Santillán-Piña, N. and Aguayo-Camargo, J.E. 2011. Facies sedimentarias turbiditicas del Terciario Inferior en la cuenca de Chicontepec, centro-oriente de México. Ingeniería, Investigación y Tecnología, 12(3), pp.337–352.

Shann, M.V., 2021. The Sureste Basin of Mexico: its framework, future oil exploration opportunities and key challenges ahead. *Geological Society, London, Special Publications*, *504*(1), pp.119–146. https://doi.org/10.1144/SP504-2019-214

Shann, M.V., Vazquez-Reyes, K., Ali, H.M. and Horbury, A.D. 2020. The Sureste Super Basin of southern Mexico. *AAPG Bulletin*, *104*(12), pp.2643-2700. https://doi.org/10.1306/09172020081

Shoemaker, S., Ducea, M., Reiners, P.W., Garver, J.I., and Campa, M.F. 2002. Cenozoic plate tectonic history of southwestern Mexico: Constraints from low temperature thermochronology: Geotemas, v. 4, p. 137–138.

Sickmann, Z.T. and Snedden, J.W. 2021. Neogene to recent evolution of the Southern Gulf of Mexico basin: Tectonic controls on deep- water sediment dispersal systems. *Basin Research*, *33*(2), pp.1240–-1265. https://doi.org/10.1111/bre.12512

Sierra-Rojas, M.I., Molina-Garza, R.S. and Lawton, T.F., 2016. The Lower Cretaceous Atzompa Formation in south-central Mexico: record of evolution from extensional backarc basin margin to carbonate platform. *Journal of Sedimentary Research*, *86*(6), pp.712–733.

Sierra-Rojas, M.I., Lawton, T.F., Martens, U., von Quadt, A., Beltrán-Triviño, A., Coombs, H., and Stockli, D.F. 2020. Early Cretaceous to Paleogene sandstone provenance and sediment-dispersal systems of the Cuicateco terrane, Mexico. *In* Southern and Central Mexico: Basement Framework, Tectonic Evolution, and Provenance of Mesozoic–Cenozoic Basins, Geological Society of America, doi:10.1130/2020.2546(10).

Simon-Labric, T., Brocard, G.Y., Teyssier, C., Beek, P.A., Fellin, M.G., Reiners, P.W., and Authemayou, C., 2013, Preservation of contrasting geothermal gradients across the Caribbean–North America plate boundary (Motagua fault, Guatemala): Tectonics, v. 32, no. 4, p. 993–1010, https://doi.org/10.1002/tect.20060.

Snedden, J.W. and Galloway, W.E., 2019. *The Gulf of Mexico sedimentary basin: Depositional evolution and petroleum applications*. Cambridge University Press. 351 p.

Snedden, J.W., Stockli, D.F., and Pasley, J. 2021. Reconstructing the Zama (Mexico) Discovery Source to Sink Story, Part II. Implications for and predictions within the depositional sink. Transactions of the GeoGulf2021 Conference, October 27–29, 2021. Austin, TX.

Solari, L.A., Torres de León, R., Hernández-Pineda, G., Solé, J., Solís-Pichardo, G., and Hernández-Treviño, T., 2007, Tectonic significance of Cretaceous–Tertiary magmatic and structural evolution of the northern margin of the Xolapa Complex: Tierra Colorada area, southern Mexico: Geological Society of America Bulletin, v. 119, p. 1265–1279, https://doi.org/10.1130/B26023.1.

Solari, L.A., García-Casco, A., Martens, U., Lee, J.K. and Ortega-Rivera, A., 2013. Late Cretaceous subduction of the continental basement of the Maya block (Rabinal Granite, central Guatemala): Tectonic implications for the geodynamic evolution of Central America. *Bulletin*, *125*(3-4), pp.625–639.

Sømme, T.O., Helland- Hansen, W., Martinsen, O.J. and Thurmond, J.B. 2009. Relationships between morphological and sedimentological parameters in source- to- sink systems: a basis for predicting semi- quantitative characteristics in subsurface systems. Basin Research, 21(4), pp. 361–387.

Sosa-Patrón, A. A., J. G. Cardenas Lopez, C. Cardenas Lara, O. Pinto Gomez, M. E. Guzzy Arredondo, M. E. Monroy Audelo, and R. Castellanos Calvo, 2009, Integrated geological interpretation and impact on the definition of Neogene plays in the Isthmus Saline Basin, Mexico, *in*C. Bartolini, and J. R. Roman Ramos, eds., Petroleum systems in the southern Gulf of Mexico: AAPG Memoir 90, p. 29–47. DOI:10.1306/13191076M903330

Stockli, D.F., Snedden, J., and Pasley, J. - Reconstructing the Zama (Mexico) Discovery Source to Sink Story, Part I. Detrital Zircon U-Pb Provenance Analysis and Implications for Sediment Source Dynamics. Transactions of the GeoGulf2021 Conference, October 27–29, 2021. Austin, TX.

Talavera-Mendoza, O., Ruiz, J., Corona-Chavez, P., Gehrels, G.E., Sarmiento-Villagrana, A., García-Díaz, J.L. and Salgado-Souto, S.A., 2013. Origin and provenance of basement metasedimentary rocks from the Xolapa Complex: New constraints on the Chortis–southern Mexico connection. *Earth and Planetary Science Letters*, *369*, pp.188–199.

Tolson, G., 2005. La falla Chacalapa en el sur de Oaxaca. *Boletín de la Sociedad Geológica Mexicana*, *57*(1), pp.111–122.

Vega-Granillo, R., Talavera-Mendoza, O., Meza-Figueroa, D., Ruiz, J., Gehrels, G.E., López-Martínez, M. and de la Cruz-Vargas, J.C., 2007. Pressure-temperature-time evolution of Paleozoic high-pressure rocks of the Acatlán Complex (southern Mexico): implications for the evolution of the Iapetus and Rheic Oceans. *Geological Society of America Bulletin*, *119*(9-10), pp.1249–1264.

Villagómez, D. 2014. The Northern Cuicateco Terrane from a thermochronological perspective and its implications on the pre-, syn- and post-Laramide deformation. Tectonic Analysis Ltd, West Sussex, UK, Cordillera Program Phase 1 technical report, 20. https://doi.org/10.13140/RG.2.2.22814.43840

Villagómez, D., Pindell, J.L. and Spikings, R. 2019. Thermal history of the crystalline basement from the western and southern Gulf of Mexico: Implications for rifting and later events. Geological Society of America Special Papers, 546, 1–18, https://doi.org/10.1130/2019.2546(16)

Villagómez, D. and Pindell, J. 2020a. Cooling and uplift history of the Chiapas Massif and its influence on sedimentation and deformation in the adjacent Sierra de Chiapas Basin. In: Martens, U. and Molina-Garza, R.S. (eds) Southern and Central Mexico: Basement Framework, Tectonic Evolution, and Provenance of Mesozoic–Cenozoic Basins. Geological Society of America, Special Papers, 546, https://doi.org/10.1130/2020.2546(17)

Villagómez, D. and Pindell, J. 2020b. Thermochronology of the southern Mexican margin (Xolapa belt), Acapulco to Puerto Angel: Crustal dynamics of a trench–trench–transform triple junction. In: Martens, U. and Molina-Garza, R.S. (eds) Southern and Central Mexico: Basement Framework, Tectonic Evolution, and Provenance of Mesozoic–Cenozoic Basins. Geological Society of America, Special Papers, 546, https://doi.org/10.1130/2020.2546(14)

Walsh, J.P., Wiberg, P.L., Aalto, R., Nittrouer, C.A. and Kuehl, S.A. 2016. Source-to-sink research: economy of the Earth's surface and its strata. *Earth Science Reviews*, *153*, pp.1–6.

Weber, B. and Hecht, L., 2003. Petrology and geochemistry of metaigneous rocks from a Grenvillian basement fragment in the Maya block: the Guichicovi complex, Oaxaca, southern Mexico. *Precambrian Research*, *124*(1), pp.41–67. https://doi.org/10.1016/S0301-9268(03)00078-0

Weber, B., Iriondo, A., Premo, W.R., Hecht, L. and Schaaf, P., 2007. New insights into the history and origin of the southern Maya block, SE México: U–Pb–SHRIMP zircon geochronology from metamorphic rocks of the Chiapas massif. *International Journal of Earth Sciences*, *96*(2), pp.253–269. https://doi.org/10.1007/s00531-006-0093-7

Weber, B., Scherer, E.E., Schulze, C., Valencia, V.A., Montecinos, P., Mezger, K. and Ruiz, J. 2010. U–Pb and Lu–Hf isotope systematics of lower crust from central-southern Mexico–Geodynamic significance of Oaxaquia in a Rodinia Realm. Precambrian Research, 182, 149–162, https://doi.org/10.1016/j.precamres.2010.07.007

Winker, C.D. and Buffler, R.T., 1988. Paleogeographic evolution of early deep-water Gulf of Mexico and margins, Jurassic to Middle Cretaceous (Comanchean). *AAPG bulletin*, *72*(3), pp.318-346. https://doi.org/10.1306/703C8C22-1707-11D7-8645000102C1865D

Winter, R., 2018, Coarse-grained deep water, slope, and basin-floor systems: Influence of tectonic processes on internal and external architecture: University of Texas PhD Dissertation, 163 pp.

Witt, C., Brichau, S. and Carter, A., 2012. New constraints on the origin of the Sierra Madre de Chiapas (south Mexico) from sediment provenance and apatite thermochronometry. *Tectonics*, *31*(6). https://doi.org/10.1029/2012TC003141

Wolfe, M.R. and Stockli, D.F., 2010. Zircon (U–Th)/He thermochronometry in the KTB drill hole, Germany, and its implications for bulk He diffusion kinetics in zircon. *Earth and Planetary Science Letters*, *295*(1-2), pp.69–82.

Worzel, J. L., Bryant, W., Beall, A. O. R. Jr, Capo, R., Dickinson, K., Foreman, H. P., Laury, R., McNeely, B. W., & Smith, L. A., 1973, Initial reports of the deep sea drilling project v. 10. Deep Sea Drilling Project Reports and Publications, p.1–748.

Zepeda-Martínez, M., Martini, M., Solari, L.A. and Mendoza-Rosales, C.C., 2021. Reconstructing the tectono-sedimentary evolution of the Early–Middle Jurassic Tlaxiaco Basin in southern Mexico: New insights into the crustal attenuation history of southern North America during Pangea breakup. *Geosphere* 17 (4): 1294–1317.

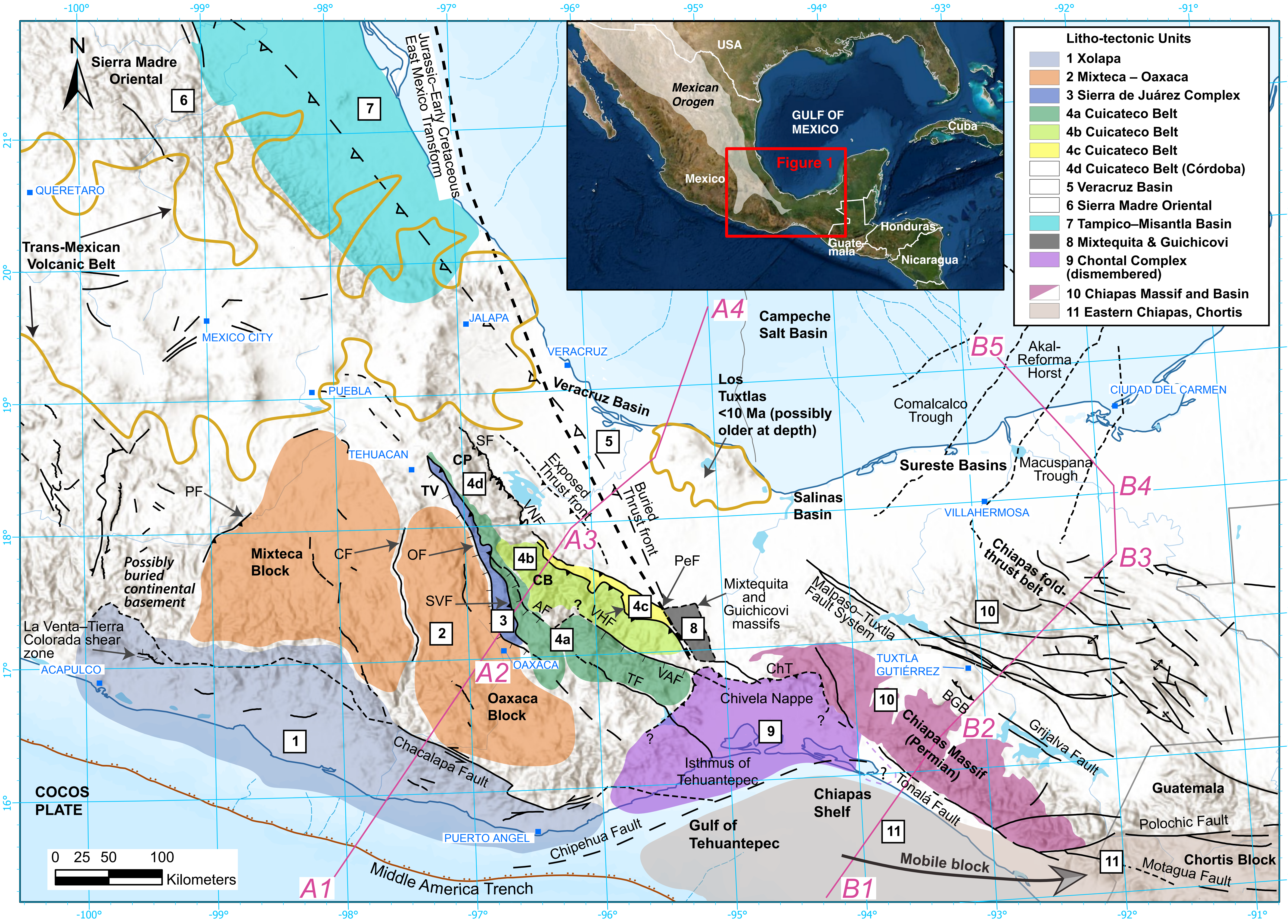
-100°
-99°
-98°
-97°
-96°
-95°
-94°
-93°
-92°
-91°
21°
20°
19°
18°
17°
16°
15°
N
Sierra Madre Oriental
6
7
Jurassic–Early Cretaceous East Mexico Transform
QUERETARO
Trans-Mexican Volcanic Belt
MEXICO CITY
JALAPA
VERACRUZ
PUEBLA
Veracruz Basin
5
TEHUACAN
SF
CP
TV
4d
PF
Exposed Thrust front
Buried Thrust front
VNF
Mixteca Block
CF
OF
4b
CB
Possibly buried continental basement
SVF
AF
?
VHF
4c
PeF
8
Mixtequita and Guichicovi massifs
3
2
4a
La Venta–Tierra Colorada shear zone
ACAPULCO
OAXACA
A1
A2
A3
A4
TF
VAF
Oaxaca Block
1
Chacalapa Fault
COCOS PLATE
PUERTO ANGEL
Chipehua Fault
Middle America Trench
0 25 50 100 Kilometers
USA
Mexican Orogen
GULF OF MEXICO
Cuba
Mexico
Figure 1
Honduras
Guatemala
Nicaragua
Litho-tectonic Units
1 Xolapa
2 Mixteca – Oaxaca
3 Sierra de Juárez Complex
4a Cuicateco Belt
4b Cuicateco Belt
4c Cuicateco Belt
4d Cuicateco Belt (Córdoba)
5 Veracruz Basin
6 Sierra Madre Oriental
7 Tampico–Misantla Basin
8 Mixtequita & Guichicovi
9 Chontal Complex (dismembered)
10 Chiapas Massif and Basin
11 Eastern Chiapas, Chortis
Campeche Salt Basin
Los Tuxtlas <10 Ma (possibly older at depth)
B5
Akal-Reforma Horst
CIUDAD DEL CARMEN
Comalcalco Trough
Sureste Basins
Macuspana Trough
Salinas Basin
B4
VILLAHERMOSA
Chiapas fold-thrust belt
B3
10
Malpaso–Tuxtla Fault System
ChT
Chivela Nappe
TUXTLA GUTIÉRREZ
10
9
?
Isthmus of Tehuantepec
BGB
Chiapas Massif (Permian)
B2
Grijalva Fault
Chiapas Shelf
Tonalá Fault
Gulf of Tehuantepec
11
Guatemala
Polochic Fault
Mobile block
11
Chortis Block
Motagua Fault
B1

Figure 1

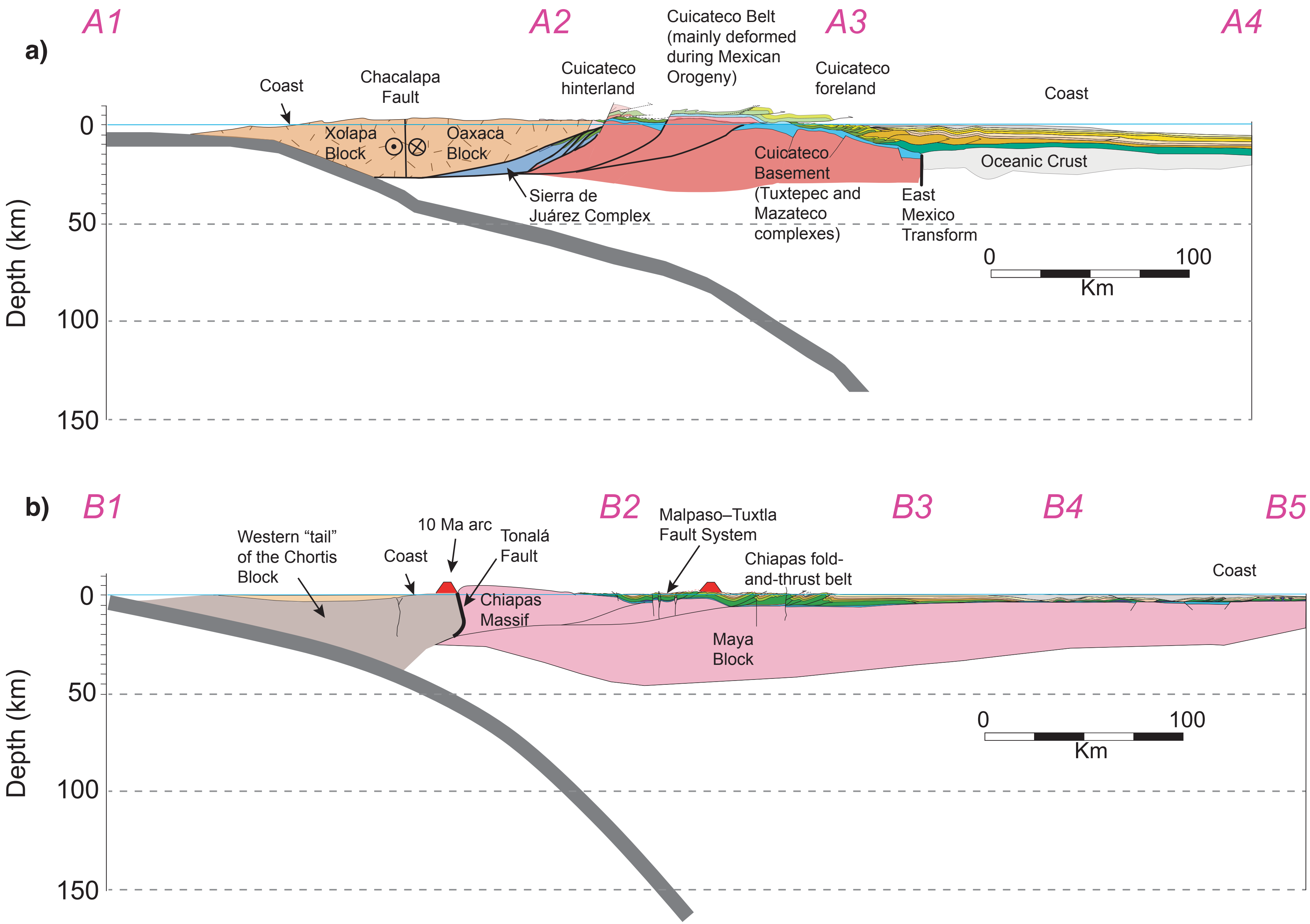
a)
A1
A2
A3
A4
Coast
Chacalapa Fault
Cuicateco hinterland
Cuicateco Belt (mainly deformed during Mexican Orogeny)
Cuicateco foreland
Coast
Xolapa Block
Oaxaca Block
Cuicateco Basement (Tuxtepec and Mazateco complexes)
Oceanic Crust
Sierra de Juárez Complex
East Mexico Transform
Depth (km)
0
50
100
150
0
100
Km
b)
B1
B2
B3
B4
B5
Western "tail" of the Chortis Block
Coast
10 Ma arc
Tonalá Fault
Malpaso–Tuxtla Fault System
Chiapas fold-and-thrust belt
Coast
Chiapas Massif
Maya Block
Depth (km)
0
50
100
150
0
100
Km

Figure 2

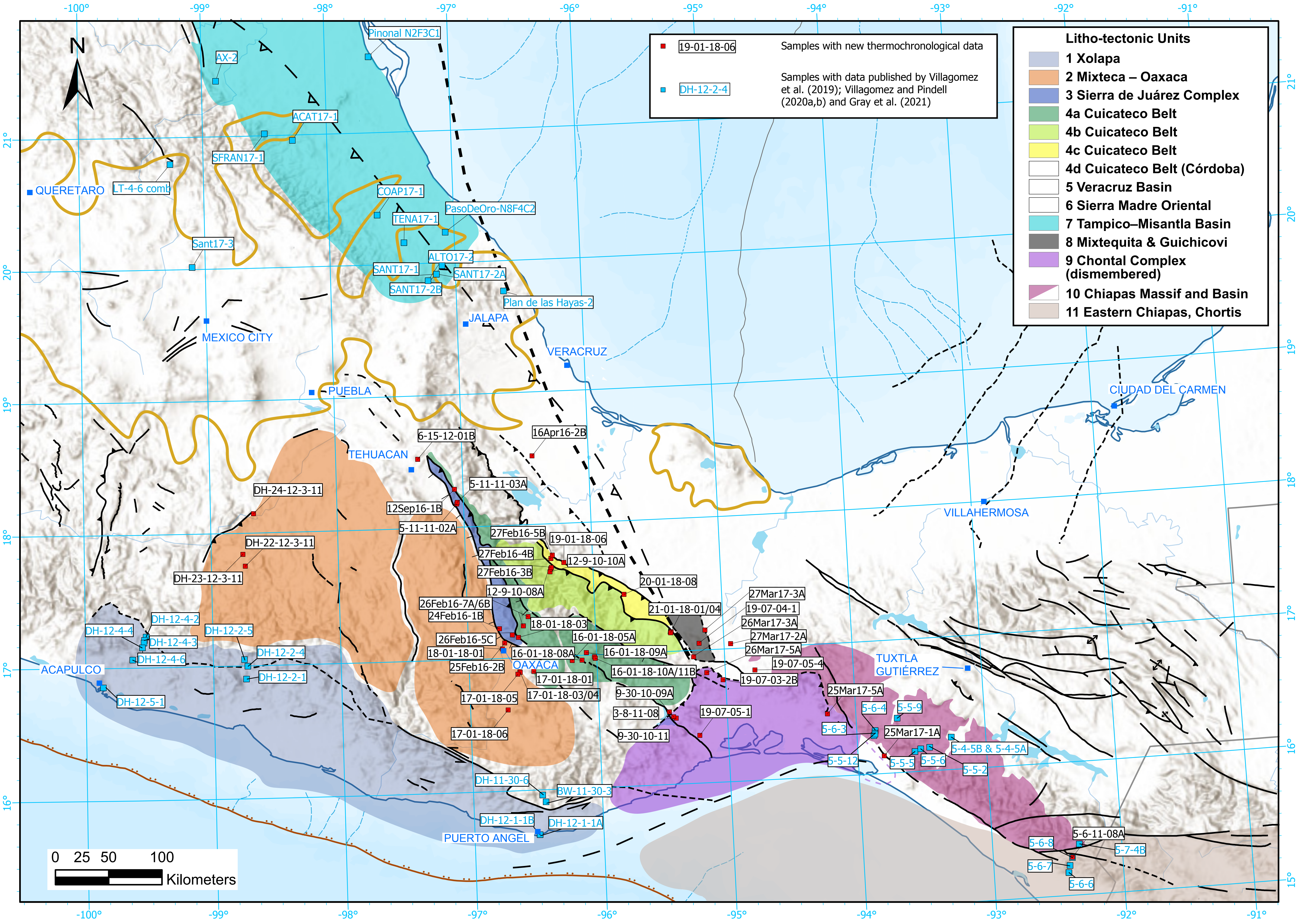
19-01-18-06 Samples with new thermochronological data
DH-12-2-4 Samples with data published by Villagomez et al. (2019); Villagomez and Pindell (2020a,b) and Gray et al. (2021)
Litho-tectonic Units
1 Xolapa
2 Mixteca – Oaxaca
3 Sierra de Juárez Complex
4a Cuicateco Belt
4b Cuicateco Belt
4c Cuicateco Belt
4d Cuicateco Belt (Córdoba)
5 Veracruz Basin
6 Sierra Madre Oriental
7 Tampico–Misantla Basin
8 Mixtequita & Guichicovi
9 Chontal Complex (dismembered)
10 Chiapas Massif and Basin
11 Eastern Chiapas, Chortis
N
0 25 50 100
Kilometers
-100°
-99°
-98°
-97°
-96°
-95°
-94°
-93°
-92°
-91°
21°
20°
19°
18°
17°
16°
15°
QUERETARO
MEXICO CITY
PUEBLA
JALAPA
VERACRUZ
TEHUACAN
OAXACA
ACAPULCO
PUERTO ANGEL
VILLAHERMOSA
CIUDAD DEL CARMEN
TUXTLA GUTIÉRREZ
Pinonal N2F3C1
AX-2
ACAT17-1
SFRAN17-1
LT-4-6 comb
COAP17-1
PasoDeOro-N8F4C2
TENA17-1
Sant17-3
ALTO17-2
SANT17-1
SANT17-2A
SANT17-2B
Plan de las Hayas-2
6-15-12-01B
16Apr16-2B
5-11-11-03A
12Sep16-1B
5-11-11-02A
DH-24-12-3-11
DH-22-12-3-11
DH-23-12-3-11
27Feb16-5B
19-01-18-06
27Feb16-4B
12-9-10-10A
27Feb16-3B
20-01-18-08
12-9-10-08A
26Feb16-7A/6B
24Feb16-1B
18-01-18-03
21-01-18-01/04
27Mar17-3A
19-07-04-1
26Mar17-3A
27Mar17-2A
26Mar17-5A
16-01-18-05A
26Feb16-5C
18-01-18-01
16-01-18-08A
16-01-18-09A
25Feb16-2B
19-07-05-4
16-01-18-10A/11B
17-01-18-01
19-07-03-2B
17-01-18-05
17-01-18-03/04
9-30-10-09A
25Mar17-5A
3-8-11-08
19-07-05-1
17-01-18-06
9-30-10-11
DH-12-4-2
DH-12-4-4
DH-12-4-3
DH-12-2-5
DH-12-4-6
DH-12-2-4
DH-12-2-1
DH-12-5-1
DH-11-30-6
BW-11-30-3
DH-12-1-1B
DH-12-1-1A
5-6-4
5-5-9
5-6-3
25Mar17-1A
5-4-5B & 5-4-5A
5-5-12
5-5-5
5-5-6
5-5-2
5-6-11-08A
5-6-8
5-7-4B
5-6-7
5-6-6

Figure 3

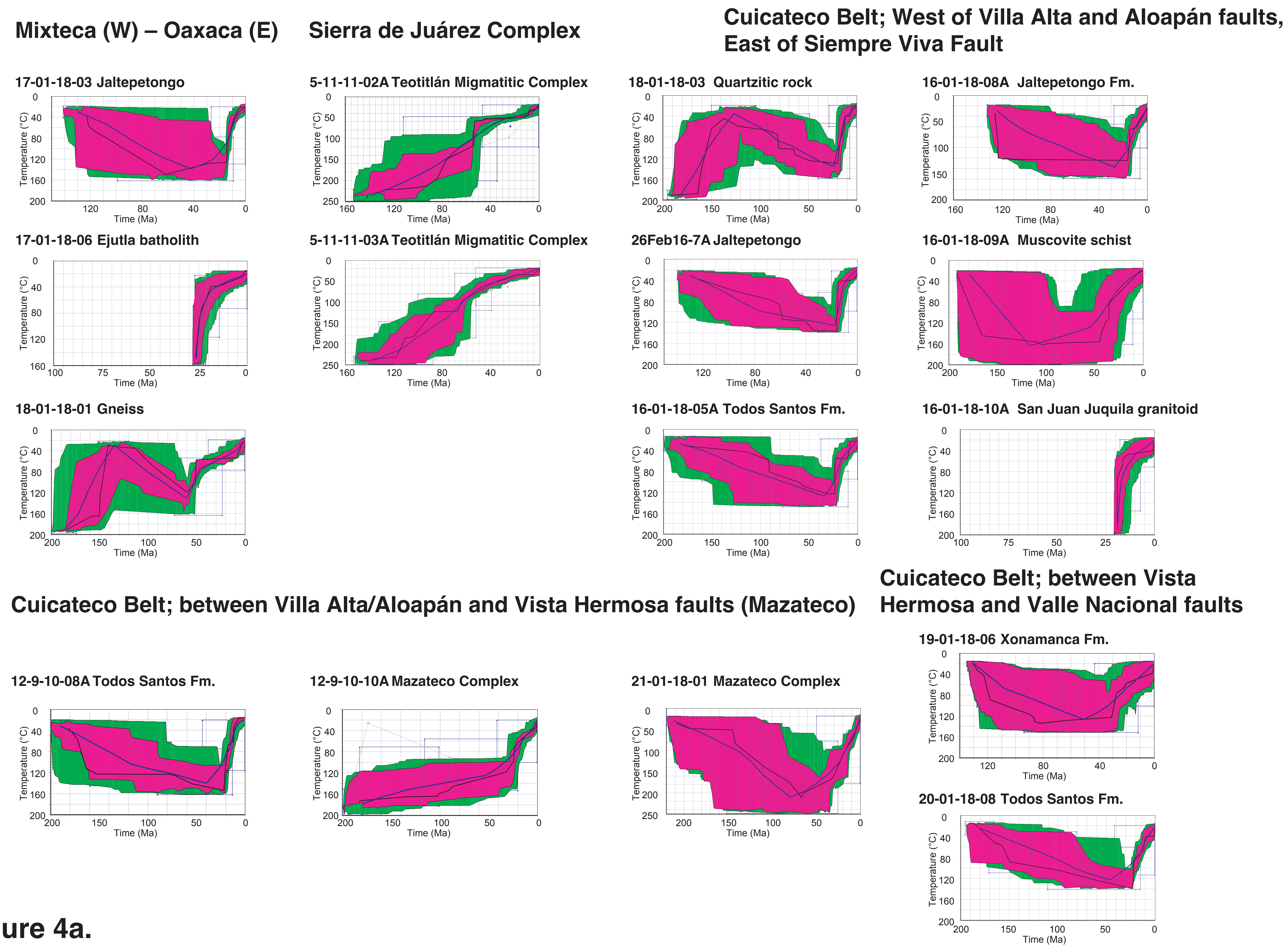
Mixteca (W) – Oaxaca (E)
Sierra de Juárez Complex
Cuicateco Belt; West of Villa Alta and Aloapán faults, East of Siempre Viva Fault
17-01-18-03 Jaltepetongo
5-11-11-02A Teotitlán Migmatitic Complex
18-01-18-03 Quartzitic rock
16-01-18-08A Jaltepetongo Fm.
17-01-18-06 Ejutla batholith
5-11-11-03A Teotitlán Migmatitic Complex
26Feb16-7A Jaltepetongo
16-01-18-09A Muscovite schist
18-01-18-01 Gneiss
16-01-18-05A Todos Santos Fm.
16-01-18-10A San Juan Juquila granitoid
Cuicateco Belt; between Villa Alta/Aloapán and Vista Hermosa faults (Mazateco)
Cuicateco Belt; between Vista Hermosa and Valle Nacional faults
19-01-18-06 Xonamanca Fm.
12-9-10-08A Todos Santos Fm.
12-9-10-10A Mazateco Complex
21-01-18-01 Mazateco Complex
20-01-18-08 Todos Santos Fm.
Temperature (°C)
Time (Ma)
0
40
80
120
160
200
50
100
150
250
0
25
50
75
100

Figure 4a.

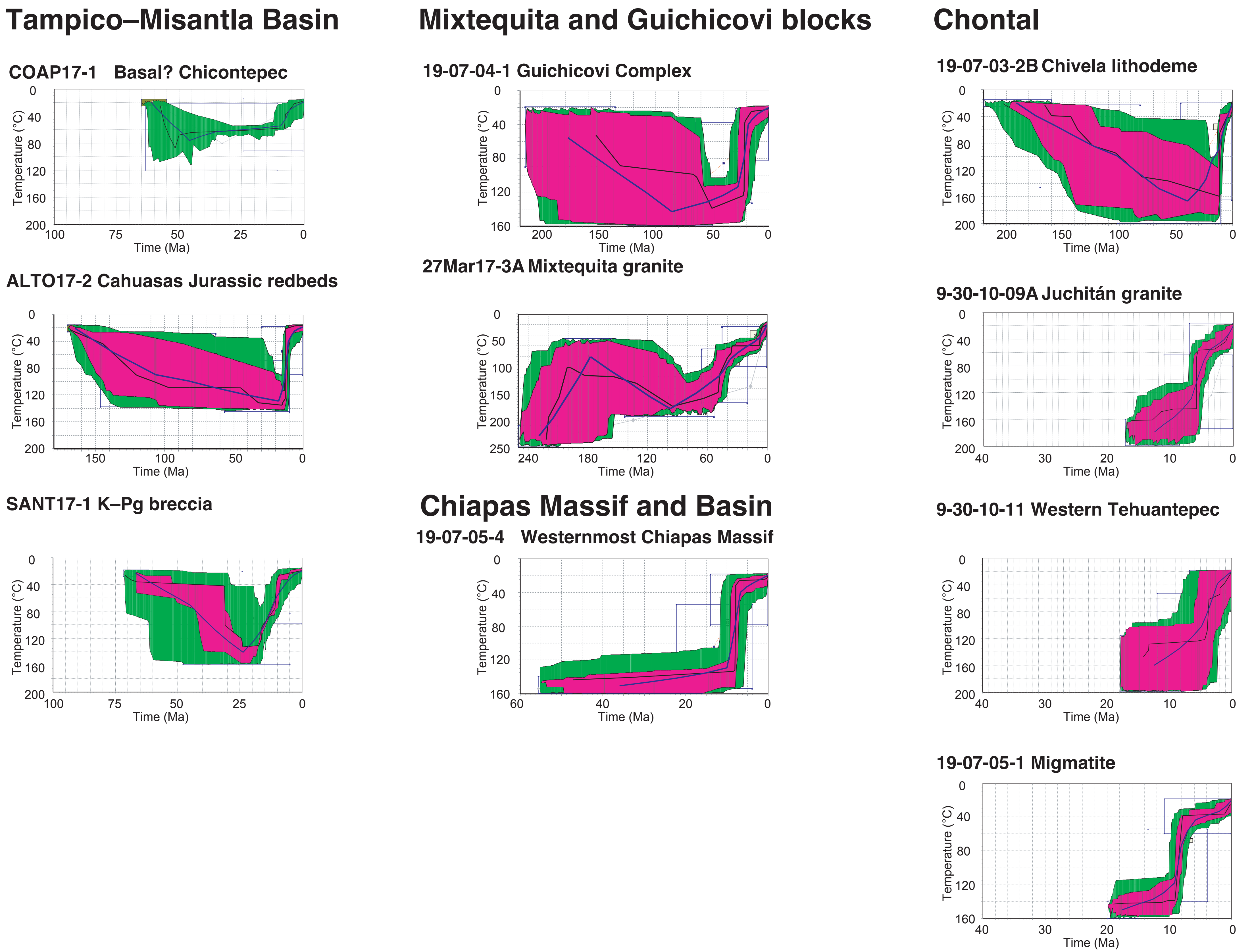
Tampico–Misantla Basin
COAP17-1 Basal? Chicontepec
ALTO17-2 Cahuasas Jurassic redbeds
SANT17-1 K–Pg breccia
Mixtequita and Guichicovi blocks
19-07-04-1 Guichicovi Complex
27Mar17-3A Mixtequita granite
Chiapas Massif and Basin
19-07-05-4 Westernmost Chiapas Massif
Chontal
19-07-03-2B Chivela lithodeme
9-30-10-09A Juchitán granite
9-30-10-11 Western Tehuantepec
19-07-05-1 Migmatite
Temperature (°C)
Time (Ma)
0
40
80
120
160
200
100
75
50
25
0
150
250
240
180
60
30
20
10

Figure 4b.

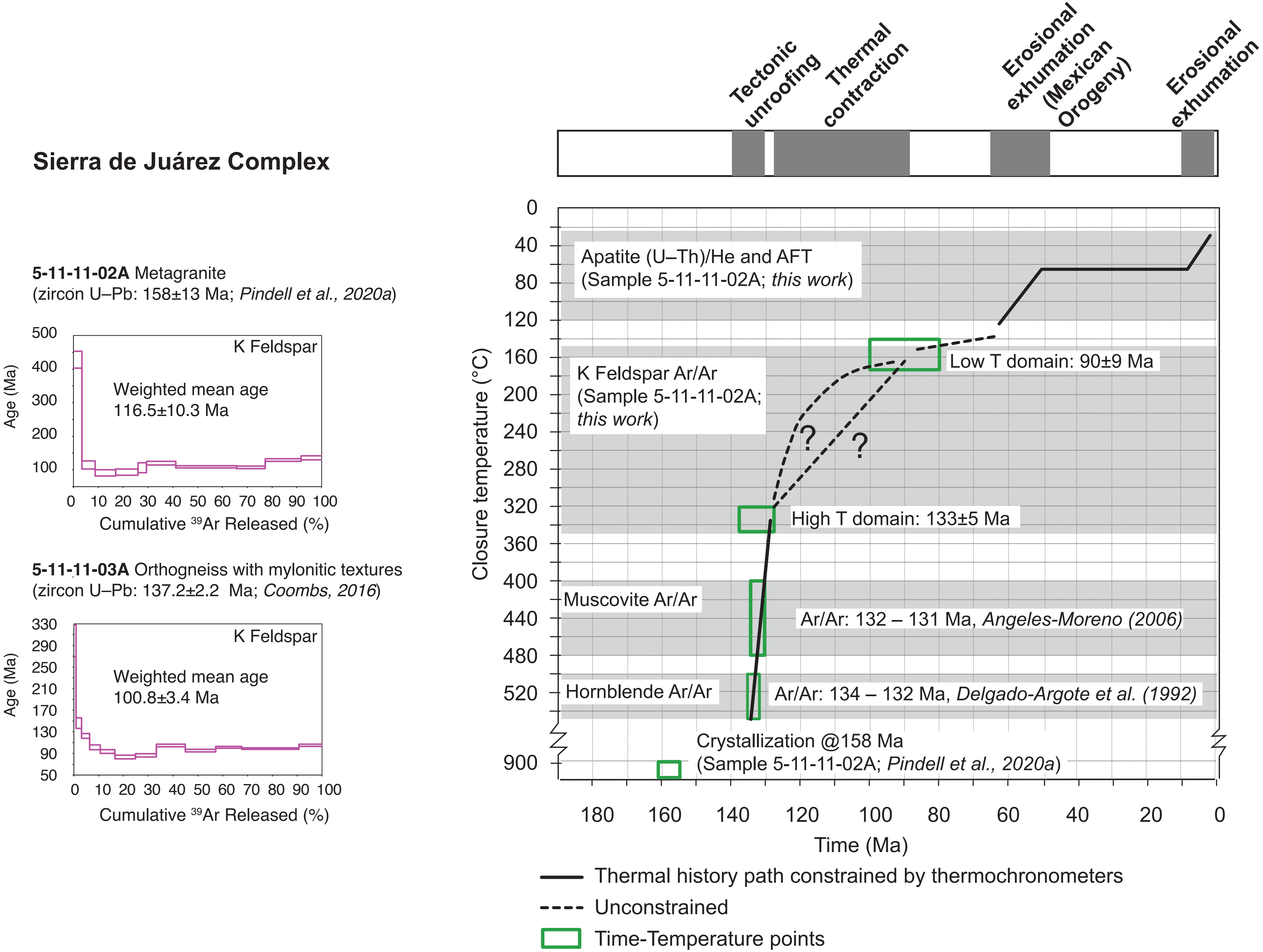
Sierra de Juárez Complex
5-11-11-02A Metagranite
(zircon U–Pb: 158±13 Ma; Pindell et al., 2020a)
K Feldspar
Weighted mean age
116.5±10.3 Ma
Age (Ma)
500
400
300
200
100
0 10 20 30 40 50 60 70 80 90 100
Cumulative 39Ar Released (%)
5-11-11-03A Orthogneiss with mylonitic textures
(zircon U–Pb: 137.2±2.2 Ma; Coombs, 2016)
K Feldspar
Weighted mean age
100.8±3.4 Ma
Age (Ma)
330
290
250
210
170
130
90
50
0 10 20 30 40 50 60 70 80 90 100
Cumulative 39Ar Released (%)
Tectonic unroofing
Thermal contraction
Erosional exhumation (Mexican Orogeny)
Erosional exhumation
Closure temperature (°C)
0
40
80
120
160
200
240
280
320
360
400
440
480
520
900
Apatite (U–Th)/He and AFT
(Sample 5-11-11-02A; this work)
K Feldspar Ar/Ar
(Sample 5-11-11-02A;
this work)
Low T domain: 90±9 Ma
?
?
High T domain: 133±5 Ma
Muscovite Ar/Ar
Ar/Ar: 132 – 131 Ma, Angeles-Moreno (2006)
Hornblende Ar/Ar
Ar/Ar: 134 – 132 Ma, Delgado-Argote et al. (1992)
Crystallization @158 Ma
(Sample 5-11-11-02A; Pindell et al., 2020a)
180
160
140
120
100
80
60
40
20
0
Time (Ma)
Thermal history path constrained by thermochronometers
Unconstrained
Time-Temperature points

Figure 5.

Figure 6

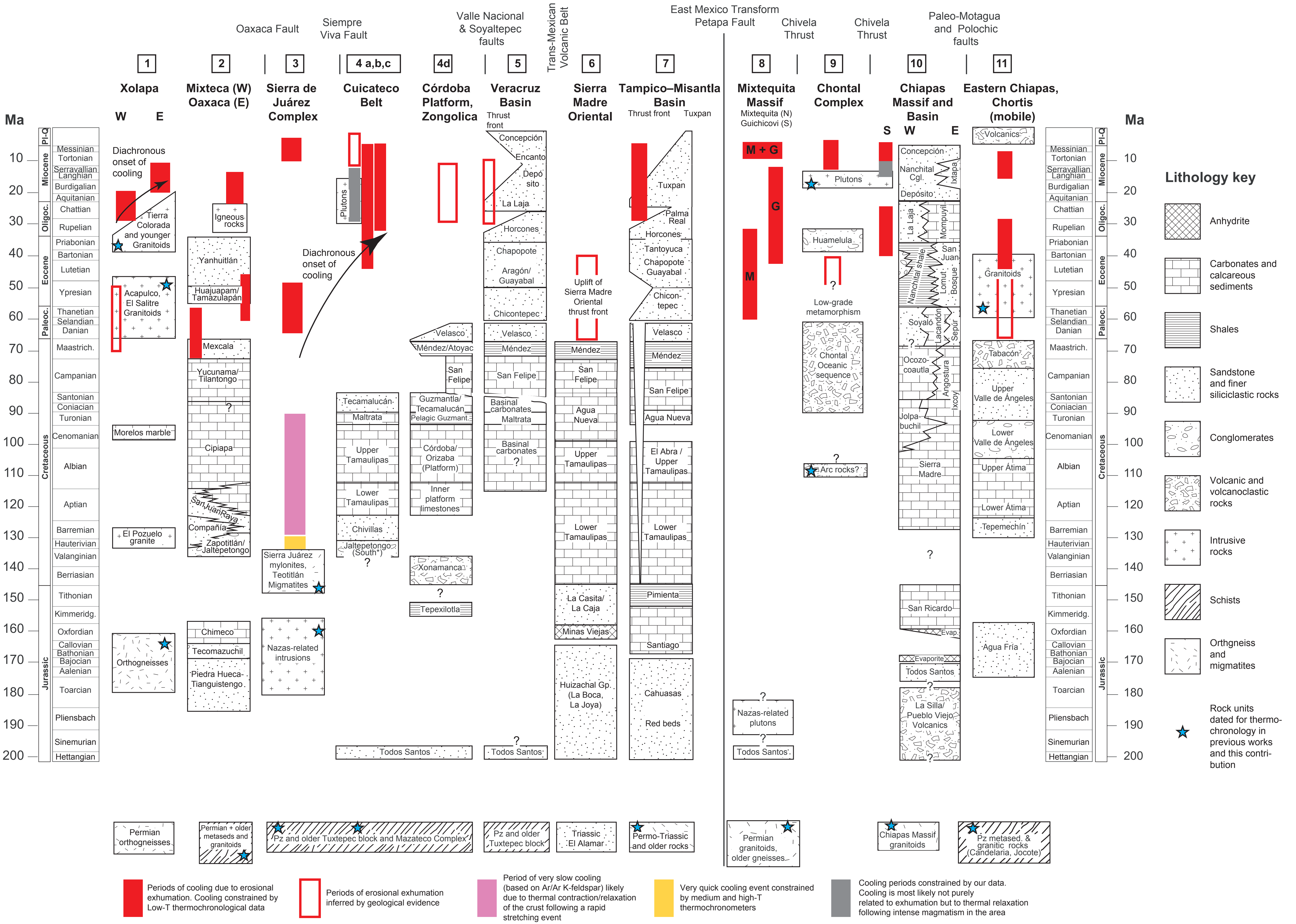

Figure 6.

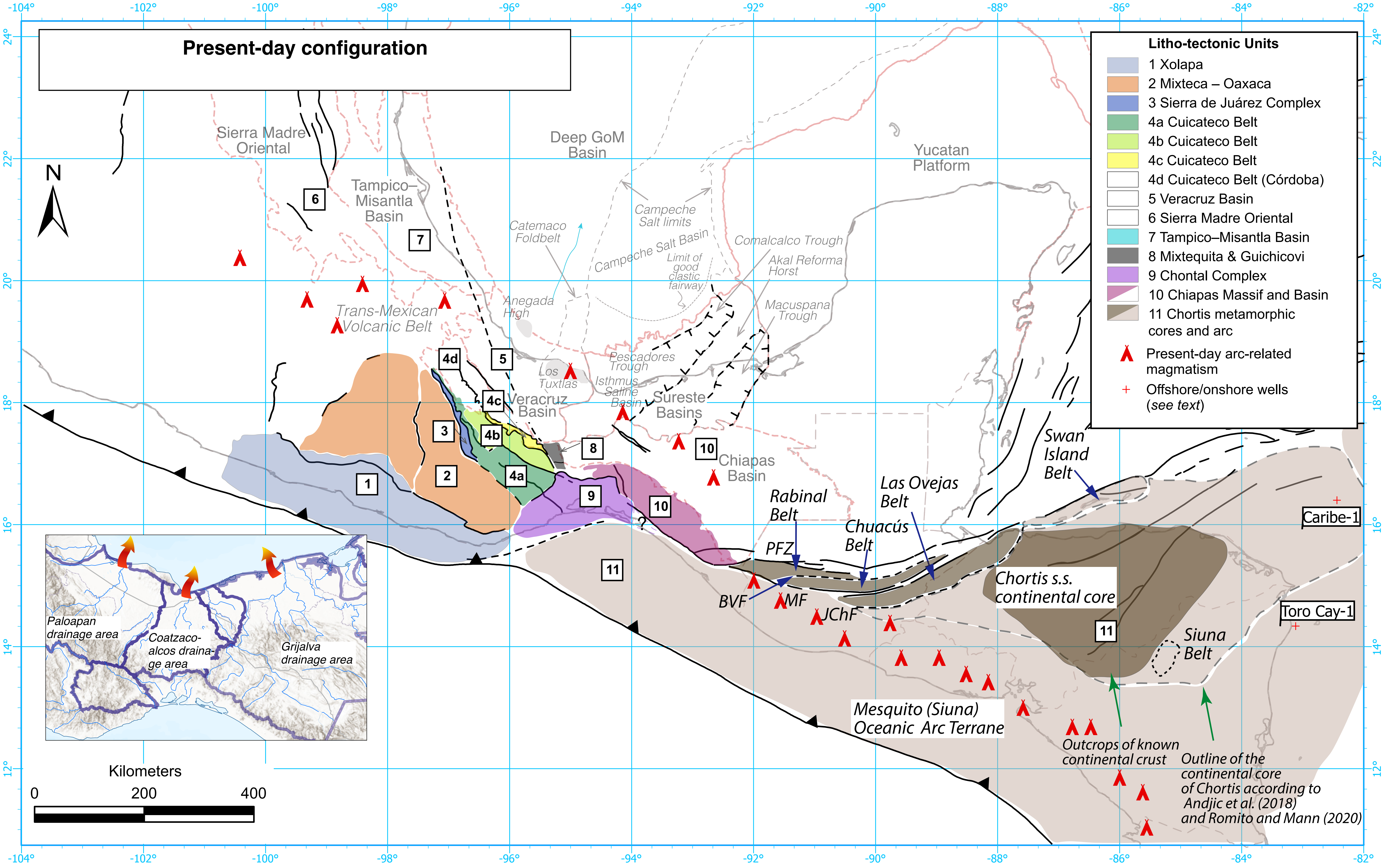
Present-day configuration
Litho-tectonic Units
1 Xolapa
2 Mixteca – Oaxaca
3 Sierra de Juárez Complex
4a Cuicateco Belt
4b Cuicateco Belt
4c Cuicateco Belt
4d Cuicateco Belt (Córdoba)
5 Veracruz Basin
6 Sierra Madre Oriental
7 Tampico–Misantla Basin
8 Mixtequita & Guichicovi
9 Chontal Complex
10 Chiapas Massif and Basin
11 Chortis metamorphic cores and arc
Present-day arc-related magmatism
Offshore/onshore wells (see text)
N
Sierra Madre Oriental
Tampico–Misantla Basin
Deep GoM Basin
Yucatan Platform
Campeche Salt limits
Catemaco Foldbelt
Campeche Salt Basin
Comalcalco Trough
Limit of good clastic fairway
Akal Reforma Horst
Macuspana Trough
Anegada High
Trans-Mexican Volcanic Belt
Los Tuxtlas
Pescadores Trough
Isthmus Saline Basin
Sureste Basins
Veracruz Basin
Chiapas Basin
Rabinal Belt
Las Ovejas Belt
Swan Island Belt
Chuacús Belt
PFZ
BVF
MF
JChF
Chortis s.s. continental core
Siuna Belt
Caribe-1
Toro Cay-1
Mesquito (Siuna) Oceanic Arc Terrane
Outcrops of known continental crust
Outline of the continental core of Chortis according to Andjic et al. (2018) and Romito and Mann (2020)
1
2
3
4a
4b
4c
4d
5
6
7
8
9
10
11
Paloapan drainage area
Coatzacoalcos drainage area
Grijalva drainage area
Kilometers
0
200
400
-104°
-102°
-100°
-98°
-96°
-94°
-92°
-90°
-88°
-86°
-84°
-82°
24°
22°
20°
18°
16°
14°
12°

Figure 7a

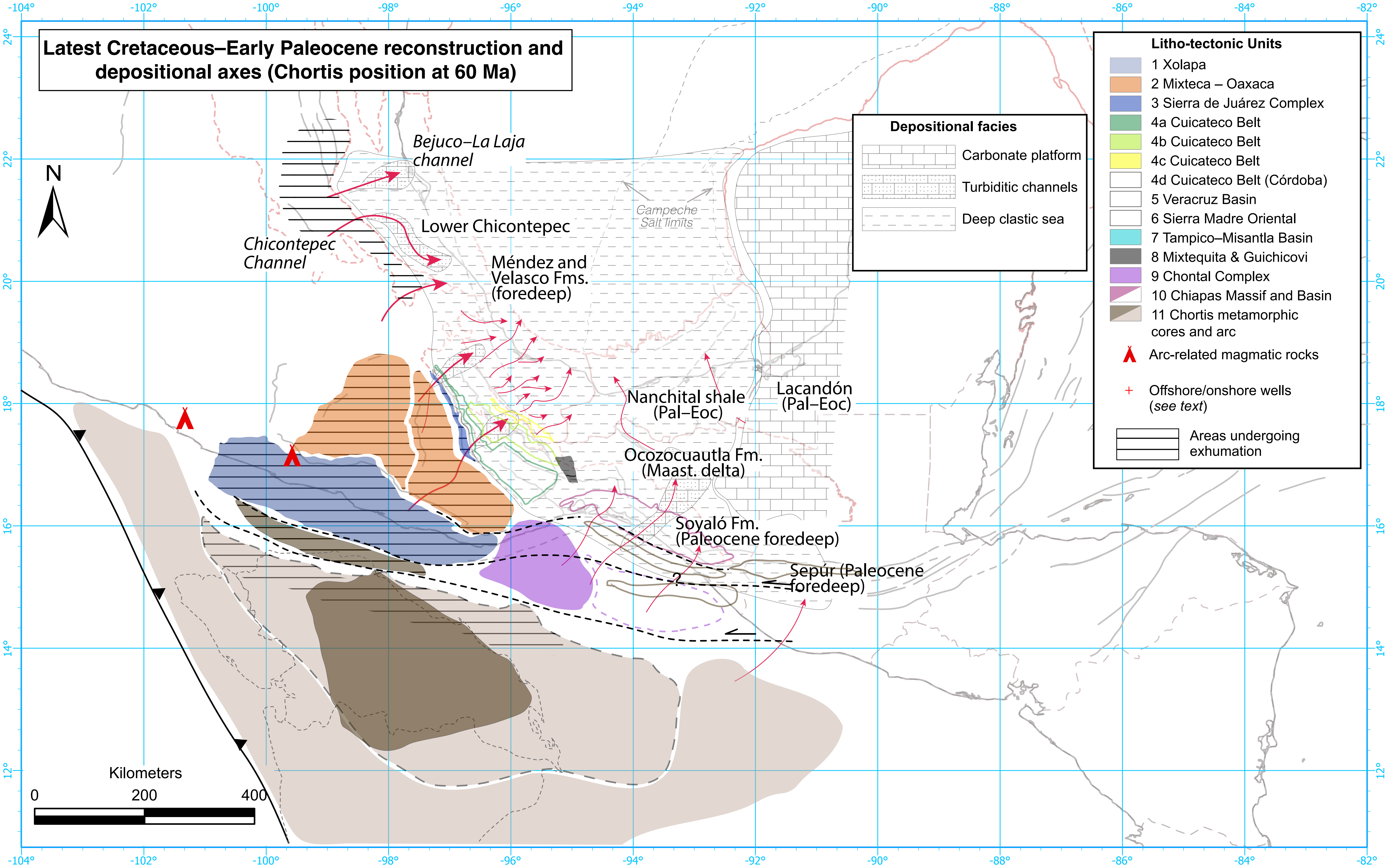
Latest Cretaceous–Early Paleocene reconstruction and depositional axes (Chortis position at 60 Ma)
N
Bejuco–La Laja channel
Chicontepec Channel
Lower Chicontepec
Méndez and Velasco Fms. (foredeep)
Campeche Salt limits
Nanchital shale (Pal–Eoc)
Lacandón (Pal–Eoc)
Ocozocuautla Fm. (Maast. delta)
Soyaló Fm. (Paleocene foredeep)
Sepúr (Paleocene foredeep)
?
Depositional facies
Carbonate platform
Turbiditic channels
Deep clastic sea
Litho-tectonic Units
1 Xolapa
2 Mixteca – Oaxaca
3 Sierra de Juárez Complex
4a Cuicateco Belt
4b Cuicateco Belt
4c Cuicateco Belt
4d Cuicateco Belt (Córdoba)
5 Veracruz Basin
6 Sierra Madre Oriental
7 Tampico–Misantla Basin
8 Mixtequita & Guichicovi
9 Chontal Complex
10 Chiapas Massif and Basin
11 Chortis metamorphic cores and arc
Arc-related magmatic rocks
Offshore/onshore wells (see text)
Areas undergoing exhumation
Kilometers
0
200
400
-104°
-102°
-100°
-98°
-96°
-94°
-92°
-90°
-88°
-86°
-84°
-82°
24°
22°
20°
18°
16°
14°
12°

Figure 7b

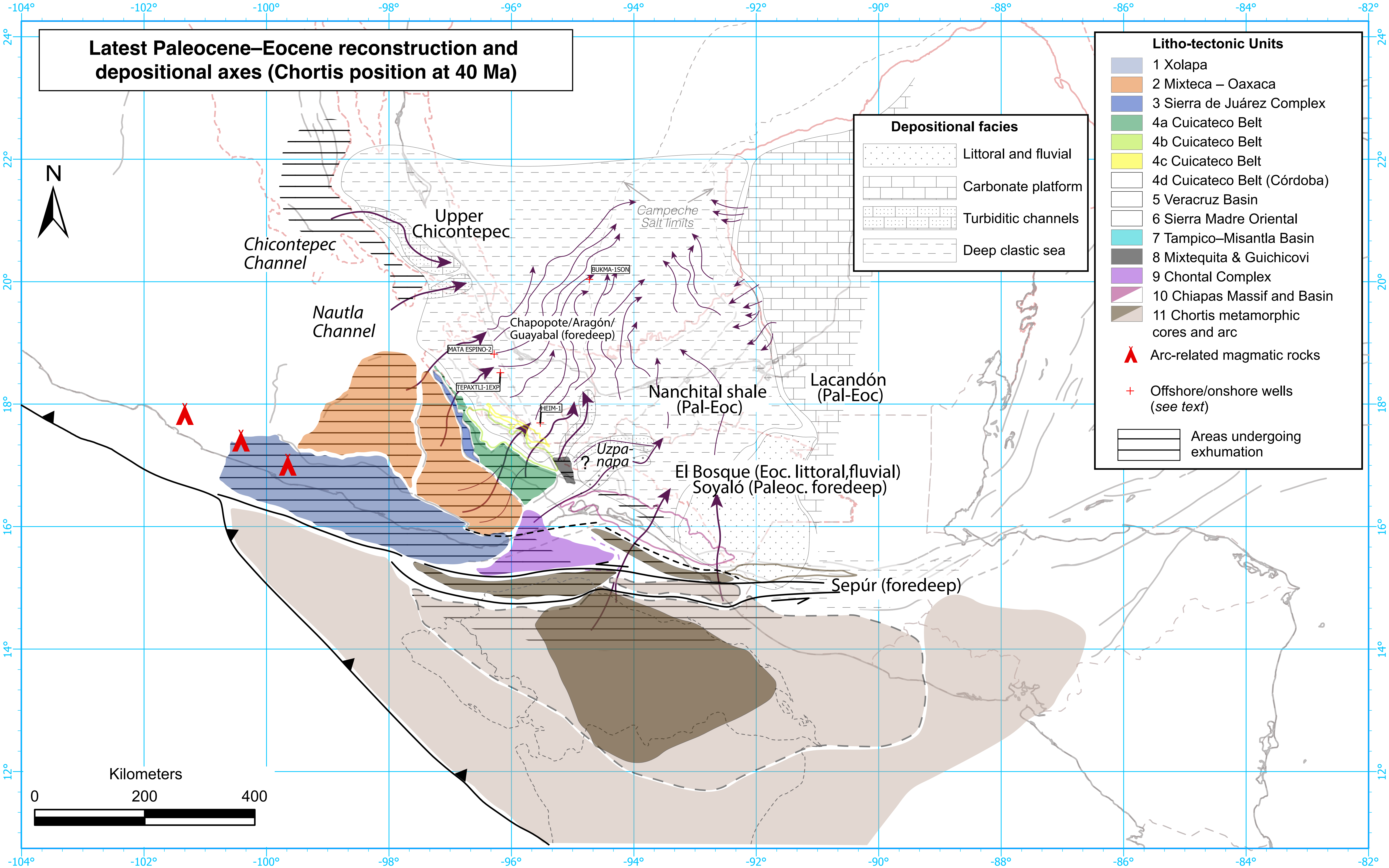
Latest Paleocene–Eocene reconstruction and depositional axes (Chortis position at 40 Ma)
N
Chicontepec Channel
Upper Chicontepec
Nautla Channel
Chapopote/Aragón/Guayabal (foredeep)
MATA ESPINO-2
TEPAXTLI-1EXP
HEIM-1
BUKMA-1SON
Campeche Salt limits
Nanchital shale (Pal-Eoc)
Lacandón (Pal-Eoc)
? Uzpa-napa
El Bosque (Eoc. littoral,fluvial)
Soyaló (Paleoc. foredeep)
Sepúr (foredeep)
Kilometers
0
200
400
Depositional facies
Littoral and fluvial
Carbonate platform
Turbiditic channels
Deep clastic sea
Litho-tectonic Units
1 Xolapa
2 Mixteca – Oaxaca
3 Sierra de Juárez Complex
4a Cuicateco Belt
4b Cuicateco Belt
4c Cuicateco Belt
4d Cuicateco Belt (Córdoba)
5 Veracruz Basin
6 Sierra Madre Oriental
7 Tampico–Misantla Basin
8 Mixtequita & Guichicovi
9 Chontal Complex
10 Chiapas Massif and Basin
11 Chortis metamorphic cores and arc
Arc-related magmatic rocks
Offshore/onshore wells (see text)
Areas undergoing exhumation
-104°
-102°
-100°
-98°
-96°
-94°
-92°
-90°
-88°
-86°
-84°
-82°
24°
22°
20°
18°
16°
14°
12°

Figure 7c

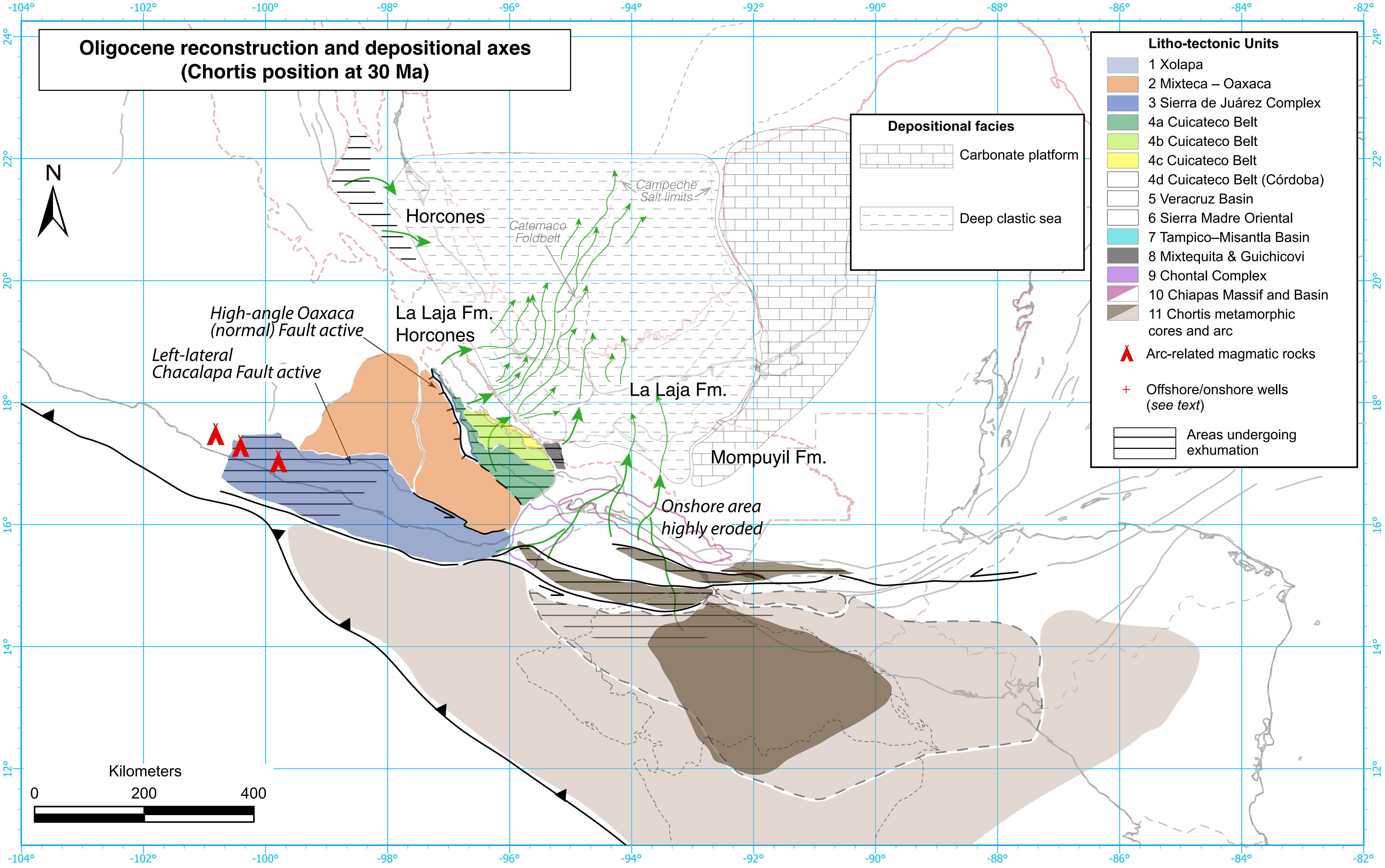
Oligocene reconstruction and depositional axes
(Chortis position at 30 Ma)
N
Horcones
Catemaco Foldbelt
Campeche Salt limits
La Laja Fm.
Horcones
High-angle Oaxaca (normal) Fault active
Left-lateral Chacalapa Fault active
La Laja Fm.
Mompuyil Fm.
Onshore area highly eroded
Depositional facies
Carbonate platform
Deep clastic sea
Litho-tectonic Units
1 Xolapa
2 Mixteca – Oaxaca
3 Sierra de Juárez Complex
4a Cuicateco Belt
4b Cuicateco Belt
4c Cuicateco Belt
4d Cuicateco Belt (Córdoba)
5 Veracruz Basin
6 Sierra Madre Oriental
7 Tampico–Misantla Basin
8 Mixtequita & Guichicovi
9 Chontal Complex
10 Chiapas Massif and Basin
11 Chortis metamorphic cores and arc
Arc-related magmatic rocks
Offshore/onshore wells (see text)
Areas undergoing exhumation
Kilometers
0
200
400
-104°
-102°
-100°
-98°
-96°
-94°
-92°
-90°
-88°
-86°
-84°
-82°
24°
22°
20°
18°
16°
14°
12°

Figure 7d

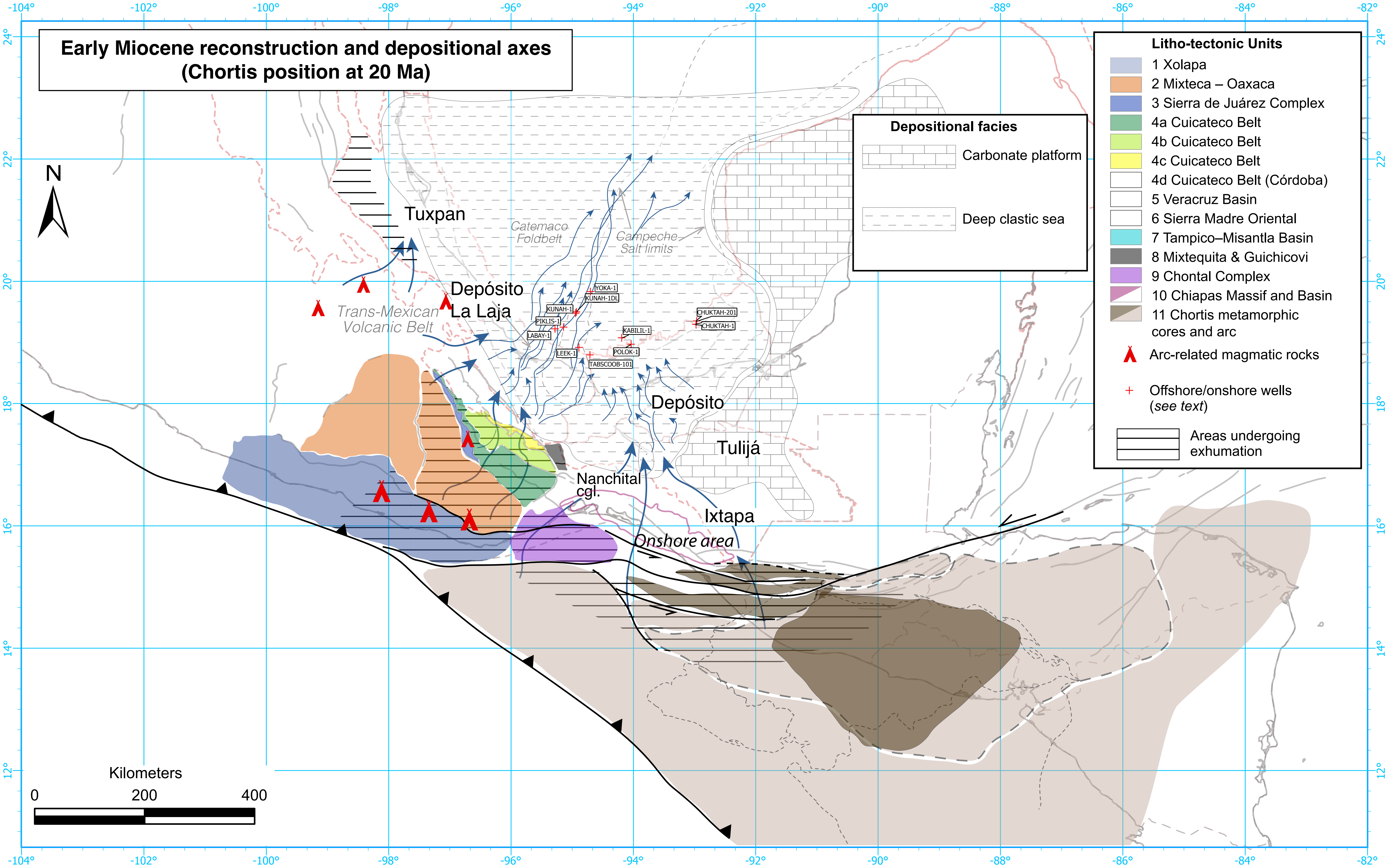
Early Miocene reconstruction and depositional axes
(Chortis position at 20 Ma)
N
Tuxpan
Catemaco Foldbelt
Campeche Salt limits
Depósito La Laja
Trans-Mexican Volcanic Belt
YOKA-1
KUNAH-1DL
KUNAH-1
PIKLIS-1
LABAY-1
LEEK-1
TABSCOOB-101
KABILIL-1
POLOK-1
CHUKTAH-201
CHUKTAH-1
Depósito
Tulijá
Nanchital cgl.
Ixtapa
Onshore area
Depositional facies
Carbonate platform
Deep clastic sea
Litho-tectonic Units
1 Xolapa
2 Mixteca – Oaxaca
3 Sierra de Juárez Complex
4a Cuicateco Belt
4b Cuicateco Belt
4c Cuicateco Belt
4d Cuicateco Belt (Córdoba)
5 Veracruz Basin
6 Sierra Madre Oriental
7 Tampico–Misantla Basin
8 Mixtequita & Guichicovi
9 Chontal Complex
10 Chiapas Massif and Basin
11 Chortis metamorphic cores and arc
Arc-related magmatic rocks
Offshore/onshore wells (see text)
Areas undergoing exhumation
Kilometers
0
200
400
-104°
-102°
-100°
-98°
-96°
-94°
-92°
-90°
-88°
-86°
-84°
-82°
24°
22°
20°
18°
16°
14°
12°

Figure 7e

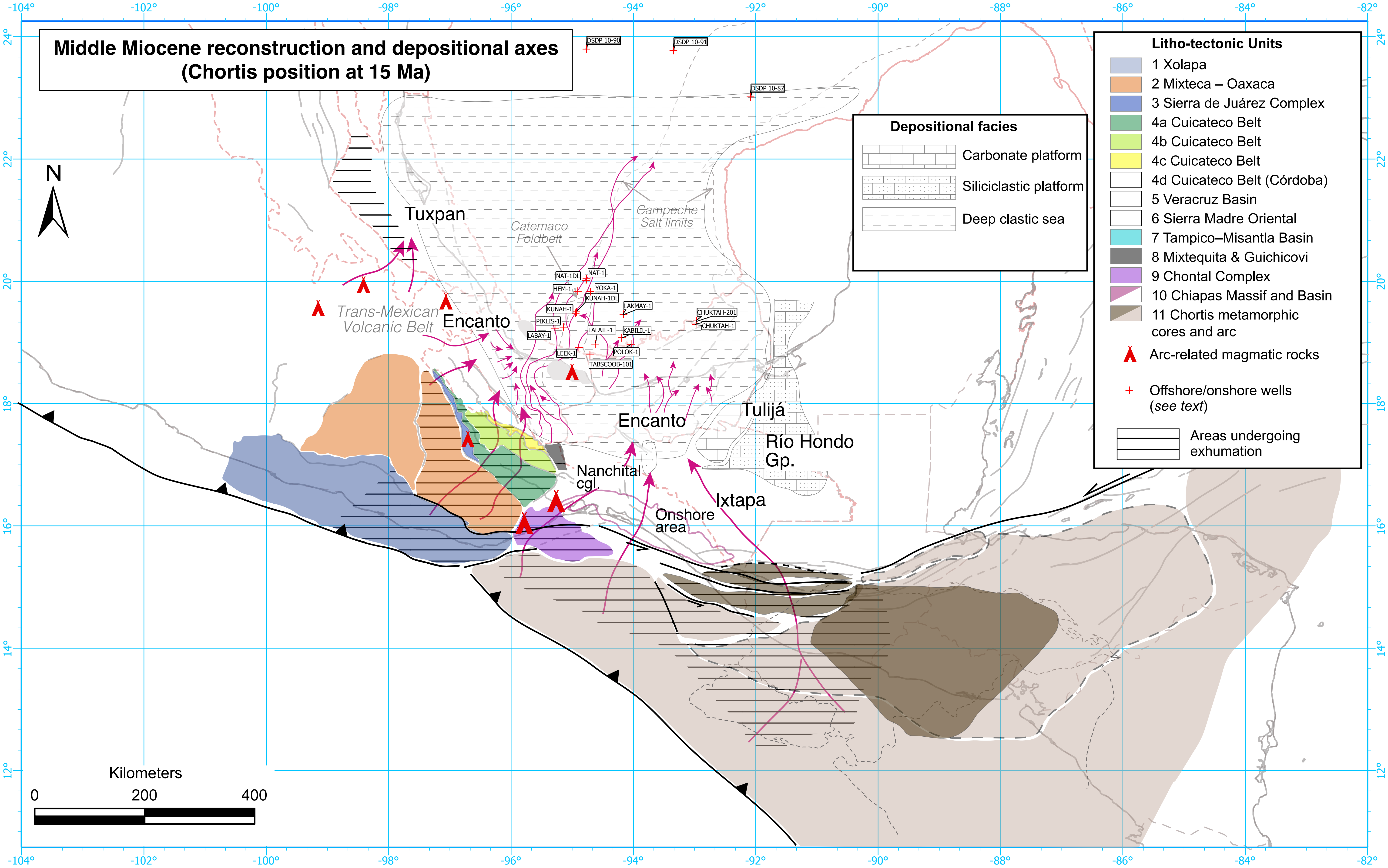
Middle Miocene reconstruction and depositional axes
(Chortis position at 15 Ma)
N
Tuxpan
Catemaco Foldbelt
Campeche Salt limits
Trans-Mexican Volcanic Belt
Encanto
Encanto
Tulijá
Río Hondo Gp.
Nanchital cgl.
Onshore area
Ixtapa
DSDP 10-90
DSDP 10-91
DSDP 10-87
NAT-1DL
NAT-1
HEM-1
YOKA-1
KUNAH-1DL
KUNAH-1
LAKMAY-1
PIKLIS-1
LABAY-1
LALAIL-1
KABILIL-1
LEEK-1
POLOK-1
TABSCOOB-101
CHUKTAH-201
CHUKTAH-1
Depositional facies
Carbonate platform
Siliciclastic platform
Deep clastic sea
Litho-tectonic Units
1 Xolapa
2 Mixteca – Oaxaca
3 Sierra de Juárez Complex
4a Cuicateco Belt
4b Cuicateco Belt
4c Cuicateco Belt
4d Cuicateco Belt (Córdoba)
5 Veracruz Basin
6 Sierra Madre Oriental
7 Tampico–Misantla Basin
8 Mixtequita & Guichicovi
9 Chontal Complex
10 Chiapas Massif and Basin
11 Chortis metamorphic cores and arc
Arc-related magmatic rocks
Offshore/onshore wells (see text)
Areas undergoing exhumation
Kilometers
0
200
400
-104°
-102°
-100°
-98°
-96°
-94°
-92°
-90°
-88°
-86°
-84°
-82°
24°
22°
20°
18°
16°
14°
12°

Figure 7f

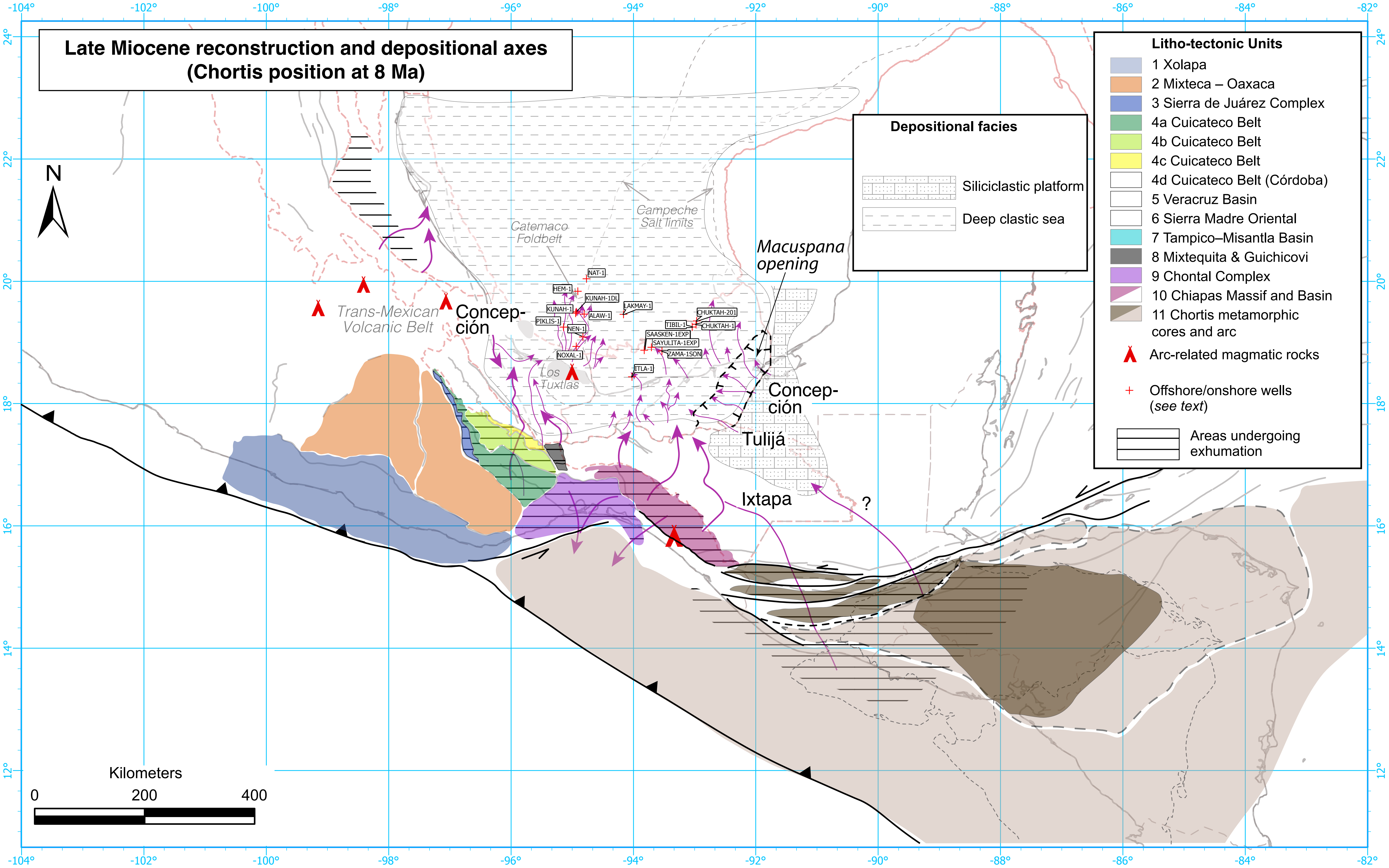
Late Miocene reconstruction and depositional axes
(Chortis position at 8 Ma)
Litho-tectonic Units
1 Xolapa
2 Mixteca – Oaxaca
3 Sierra de Juárez Complex
4a Cuicateco Belt
4b Cuicateco Belt
4c Cuicateco Belt
4d Cuicateco Belt (Córdoba)
5 Veracruz Basin
6 Sierra Madre Oriental
7 Tampico–Misantla Basin
8 Mixtequita & Guichicovi
9 Chontal Complex
10 Chiapas Massif and Basin
11 Chortis metamorphic cores and arc
Arc-related magmatic rocks
Offshore/onshore wells (see text)
Areas undergoing exhumation
Depositional facies
Siliciclastic platform
Deep clastic sea
N
Kilometers
0
200
400
Trans-Mexican Volcanic Belt
Concep-ción
Catemaco Foldbelt
Campeche Salt limits
Macuspana opening
Los Tuxtlas
Concep-ción
Tulijá
Ixtapa
?
NAT-1
HEM-1
KUNAH-1DL
KUNAH-1
ALAW-1
LAKMAY-1
PIKLIS-1
NEN-1
NOXAL-1
CHUKTAH-201
TIBIL-1
CHUKTAH-1
SAASKEN-1EXP
SAYULITA-1EXP
ZAMA-1SON
ITLA-1
-104°
-102°
-100°
-98°
-96°
-94°
-92°
-90°
-88°
-86°
-84°
-82°
24°
22°
20°
18°
16°
14°
12°

Figure 7g

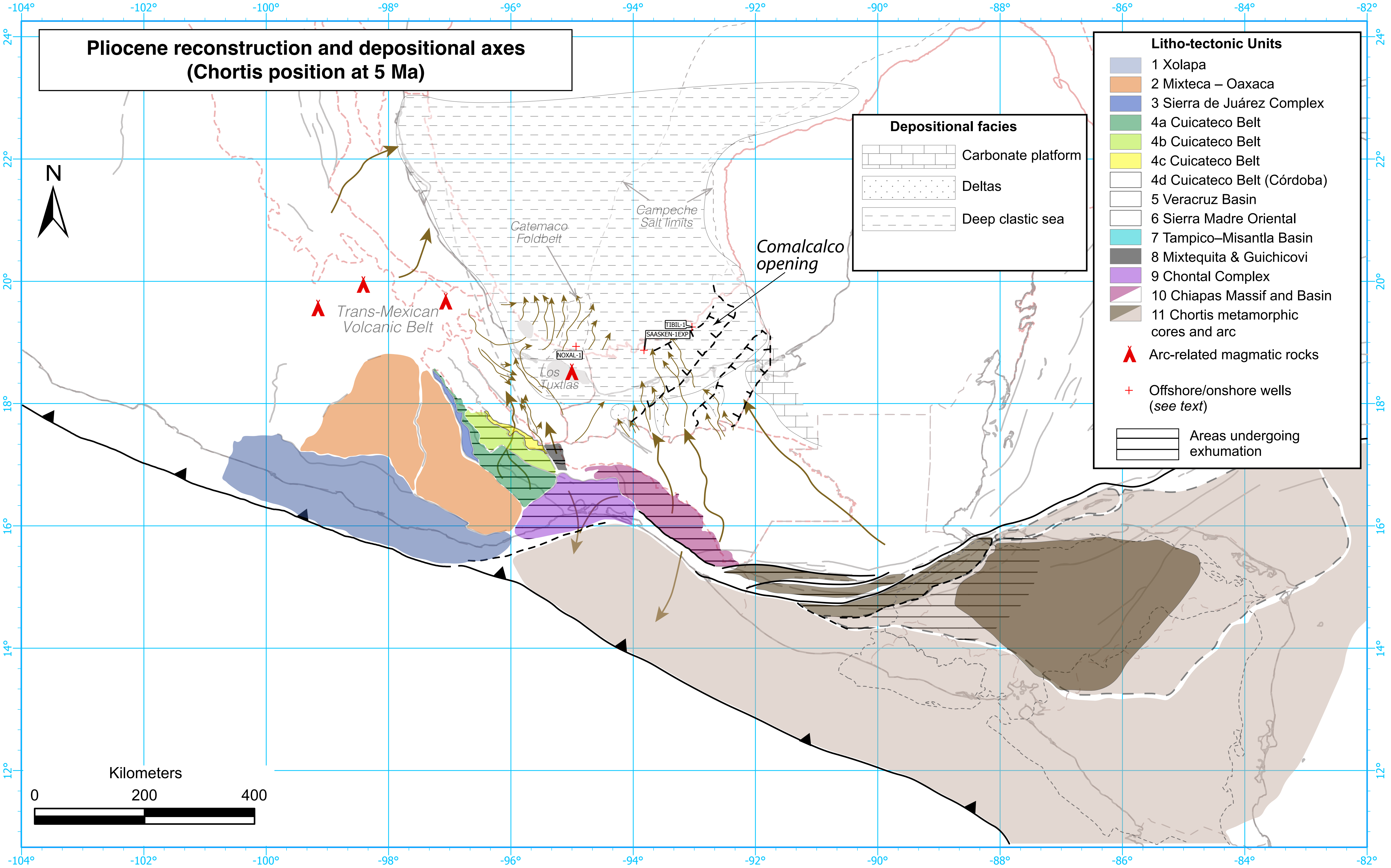
Pliocene reconstruction and depositional axes
(Chortis position at 5 Ma)
N
Catemaco Foldbelt
Campeche Salt limits
Comalcalco opening
Trans-Mexican Volcanic Belt
Los Tuxtlas
TIBIL-1
SAASKEN-1EXP
NOXAL-1
Depositional facies
Carbonate platform
Deltas
Deep clastic sea
Litho-tectonic Units
1 Xolapa
2 Mixteca – Oaxaca
3 Sierra de Juárez Complex
4a Cuicateco Belt
4b Cuicateco Belt
4c Cuicateco Belt
4d Cuicateco Belt (Córdoba)
5 Veracruz Basin
6 Sierra Madre Oriental
7 Tampico–Misantla Basin
8 Mixtequita & Guichicovi
9 Chontal Complex
10 Chiapas Massif and Basin
11 Chortis metamorphic cores and arc
Arc-related magmatic rocks
Offshore/onshore wells (see text)
Areas undergoing exhumation
Kilometers
0
200
400
-104°
-102°
-100°
-98°
-96°
-94°
-92°
-90°
-88°
-86°
-84°
-82°
24°
22°
20°
18°
16°
14°
12°

Figure 7h

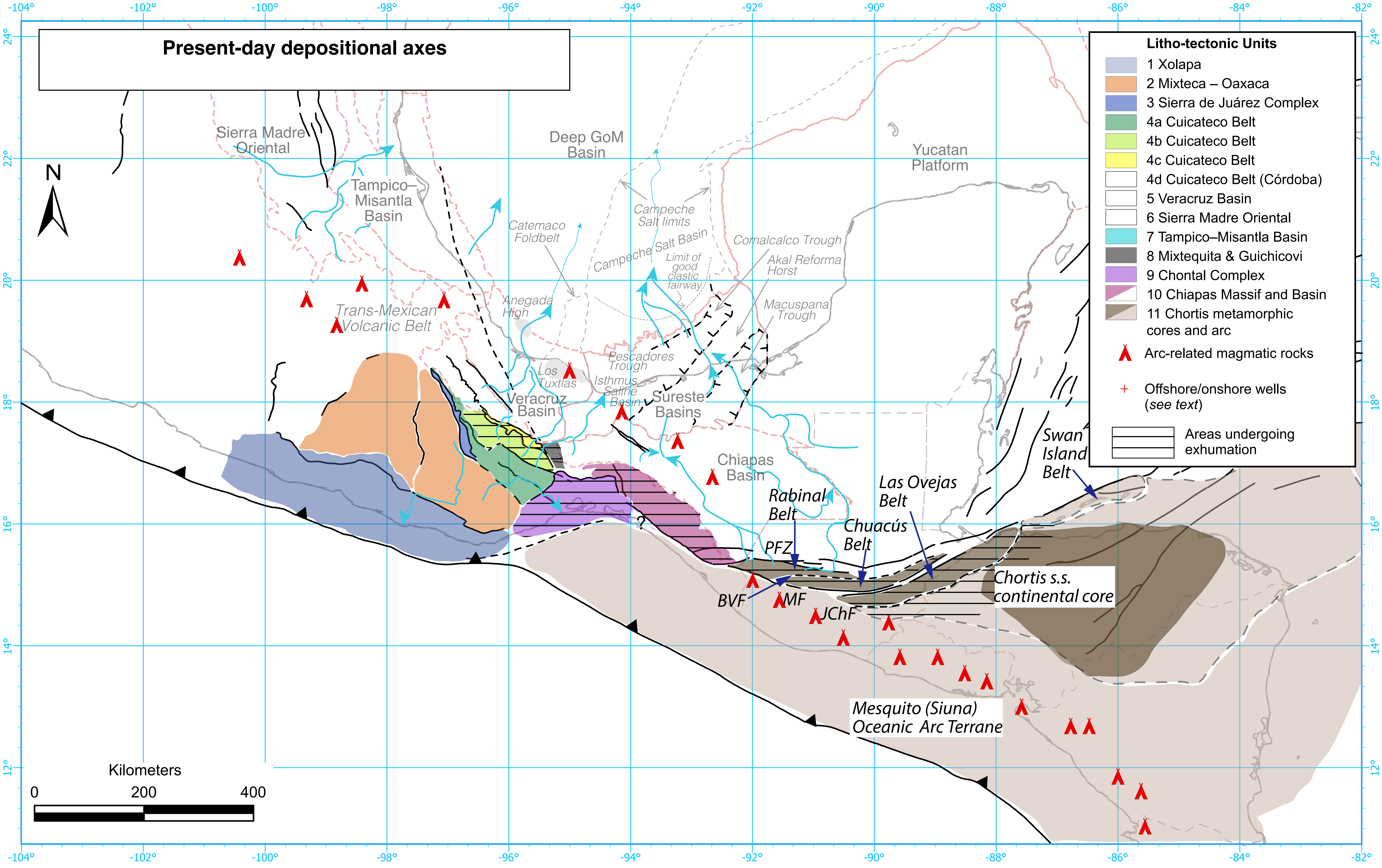
Present-day depositional axes
Litho-tectonic Units
1 Xolapa
2 Mixteca – Oaxaca
3 Sierra de Juárez Complex
4a Cuicateco Belt
4b Cuicateco Belt
4c Cuicateco Belt
4d Cuicateco Belt (Córdoba)
5 Veracruz Basin
6 Sierra Madre Oriental
7 Tampico–Misantla Basin
8 Mixtequita & Guichicovi
9 Chontal Complex
10 Chiapas Massif and Basin
11 Chortis metamorphic cores and arc
Arc-related magmatic rocks
Offshore/onshore wells (see text)
Areas undergoing exhumation
N
Sierra Madre Oriental
Tampico–Misantla Basin
Deep GoM Basin
Yucatan Platform
Campeche Salt limits
Catemaco Foldbelt
Campeche Salt Basin
Comalcalco Trough
Akal Reforma Horst
Limit of good clastic fairway
Macuspana Trough
Anegada High
Trans-Mexican Volcanic Belt
Pescadores Trough
Los Tuxtlas
Isthmus Saline Basin
Sureste Basins
Veracruz Basin
Chiapas Basin
Swan Island Belt
Las Ovejas Belt
Rabinal Belt
Chuacús Belt
PFZ
BVF
MF
JChF
Chortis s.s. continental core
Mesquito (Siuna) Oceanic Arc Terrane
Kilometers
0
200
400
-104°
-102°
-100°
-98°
-96°
-94°
-92°
-90°
-88°
-86°
-84°
-82°
24°
22°
20°
18°
16°
14°
12°

Figure 7i

Table 1. Zircon U–Pb results

Sample	Unit	Lithology	Locality	Elevation (m)	LAT	LON	Grain dated	Main age populations
Mixteca (W) – Oaxaca (E)								
6-15-12-01B	Cobble in detrital Chivillas Fm.	Jurassic granodiorite	Tehuacán–Orizaba,	ND	18.52087	-97.35118	39	The granite cobble mostly contains Mesoproterozoic zircon with a range of inherited ages. One Jurassic age may correspond to the time of magmatism.
18-01-18-01	Oaxaqueno, foliated basement sample covered by Lower K Jaltepetongo	Coarse to medium grained metamorphic rock		1466	17.06959	-96.73631	110	Youngest population: 820 - 870 Ma. Other populations from 920-970 Ma, 1000-1350 Ma
17-01-18-01	San Bartolomé Quialana	Plutonic Rock- Granodiorite- (Qz, Hb, Plg,Bt). Mafic enclaves. 29 Ma	San Bartolomé Quialana, Block west of Tlacolula. East Oaxaca City	1787	16.89447	-96.49601	23	Weightead mean of 29.1±0.19 Ma
17-01-18-04	Crystal Tuff	Crystal Tuff		1810	16.88886	-96.60350	19	Youngest population: 33.31 ± 0.16 Ma. Other populations from 400, 1000-1200 Ma
17-01-18-05	Andesitic tuff	Felsic volcanic rock- subhedral crystal (Hb, Kfs,Plg)	S of Oaxaca City	1743	16.87530	-96.62229	12	Weighted mean age of 23.1±0.1 Ma
17-01-18-06	Ejutla batholith	Qtz monzodiorite,(Qz,Plg, Bt,Hbl)	S of Oaxaca City	1561	16.60958	-96.70852	30	Weighted mean age of 25.32±0.32 Ma
Sierra de Juárez Complex								
Between Siempre Viva Fault and Oaxaca Fault (Teotitlán migmatitic Belt / Sierra de Juárez mylonite complex)								
20-01-30-13A	KnapArLu, mylonite with metasedimentary protolith road to Teococuilco (Oaxaca myl		Road to Teocuico	ND	17.31000	-96.67482	95.0	Meso and Neoproterozoic zircons moslty, a single zircon is ca 415 Ma
Cuicateco Belt								
West of Villa Alta and Aloapán faults, East of Siempre Viva Fault:								
16-01-18-10A	San Juan Juquila	Intrusive contact, Felsic rock (intrusive sample).	East Oaxaca City	2087	16.98304	-96.01800	30	Weighted mean age of 17.57±0.28 Ma
16-01-18-11B	San Juan Juquila	Plutonic Rock- Granite (weathered sample)	East Oaxaca City	1995	16.97187	-96.01236	14	Weighted mean age of 17.30 ± 0.1
Veracruz Basin								
16Apr16-2B	Quaternary		Tetela	ND	18.51636	-96.44598	317	Youngest DZ 0.55 ± 0.04 Ma. Other populations from 2 Ma-18 Ma, 80, 100, 270, >900 Ma
Tampico–Misantla Basin								
COAP17-1	Basal? Chicontepec above thrust over eoc	Sandstone		171	20.37653	-97.61215	108	Youngest DZ about 59 Ma, population 60-100 Ma, 110-162 Ma, 215-290 Ma, >350Ma-2.6 Ga
SANT17-2A	Basal Chicontepec above K/T breccia	Sandstone	Santiago	484	19.91593	-97.15263	107	Youngest DZ about 65 Ma, population 65-120 Ma, 140-200 Ma, 235-300 Ma, >325Ma-1.9 Ga
SANT17-2B	Chicontepec (Middle and Upper)	Conglomeratic sandstone		301	19.97935	-97.10584	108	Youngest DZ about 55 Ma, population 55-107 Ma, 253-280 Ma, >335Ma-3.1 Ga
SFRAN17-1	Chicontepec (Middle and Upper)	Carbonate-rich volcanosediment		973	21.01527	-98.50159	109	Youngest DZ about 52 Ma, population 55-86 Ma, 104-183 Ma, 250-277, >470 Ma-2.2 Ga
TENA17-1	Oligocene	Medium- Fine-grained sandstone. Volcanoclastic		204	20.16197	-97.40399	108	Youngest DZ about 38 Ma, population 38-93 Ma, 120-176 Ma, 195-280, >335 Ma-2.6 Ga

A more detailed document with the methodology and raw analytical data are presented in Appendixes 2 and 3

Table 2. $^{40}Ar/^{39}Ar$ results

Sample	Unit	Lithology	Locality	Elevation (m)	LAT	LON	Phase	WM $^{40}Ar/^{39}Ar$ age ± 2σ (Ma)	Total Fusion age±2σ (Ma)	Inverse Isochron age±2σ (Ma)	MSWD[1]	Observations
Sierra de Juárez Complex												
Between Siempre Viva Fault and Oaxaca Fault (Teotitlán migmatitic Belt / Sierra de Juárez mylonite complex)												
5-11-11-02A	Teotitlán Migmatitic Suite, Zr U/Pb 158 Ma	Orthogneiss	E Teotitlán	1604	18.17367	-97.05451	K feldspar	116.50 ± 10.29	124.70 ± 2.18	81.00 ± 42.25	21.41	Age gradient (91 - 135 Ma)
5-11-11-03A	Teotitlán Migmatitic Suite, Zr U/Pb 137 Ma	Migmatitic orthogneiss	E Teotitlán	1804	18.18604	-97.04982	K feldspar	100.74 ± 3.38	101.23 ± 0.90	93.70 ± 22.57	15.56	Flat region (approximately 101 Ma), excess Ar

WM: Weighted mean age over >3 contiguous heating steps that yield distinguishable ages that differ by less than 5%, and span > 50% ^{39}Ar released

[1] Mean Square of Weighted Deviates of the inverse isochron linear regression

Zircon U-Pb published by Pindell et al. (2020a) and Coombs (2016)

Table 3

Table 3. Apatite Fission Track results

Sample	Unit	Lithology	Locality	Elevation (m)	LAT	LON	Grains	Ns	Total area cm^2	U average (ppm)	Pooled AFT age (§)	95%-CI (Ma)	95%+CI (Ma)	Chi-squared	Primary Zeta	+/- 1 sigma	MTL µm (1)	SE	SD	MTL proj. µm (2)	N (#)	Dpar average µm
Mixteca (W) – Oaxaca (E)																						
17-01-18-03 *	Jaltepetongo, intruded by 28 Ma San Bartolomé Quialana batholith	Arkosic sandstone		1721	16.89245	-96.60584	40	501	1.0E-03	45.1	14.2	1.3	1.4	63.8	8.3	0.1	14.59	0.10	1.03	15.35	106	1.9
17-01-18-06 *	Ejutla batholith (Zr U/Pb age 25 Ma; this work)	Qtz monzodiorite,(Qz,Plg, Bt,Ho)	S of Oaxaca City	1561	16.60958	-96.70852	40	84	1.4E-03	0.4	25.0	5.0	6.2	59.7	8.3	0.1	14.47	0.13	1.19	15.29	85	2.0
18-01-18-01 *	Oaxaqueno, foliated basement sample covered by Lower K Jaltepetongo	Coarse to medium grained metamorphic rock		1466	17.06959	-96.73631	40	1182	1.0E-03	37.2	50.5	3.9	4.2	73.5	8.3	0.1	13.49	0.13	1.41	14.67	127	2.1
DH-22-12-3-11	Acatlan, Upper Pz (Olinala Fm?)	Fine-grained volcanoclastic sandstones		1415	17.75084	-98.73439	35	562	1.7E-03	104.0	83.2	7.6	8.3	72.9	6.2	0.1	ND	ND	ND	ND	ND	ND
DH-23-12-3-11	Cosoltepec Fm, Acatlan (Pz)	Fine-grained sandstones (very deformed, slighty metamorphosed)		1688	17.84033	-98.75138	24	1254	6.6E-04	590.9	70.2	5.3	5.7	71.3	6.2	0.1	ND	ND	ND	ND	ND	ND
DH-24-12-3-11	Cosoltepec Fm, Acatlan (Pz)	Graywacke interbedded within phyllites (very deformed, slightly metamorphosed)		1279	18.14525	-98.66060	29	856	7.5E-04	455.7	62.4	5.0	5.4	80.9	6.2	0.1	ND	ND	ND	ND	ND	ND
Sierra de Juárez Complex																						
Between Siempre Viva Fault and Oaxaca Fault (Teotitlán migmatitic Belt / Sierra de Juárez mylonite complex)																						
5-11-11-02A **	Teotitlán Migmatitic Suite, Zr U/Pb 158 Ma (Pindell et al., 2020a)	Orthogneiss	E Teotitlán	1604	18.17367	-97.05451	26	527	1.6E-03	9.2	51.9	5.6	6.3	42.5	9.1	0.2	12.97	0.24	1.15	14.37	92	1.2
5-11-11-03A **	Teotitlán Migmatitic Suite, Zr U/Pb 137 Ma (Coombs 2016)	Migmatitic orthogneiss	E Teotitlán	1804	18.18604	-97.04982	31	572	2.7E-03	5.6	57.2	6.0	6.7	51.1	9.1	0.2	12.84	0.22	1.34	14.26	151	1.3
Cuicateco Belt																						
West of Villa Alta and Aloapán faults, East of Siempre Viva Fault:																						
16-01-18-10A *	San Juan Juquila (Zr U/Pb age 17.6 Ma; this work)	Intrusive contact- Felsic rock (intrusive sample).	East Oaxaca City	2087	16.98304	-96.01800	22	21	2.4E-04	10.5	17.9	6.4	10.0	14.8	8.3	0.1	14.39	0.21	0.88	14.93	19	2.0
16-01-18-09A *	Metamorphic Complex, Zr U/Pb 180 Ma (Pindell et al. 2020)	Muscovite-rich schist	East Oaxaca City	2021	17.01785	-96.08020	29	17	3.5E-04	1.2	33.9	16.8	33.2	101.1	8.3	0.1	14.03	0.38	1.53	14.89	17	1.8
16-01-18-08A *	Jaltepetongo Fm.	Tabular Sandstone (fine size)		1877	16.96214	-96.11690	39	99	4.6E-04	19.4	14.9	2.8	3.4	87.7	8.3	0.1	13.98	0.20	1.31	14.96	46	1.8
16-01-18-05A *	Todos Santos	Tabular red fine-grained sandstone		1653	16.96250	-96.19340	38	91	5.0E-04	15.1	22.2	4.3	5.3	56.4	8.3	0.1	14.18	0.15	1.12	15.03	56	1.8
26Feb16-7A *	Jaltepetongo	Masive quartzose sandstone. distal facies of turbidites.	Quarry by the road from Oaxaca to Tuxtepec, 3 km before Guelatao	1525	17.30611	-96.52531	40	77	5.3E-04	14.0	15.4	3.2	4.1	45.4	8.3	0.1	14.25	0.20	1.27	15.15	40	2.3
18-01-18-03 *	Complejo Oaxaqueño	Quartzitic rock		2482	17.15195	-96.60720	25	81	3.2E-04	19.1	17.6	3.6	4.5	69.4	8.3	0.1	14.26	0.31	1.27	15.14	18	1.9
Between Villa Alta/Aloapán and Vista Hermosa faults (Mazateco Complex)																						
12-9-10-08A *	Todos Santos Fm. (West of VH Fault)	Red very fine sandstone. Shows thermal effect, cooked		1316	17.65928	-96.33430	45	135	5.7E-04	25.8	20.4	3.3	4.0	72.5	8.3	0.1	14.65	0.21	1.47	15.32	52	2.1
12-9-10-10A *	Mazateco Complex. (West of VH Fault)	Quartzite		1423	17.63692	-96.33977	40	55	6.6E-04	5.6	23.0	5.5	5.5	26.1	8.3	0.1	13.75	0.19	1.40	14.71	54	2.0
21-01-18-01 *	Mazateco (SW of VH Fault)	Low grade metasediment		377	17.14588	-95.40940	15	57	2.2E-04	26.9	15.6	3.7	4.8	20.2	8.3	0.1	13.17	0.81	3.35	14.28	18	1.8
Between Vista Hermosa and Valle Nacional faults																						
20-01-18-08 *	Todos Santos (East of VH Fault)	Sandstone and mudstone with tectonic foliation.	Contact zones between basement and Todos Santos Fm, along the Vista Hermosa Fault	158	17.44420	-95.76623	39	296	9.4E-04	27.5	20.9	2.4	2.8	75.5	8.3	0.1	13.47	0.27	1.85	14.67	49	1.8
19-01-18-06 *	Fm. Xonamanca?, (East of VH Fault)	Sublitharenite		370	17.70332	-96.22829	12	67	9.0E-05	44.3	27.6	7.1	9.5	54.2	8.3	0.1	13.12	0.58	1.42	14.43	7	2.0
19-01-18-10*	Todos Santos (East of VH Fault)	Sandstone		358	17.64434	-96.15566	40	161	5.6E-04	26.9	19.7	3.0	3.6	90.9	8.3	0.1	13.86	13.86	1.47	14.84	53	1.8

Table 3 (continued). Apatite Fission Track results

Sample	Unit	Lithology	Locality	Elevation (m)	LAT	LON	Grains	Ns	Total area cm2	U average (ppm)	Pooled AFT age (§)	95%-CI (Ma)	95%+CI (Ma)	Chi-squared	Primary Zeta	+/- 1 sigma	MTL µm (1)	SE	SD	MTL proj. µm (2)	N (#)	Dpar average µm
Tampico–Misantla Basin																						
ACAT17-1 *	Chicontepec. MDA 55 Ma (Cossey et al., 2019)	Carbonate-rich volcanosediment	Chicontepec channel at Acatapec	465	20.96020	-98.27656	40	223	1.8E-03	3.6	57.0	7.4	8.4	32.0	8.3	0.1	14.16	0.17	2.08	15.11	152	3.5
ALTO17-2 *	Cahuasas redbeds,	Red tuff (Nazas?), coarse-medium grained		1059	19.86862	-97.22115	40	48	1.2E-03	12.9	11.8	3.0	4.0	58.6	8.3	0.1	14.28	0.37	1.44	15.03	16	2.2
SANT17-1	K/T, K-Pg breccia	Breccia	Santiago	484	19.91593	-97.15263	40	500	1.6E-03	56.4	16.2	1.5	1.7	323.7	8.3	0.1	13.98	0.15	1.82	14.95	140	2.4
COAP17-1 *	Basal? Chicontepec above thrust over eocene	Sandstone		171	20.37653	-97.61215	40	313	9.9E-04	19.5	56.6	6.3	7.1	63.0	8.3	0.1	13.38	0.16	1.64	14.54	112	2.8
Mixtequita (N) & Guichicovi (S) blocks																						
27Mar17-3A	Mixtequita granite, Permo-Triassic	Granite		153	17.14763	-95.14480	25	41	3.8E-03	4.4	42.0	3.5	3.5	ND	12.0	0.2	12.93	0.20	1.56	ND	58	ND
19-07-04-1	Guichicovi Complex, Precambrian	Granulitic gneiss	Sarabia River		17.04996	-95.19520	36	22	8.8E-04	1.8	23.1	8.0	12.3	5.9	8.3	0.1	14.48	0.16	0.86	15.20	29	1.8
Chontal																						
19-07-03-2B	Chivela lithodeme, Cretaceous	Coarse grained phyllite	Ajal town	188	16.76736	-95.02154	36	98	5.3E-04	19.4	11.4	2.1	2.6	37.6	8.3	0.1	14.18	0.14	0.84	14.95	35	1.8
9-30-10-09A	Juchitan, Western Tehuantepec Tertiary magmatic rocks	Biotite tonalite or granodiorite		ND	16.50632	-95.42106	40	122	1.5E-03	20.6	5.7	1.0	1.2	61.0	8.3	0.1	14.17	0.17	1.16	15.01	50	1.6
9-30-10-11	Western Tehuantepec Tertiary magmatic rocks	Biotite Granodiorite/Tonalite		ND	16.54434	-95.45190	6	9	1.8E-04	13.4	4.1	2.1	4.2	4.4	8.3	0.1	14.21	0.44	0.98	15.06	6	1.5
3-8-11-08	Western Tehuantepec Tertiary magmatic rocks	Biotite tonalite Zoned plagioclase	New highway to Oaxaca	220	16.49542	-95.40132	29	284	1.7E-03	14.2	7.1	0.9	1.0	278.4	6.2	0.1	ND	ND	ND	ND	ND	ND
19-07-05-1	Migmatite, Appears to intrude K phyllites	Migmatite	Tehuantepec town	ND	16.35775	-95.22333	40	378	1.4E-03	100.3	8.7	1.0	1.1	229.5	8.3	0.1	14.13	0.09	0.95	14.98	115	1.8
Chiapas Massif and Basin																						
19-07-05-4	Westernmost Chiapas Massif	Porphyritic granite	Road to Sta. María Chimalapa	300	16.82889	-94.76931	37	37	5.8E-04	20.6	8.3	2.5	3.5	34.4	8.3	0.1	14.45	0.14	0.69	15.14	25	1.8

(§) Pooled age calculated by pooling the spontaneous fission tracks and U content obtained from the individual grains.

MTL—mean track length (1) measured, (2) c-axis corrected); Dpar — mean etch pit diameter; SE — Standard deviation; SD — Standard deviation

Ns: Number of spontaneous fission tracks counted over the total area.

N#: Number of fission track lengths measured.

Laser spot size: 16 µm. LA–ICP–MS Zeta method

** AFT ages published by Gray et al. (2021) integrated into the new thermal models ** AFT ages published by Villagomez (2014)*

Table 4. Apatite (U–Th)/He data

Sample	Unit	Lithology	Locality	Elevation (m)	LAT	LON	Age (Ma)	±2σ (Ma)	U (ppm)	Th (ppm)	^{147}Sm (ppm)	[U]e	Th/U	He (nmol/g)	Mass (µg)	Alpha correction (F_T)	Effective radius (µm)
Sierra de Juárez Complex																	
Between Siempre Viva Fault and Oaxaca Fault (Teotitlán migmatitic Belt / Sierra de Juárez mylonite complex)																	
5-11-11-02A	Teotitlán Migmatitic Suite, Zr U/Pb 158 Ma (Pindell et al., 2020a)	Orthogneiss	E Teotitlán	1604	18.17367	-97.05451	**17.4**	**1.0**	21.9	14.2	22.3		0.7	1.5		0.6	39.4
							16.0	**1.0**	7.8	2.5	21.1		0.3	0.6		0.8	60.6
							14.8	**0.9**	7.6	2.2	25.2		0.3	0.5		0.8	63.4
							20.5	1.2	8.4	1.8	15.9		0.2	0.7		0.7	52.7
							21.5	1.3	10.2	3.1	25.1		0.3	0.9		0.7	45.3
							18.2	**1.1**	5.2	1.5	13.7		0.3	0.4		0.8	65.1
					Weighted mean		**16.4**	**0.5**	**10.6**	**5.1**	**20.6**		**0.4**	**0.7**		**0.7**	**57.1**
Cuicateco Belt																	
Between Villa Alta/Aloapán and Vista Hermosa faults (Mazateco Complex)																	
21-01-18-01	Mazateco (SW of VH Fault)	Low grade Metasediment (Paleozoic?)		377	17.14588	-95.40940	**7.5**	**0.4**	7.8	19.9	100.6	12.9	2.5	0.3	1.2	0.6	38.5
							82.0	4.9	32.7	77.7	161.7	51.4	2.4	13.2	0.9	0.6	34.3
							7.2	**0.4**	1.7	2.0	26.7	2.2	1.2	0.1	5.8	0.8	62.7
							4.9	**0.3**	54.7	96.2	55.9	77.1	1.8	1.5	6.2	0.8	63.5
					Weighted mean		**6.0**	**0.2**	**21.4**	**39.4**	**61.0**	**30.8**	**1.8**	**0.6**	**4.4**	**0.7**	**54.9**
Tampico–Misantla Basin																	
ACAT17-1 *	Chicontepec. MDA 55 Ma (Cossey et al., 2019)		Chicontepec channel at Acatapec	465	20.96020	-98.27656	**15.9**	**1.0**	12.6	39.9	156.8	22.6	3.2	1.4	3.5	0.7	50.3
							15.4	**0.9**	4.3	32.3	146.2	12.5	7.4	0.8	6.0	0.7	60.7
							13.3	**0.8**	3.8	19.4	152.4	9.0	5.1	0.5	6.1	0.7	60.6
							15.2	**6.1**	3.7	21.7	130.5	9.4	5.9	0.6	5.8	0.7	63.9
					Weighted mean		**14.8**	**0.2**	**6.1**	**28.3**	**146.4**	**13.4**	**5.4**	**0.8**	**5.3**	**0.7**	**58.9**
COAP17-1 *	Basal? Chicontepec above thrust over Eocene	Sandstone		171	20.37653	-97.61215	16.4	1.0	3.3	17.4	223.6	8.4	5.3	0.6	2.6	0.7	48.9
							10.3	**0.6**	10.1	26.2	127.4	16.8	2.6	0.6	2.3	0.7	44.5
							9.6	**0.6**	3.5	43.6	147.0	14.3	12.3	0.4	1.0	0.6	34.4
							9.9	**0.4**	11.4	44.4	109.2	22.2	3.9	0.7	1.1	0.6	36.5
					Weighted mean		**9.9**	**0.3**	**8.4**	**38.0**	**127.9**	**17.8**	**6.3**	**0.6**	**1.5**	**0.6**	**38.4**
ALTO17-2 *	Cahuasas redbeds, Mid-Jurassic (Max. dep. age: 167 Ma)	Red tuff (Nazas?)		1059	19.86862	-97.22115	**12.2**	**0.7**	6.0	12.8	115.9	9.5	2.1	0.5	4.0	0.7	50.9
							13.4	**0.8**	2.9	56.5	121.5	16.5	19.7	0.8	1.4	0.6	39.7
							11.7	**0.7**	3.0	5.7	198.3	5.3	1.9	0.2	1.3	0.6	38.7
					Weighted mean		**12.3**	**0.4**	**3.9**	**25.0**	**145.2**	**10.4**	**7.9**	**0.5**	**2.2**	**0.6**	**43.1**
Mixtequita (N) & Guichicovi (S) blocks																	
27Mar17-3A	Mixtequita granite, Permo-Triassic	Granite		153	17.14763	-95.14480	**7.2**	**0.4**	4.7	4.4	90.8	6.2	0.9	0.2	3.5	0.7	49.8
							10.9	**0.7**	6.0	2.8	103.4	7.1	0.5	0.3	1.5	0.6	39.4
							12.5	**0.8**	5.7	4.3	84.1	7.1	0.8	0.4	3.6	0.7	51.4
							6.8	**0.4**	4.0	3.2	97.5	5.2	0.8	0.1	2.0	0.6	39.4
							8.8	**0.5**	4.5	3.2	70.1	5.6	0.7	0.2	1.5	0.6	39.5
					Weighted mean		**8.2**	**0.2**	**5.0**	**3.6**	**89.2**	**6.2**	**0.7**	**0.2**	**2.4**	**0.7**	**43.9**
Chiapas Massif and Basin																	
27Mar17-2A	Chiapas (Mixtequita) granite	Granite		86	17.03590	-94.94886	**10.9**	**0.7**	9.2	4.5	247.4	11.5	0.5	0.5	3.9	0.7	54.9
							15.7	**0.9**	22.0	3.9	314.2	24.5	0.2	1.7	8.0	0.8	70.0
							16.3	**1.0**	15.5	6.7	311.5	18.6	0.4	1.2	2.6	0.7	49.2
					Weighted mean		**13.3**	**0.5**	**15.6**	**5.0**	**291.0**	**18.2**	**0.4**	**1.1**	**4.8**	**0.7**	**58.0**

[U]e = effective Uranium concentration. (U-Th)/He data, numbers in bold indicate the aliquots (one grain per aliquot) used to calculate the weighted mean (see text)

** Apatite (U–Th)/He ages published by Gray et al. (2021), integrated into the new thermal models*

Table 5. Zircon (U–Th)/He data

Sample	Unit	Lithology	Locality	Elevation (m)	LAT	LON	Zircon (U–Th)/He Age (Ma)	±2σ (Ma)	U (ppm)	Th (ppm)	^{147}Sm (ppm)	[U]e	Th/U	He (nmol /g)	Mass (μg)	Alpha correction (Fт)	Effective radius (μm)
Mixteca (W) – Oaxaca (E)																	
25Feb16-2B	Jaltepetongo Fm.	Laminated metasandstones and filites, rich on quartz and feldspar.	Oaxaca City	ND	17.11408	-96.71640	18.0	1.4	33.4	31.8	1.1	40.7	1.0	3.7	138.6	0.9	154.9
							16.9	1.4	22.0	4.9	0.5	23.1	0.2	1.9	52.1	0.9	110.8
							39.6	3.2	117.0	27.8	2.1	123.4	0.2	22.8	26.5	0.9	88.2
					Weighted mean		**Discordant single grain ages. Samples was probably only partially reset**										
Sierra de Juárez Complex																	
Between Siempre Viva Fault and Oaxaca Fault (Teotitlán migmatitic Belt / Sierra de Juárez mylonite complex)																	
26Feb16-5C	Sierra de Juárez Complex	Amphibolite		3100	17.17224	-96.65426	23.4	1.9	34.2	7.0	0.4	35.9	0.2	3.9	21.2	0.9	81.1
							31.4	2.5	36.7	6.2	0.7	38.2	0.2	5.6	28.5	0.9	90.7
							88.6	7.1	67.4	19.4	5.4	71.9	0.3	29.3	20.9	0.8	78.3
					Weighted mean		**Discordant single grain ages. Samples was probably only partially reset**										
24Feb16-1B	Southermost Sierra de Juárez Complex	Filonite, banded with white mica. Low metamorphic grade	Road from San Juan Bautista Guelache to Teocuilco	2150	17.22260	-96.75324	**16.7**	**1.3**	67.1	20.5	1.0	71.8	0.3	5.5	18.0	0.8	76.8
							20.5	**1.6**	204.3	25.6	1.6	210.2	0.1	19.6	18.0	0.8	75.4
							19.0	**1.5**	51.6	21.3	1.5	56.5	0.4	4.8	12.3	0.8	66.6
					Weighted mean		**18.5**	**0.4**	**107.7**	**22.4**	**1.4**	**112.8**	**0.3**	**10.0**	**16.1**	**0.8**	**73.0**
Cuicateco Belt																	
West of Villa Alta and Aloapán faults, East of Siempre Viva Fault:																	
26Feb16-6B	Miocene dacite	Dacitic porphyry	Las Animas-Ixtepeji		17.23741	-96.56561	**16.0**	**1.3**	240.2	49.4	6.7	251.6	0.2	19.2	45.5	0.9	100.2
							14.0	**1.1**	93.0	20.3	9.4	97.8	0.2	6.4	30.3	0.9	86.6
							18.4	**1.5**	131.4	22.7	3.6	136.6	0.2	11.0	10.7	0.8	60.7
					Weighted mean		**15.7**	**0.4**	**154.9**	**30.8**	**6.6**	**162.0**	**0.2**	**12.2**	**28.8**	**0.9**	**82.5**
Between Villa Alta/Aloapán and Vista Hermosa faults (Mazateco Complex)																	
27Feb16-3B	Todos Santos (SW of Vista Hermosa Fault)	Red sandstone, masive with quartz, feldspar and lithics.	Mazateco Complex, Guelatao to Tuxtepec	ND	17.66895	-96.32819	56.2	4.5	23.4	13.1	1.3	26.4	0.6	6.6	14.3	0.8	67.0
							35.5	**2.8**	178.3	36.9	2.5	186.8	0.2	29.4	11.4	0.8	65.7
							32.6	**2.6**	194.1	31.3	1.4	201.3	0.2	29.6	13.6	0.8	70.0
							26.3	**2.1**	421.7	156.8	7.4	457.9	0.4	55.6	23.2	0.9	82.5
					Weighted mean		**30.5**	**1.4**	**204.4**	**59.5**	**3.1**	**218.1**	**0.3**	**30.3**	**15.7**	**0.8**	**71.3**
21-01-18-01	Mazateco (SW of Vista Hermosa Fault)	Low grade Metased		377	17.14588	-95.40940	**37.2**	**3.0**	379.3	16.7	0.0	383.1	0.0	54.7	2.6	0.7	38.3
							39.6	**3.2**	448.1	121.9	1.0	476.1	0.3	82.1	9.7	0.8	60.4
							39.6	**3.2**	54.1	12.9	1.3	57.0	0.2	9.6	7.4	0.8	54.8
					Weighted mean		**38.7**	**1.8**	**293.8**	**50.5**	**0.8**	**305.4**	**0.2**	**48.8**	**6.6**	**0.8**	**51.2**
Between Vista Hermosa and Valle Nacional faults																	
27Feb16-4B	Todos Santos (NE of Vista Hermosa Fault)	Very fine to medium-grained sandstone	Mazateco Complex, Guelatao to Tuxtepec		17.73676	-96.32892	49.3	3.9	56.7	15.5	0.0	60.2	0.3	13.1	10.7	0.8	63.4
							66.6	5.3	47.8	26.6	1.3	54.0	0.6	16.1	14.2	0.8	69.7
							25.8	2.1	520.5	116.4	13.3	547.4	0.2	65.0	21.4	0.9	80.3
					Weighted mean		**Discordant single grain ages. Samples was probably only partially reset**										
27Feb16-5B	Todos Santos? Xonamanca? (NE of Vista Hermosa Fault)	Coarse-grained sandstone	Mazateco Complex, Guelatao to Tuxtepec		17.76214	-96.31636	76.9	6.2	105.1	39.1	1.2	114.2	0.4	39.5	15.3	0.8	69.7
							138.7	11.1	48.7	18.3	2.1	52.9	0.4	35.9	59.7	0.9	116.2
							71.5	5.7	133.2	59.4	3.0	146.8	0.4	48.3	21.9	0.8	79.2
					Weighted mean		**Discordant single grain ages. Samples was probably only partially reset**										
Tampico–Misantla Basin																	
SANT17-1 *	K/T, K-Pg breccia	Breccia	Santiago	484	19.91593	-97.15263	238.8	19.1	28.5	14.6	1.7	31.9	0.5	36.4	32.3	0.9	92.7
							77.9	6.2	127.5	41.1	1.0	137.0	0.3	46.9	9.6	0.8	62.7
							228.9	18.3	110.0	26.6	1.5	116.1	0.2	120.7	12.5	0.8	68.6
					Weighted mean		**Discordant single grain ages. Samples was probably only partially reset**										
Mixtequita (N) & Guichicovi (S) blocks																	
27Mar17-3A	Mixtequita granite, Permo-Triassic	Granite		153	17.14763	-95.14480	**117.3**	**9.4**	41.1	12.7	0.4	44.1	0.3	23.7	21.1	0.8	76.2
							104.0	**8.3**	41.1	15.6	0.0	44.7	0.4	21.1	18.0	0.8	73.2
							106.1	**8.5**	21.9	7.2	0.0	23.5	0.3	11.4	18.1	0.8	72.9
					Weighted mean		**108.6**	**5.0**	**34.7**	**11.8**	**0.1**	**37.4**	**0.3**	**18.7**	**19.1**	**0.8**	**74.1**
26Mar17-3A	Petapa (South Guichicovi, East of Vista Hermosa Fault), Precambrian	Precambrian metasediment	La Maceta-Loma Santa Cruz	ND	16.95053	-95.24303	**30.6**	**2.4**	109.2	26.8	1.5	115.3	0.2	15.5	12.7	0.8	63.1
							32.3	**2.6**	158.1	48.1	0.9	169.2	0.3	25.4	32.2	0.9	85.1
					Weighted mean		**31.4**	**1.8**	**133.6**	**37.5**	**1.2**	**142.3**	**0.3**	**20.4**	**22.4**	**0.8**	**74.1**
26Mar17-5A	Petapa (South Guichicovi), Precambrian	Precambrian metaconglomerate	Santo Domingo Petapa	ND	16.82660	-95.14648	**41.8**	**3.3**	160.6	31.4	0.0	167.9	0.2	28.3	4.0	0.7	45.3
							42.9	**3.4**	145.4	62.2	0.0	159.7	0.4	26.8	2.9	0.7	41.6
							42.0	**3.4**	331.2	156.6	33.4	367.4	0.5	60.4	2.8	0.7	41.6
							44.1	**3.5**	144.7	76.1	1.4	162.3	0.5	30.6	6.7	0.8	56.1
					Weighted mean		**42.7**	**1.7**	**195.5**	**81.6**	**8.7**	**214.3**	**0.4**	**36.6**	**4.1**	**0.7**	**46.2**
Chontal																	
25Mar17-5A	Chivela sedimentary	Coarse sandstone	General Pascual	ND	16.47059	-94.22151	36.0	2.9	0.5	-1.8	2.9	0.1	-3.3	0.0	6.4	0.8	68.4
							13.9	1.1	16.8	7.3	0.8	18.5	0.4	1.2	12.0		
					Weighted mean		**Discordant single grain ages. Samples was probably only partially reset**										
Chiapas Massif and Basin																	
25Mar17-1A	Chiapas Massif, Triassic	Migmatite	Tapachula-Juchitla	ND	16.13137	-93.79774	**7.1**	**0.6**	115.1	25.3	0.0	120.9	0.2	3.4	3.3	0.7	41.0
							7.2	**0.6**	120.8	22.4	0.0	126.0	0.2	3.9	7.8	0.8	57.5
							7.7	**0.6**	135.2	20.3	-0.6	139.8	0.2	4.9	15.1	0.8	72.2
							9.4	**0.8**	215.1	31.3	0.0	222.3	0.1	8.2	3.5	0.7	42.3
					Weighted mean		**7.7**	**0.3**	**146.5**	**24.8**	**-0.2**	**152.2**	**0.2**	**5.1**	**7.5**	**0.8**	**53.3**
27Mar17-2A	Chiapas (Mixtequita) granite	Granite		86	17.03590	-94.94886	59.3	4.7	39.1	7.5	0.0	40.8	0.2	9.3	2.4	0.7	38.6
							80.7	6.5	31.0	5.7	-3.1	32.3	0.2	10.1	3.0	0.7	39.5
							94.4	7.6	70.0	121.6	-5.1	98.0	1.7	33.5	1.8	0.7	34.7
					Weighted mean		**Discordant single grain ages. Samples was probably only partially reset**										

[U]e = effective Uranium concentration. (U-Th)/He data, numbers in bold indicate the aliquots (one grain per aliquot) used to calculate the weighted mean (see text)

** Zircon (U–Th)/He age published by Gray et al. (2021), integrated into the new thermal models*

Table 6. Zircon Fission Track results

Sample	Unit	Lithology	Locality	Elevation (m)	LAT	LON	Grains	Ns	Total area cm2	U average (ppm)	Pooled AFT age (§)	95%-CI (Ma)	95%+CI (Ma)	Chi-squared	Primary Zeta	+/- 1 sigma
Cuicateco Belt																
Between Villa Alta/Aloapán and Vista Hermosa faults (Mazateco Complex)																
21-01-18-04	Mazateco (SW of Vista Hermosa Fault)	Metamorphic rock- schistose texture	Mazateco	543	17.13892	-95.41451	25	1435	1.6E-04	316.2	40.6	2.3	2.4	22.5	0.0401	0.0005

(§) Pooled age calculated by pooling the spontaneous fission tracks and U content obtained from the individual grains.

Table 7. Key wells drilled by the state-owned petroleum company (Pemex) and other international operators in onshore and offshore areas

WELL NAME	LOCATION*	WELL TYPE	FIELD	STATUS	HYDROCARBON TYPE	MEASURED DEPTH (m)	TRUE VERTICAL DEPTH (m)	DRILLING COMPLETION YEAR	PLAY	LITHOLOGY	FACIES
ALAW-1	Ultradeep waters	Exploration	N/A	Dry gas producer	Dry gas	5279	5279	2015	Upper Miocene		
AMATL-1EXP	Shallow waters	New-field wildcat	N/A	Oil and gas producer		3800	3090	2020	Lower Pliocene		
BUKMA-1SON	Ultradeep waters	Stratigraphic test well	N/A	Non-commercial gas and condensate	Gas condensate	7377	7373	2018	Middle Eocene		
CAHUA-1EXP	Shallow waters	New-field wildcat	CAHUA	Gas and condesate discovery	Gas condensate	2984	2973	2017	Upper Pliocene		
CHELEM-1	Deep waters	Exploration	N/A	Dry gas producer		3125	3125	2008	Pliocene		
CHINWOL-1EXP	Deep waters	New-field wildcat	N/A	Oil discovery (P&A)	Oil	1850	1813	2020	Lower Pliocene (3 zones)		
CHUKTAH-1	Shallow waters	Exploration		P&A, dry		4968	4968	1999	Lower, Middle, Upper Miocene		
CHUKTAH-201	Deep waters	Exploration		P&A, dry		4901	4901	2004	Lower, Middle, Upper Miocene		
HEIM-1	Onshore	Exploration	N/A	P&A		5004	5004	1983	Middle Eocene		
HEM-1	Ultradeep waters	Exploration	HEM	Suspended, wet gas	Wet gas	4429	4429	2015	Middle, Upper Miocene		
ITLA-1	Shallow waters	Exploration	ITLA	Oil discovery	Oil	3235	3235	2015	Upper Miocene		
KABILIL-1	Deep waters	Exploration	N/A	P&A, dry		5350	5196	2004	Lower Miocene		
KUNAH-1	Ultradeep waters	Exploration	KUNAH	Wet gas producer (5 zones)	Wet gas	4550	4550	2009	Lower, Middle, Upper Miocene	Litharenite	Turbidite channel, basin floor fan
KUNAH-1DL	Ultradeep waters	Appraisal well	KUNAH	Wet gas producer	Wet gas	4515	4471.5	2012	Lower, Middle, Upper Miocene	Litharenite	Turbidite channel, basin floor fan
LABAY-1	Ultradeep waters	Exploration	LABAY	Dry gas discovery, P&A	Dry gas	3362	3362	2009	Lower Miocene		
LAKACH-1	Deep waters	Exploration	LAKACH	Dry gas discovery, P&A	Dry gas	3813	3813	2006	Middle Pliocene	Litharenite	
LAKMAY-1	Deep waters	Exploration	N/A	Dry, P&A		2600	2417	2014	Middle, Upper Miocene		
LALAIL-1	Deep waters	Exploration	LALAIL	Gas and condensate producer	Dry gas	3815	3787.1	2007	Middle Miocene	Calc./volc. Litharenite	Submarine fan
LEEK-1	Deep waters	Exploration	LEEK	Wet gas producer	Wet gas	3700	3642.1	2009	Lower Miocene	Volcanic-rich litharenite	Base of slope channel
MATA ESPINO-2	Onshore	Exploration	MATA ESPINO	Condensate	Gas condensate	3804.5	3804.5	1956	Upper Eocene		
NAT-1	Ultradeep waters	Exploration	NAT	Wet gas producer		5531	5531	2014	Middle, Upper Miocene	Feldspathic litharenite	Basin floor turbidite channel, channel levee
NAT-1DL	Ultradeep waters	Appraisal well	NAT	Wet gas producer	Wet gas	4569	4349	2015	Middle Miocene		
NEN-1	Ultradeep waters	Exploration	NEN	Dry gas producer	Dry gas	4350	4350	2011	Upper Miocene		
NOXAL-1	Deep waters	Exploration	NOXAL	Dry gas producer	Dry gas	3640	3640	2006	Upper Miocene, Lower Pliocene	Calcareous litharenite	
OCTLI-1EXP	Shallow waters	New-field wildcat	OCTLI	Oil and gas discovery	Oil and gas	2580	2190	2017	Upper Pliocene		
PIKLIS-1	Ultradeep waters	Exploration	PIKLIS	Gas and condensate discovery	Wet gas	5431	5431	2011	Lower, Upper Miocene		
POLOK-1EXP	Deep waters	New-field wildcat	N/A	Oil discovery	Oil	2620	2529.6	2020	Lower Miocene (2 zones)		
SAASKEN-1EXP	Shallow waters	New-field wildcat	N/A	P&A	Oil	3830	3688	2020	Upper Miocene, Pliocene		
SAYULITA-1 EXP	Shallow waters	New-field wildcat	SAYULITA	P&A, oil discovery	Oil	1758	1931	2021	Upper Miocene		
TABSCOOB-1	Shallow waters	Exploration	TABSCOOB	Gas and condensate discovery	Oil	6900	6900	1997	Middle Pliocene		
TABSCOOB-101	Shallow waters	Exploration	TABSCOOB	Dry gas producer	Gas	3150	3150	2006	Lower Miocene		
TECOALLI-1	Shallow waters	Exploration	TECOALLI	Oil and gas discovery	Oil and gas	3930	3930	2008	Lower Pliocene		Fluvial-deltaic mouth bars
TEPAXTLI-1EXP	Onshore	New-field wildcat	PERDIZ	P&A	Non disclosed	7283	7859	2021	Eocene		
TIBIL-1	Shallow waters	Exploration	N/A	Oil discovery (P&A)	Oil	4334	4334	2005	Upper Miocene, Pliocene		
XAXAMANI-1	Shallow waters	Exploration	XAXAMANI	Gas and oil discovery	Oil	1990	1990	2003	Lower, Middle Pliocene		
YOKA-1	Ultradeep waters	Exploration	N/A	P&A; non-commercial wet gas	Wet gas	4573	4573	2014	Lower Miocene	Feldspathic litharenite	
ZAMA-1SON	Shallow waters	Stratigraphic test well	ZAMA	Oil discovery	Oil	4109	4109	2017	Upper Miocene	Feldspathic litharenite	Slope channel turbidites
Other wells from DSDP											
DSDP 10-87	Ultradeep waters	Stratigraphic test well					700	1970	Middle Miocene	Sandy silt	
DSDP 10-90	Ultradeep waters	Stratigraphic test well					768	1970	Middle Miocene	Quartz rich clay mineral rich sand	
DSDP 10-91	Ultradeep waters	Stratigraphic test well					900	1970	Middle Miocene	Pebbly coarse sand	

* Location definition according to the database https://mapa.hidrocarburos.gob.mx (Comisión Nacional de Hidrocarburos)

Shallow waters: 0 – 500m; Deep waters: 500 – 1000m; Ultradeep waters: >1000m (meters below sea level)

P&A: Plugged and abandoned